Auburn University

B-424 (2)

DEVELOPMENT OF P-Y CURVES FOR PIEDMONT RESIDUAL SOILS

Prepared by

Michael Simpson, Graduate Research Assistant
Dan A. Brown, Gottlieb Associate Professor of Civil Engineering

Highway Research Center
Harbert Engineering Center
Auburn University, Alabama 36849-5337

FEBRUARY 2003

DEVELOPMENT OF P-Y CURVES FOR PIEDMONT RESIDUAL SOILS

Project No. B-424 (2)

Prepared by

Michael Simpson
Dan A. Brown

Department of Civil Engineering
Auburn University

ABSTRACT

DEVELOPMENT OF P-Y CURVES FOR PIEDMONT RESIDUAL SOILS

P-y curves can be used to predict a piles response to lateral loading. Computer programs such as COM624 incorporate many p-y criteria which include: soft clay, stiff clay below the water table, stiff clay above the water table, sand, and vuggy limestone. A computer program can easily predict deflections and moments along the length of a pile by using known soil strength parameters. But, there is no specific criterion for producing p-y curves for residual soils; therefore accurate computer solutions predicting pile behavior to lateral loading in residual soils cannot be obtained. The behavior of residual soils cannot be captured using these other criterion for developing p-y curves. A research project was conducted at the Auburn University Geotechnical Test Site to create a method to develop p-y curves for Piedmont residual soils.

Five full-scale lateral load tests and several in-situ tests to observe soil strength were performed at the test site and analyzed. The data were used to backcalculate p-y curves for the residual soil present at this site.

Linear p-y curves were input to COM624 until the pile deflections calculated matched those measured in the field. The slopes of these p-y curves (k) were plotted versus depth. A trend was observed between these k values and the in-situ soil tests

performed at the site. A simple p-y relation was used to generate p-y curves by correlating the in-situ data with the k values.

Deflections produced by COM624 were checked by comparison with the deflections measured in the field. The deflections calculated were accurate and conservative. The deflected shape of the pile was also similar to those observed in the field tests.

A useful p-y criterion was developed for Piedmont residual soils. P-y curves can be generated using data from an in-situ test performed in the residual soil. With these p-y curves, computer programs can be used to quickly and accurately predict pile behavior under lateral loading

Style manual or journal used: ASCE Author's Guide to Journals, Books, and Reference Publications

Computer software used: Microsoft Word, Microsoft Excel, COM624

TABLE OF CONTENTS

LIST OF FIGURES

LIST OF TABLES

CHAPTER 1

INTRODUCTION

1.1 General

A drilled shaft consists of a drilled hole that is filled with fluid concrete, which can be reinforced by lowering a rebar cage into the excavation. A drilled shaft that is sized adequately and reinforced properly can sustain large lateral loads created by earth pressures, wind pressures, water pressures, earthquakes, impact loads, etc. Drilled shafts are used often in the case of a large lateral load for structures such as bridges, towers, and signs. The economic advantage of drilled shafts often occurs as a result of the fact that a large diameter drilled shaft can be installed to replace groups of driven piles (O'Neill and Reese, 1999).

The solution to the lateral load problem involves the pile deflection and the reaction of the soil in which it is embedded. The deflection caused by the lateral loading of a shaft creates reactions in the soil, where the equations of static equilibrium must be satisfied. The problem created is a soil-structure-interaction problem, which requires numerical relationships between the pile deflection and soil reaction. In order to understand the pile behavior under lateral loading, some knowledge of the soil response must be obtained. Analysis of the data from full-scale load tests provides the best means to develop full understanding of a particular soil.

Computer programs such as FHWA COM624 are used in the analysis of laterally loaded piles. With the input of known soil parameters, the computer program can predict deflections and moments along the pile. This is possible because the program has p-y criteria for certain soil types such as sand, clay above the water table, and clay below the water table. But the program lacks a p-y criterion for Piedmont residual soils. These soils cannot be modeled with the traditional p-y curves used in such a program. Residual soils are weathered in-place and do not have engineering characteristics similar to sedimentary deposits. Therefore, a criterion for developing p-y curves for Piedmont residual soils is needed.

1.2 Objectives

The objectives of this research is as follows:

1. Six full-scale static lateral load tests were conducted in Piedmont residual soil at the Spring Villa geotechnical test site located in Opelika, Alabama. Five of the shafts were constructed without defects and one constructed with defects. This research includes analysis of the data produced from the testing of the five non-defective shafts.
2. From the analysis, recommendations for computing p-y curves for laterally loaded piles in the piedmont residuum will be presented.

CHAPTER 2

BACKGROUND

2.1 Introduction

There is not currently a design procedure for p-y curves for laterally loaded drilled shafts in piedmont soils. Much research can be found in literature with respect to laterally loaded piles in many different geologic settings. Yet, there is little knowledge for geotechnical practice in piedmont residual soils. The literature on piedmont residual soils reflects the knowledge of the geology, but the lack of research on design procedures.

There are many design methods for laterally loaded drilled shafts in soil. The p-y method is the most widely used for the design of drilled shafts under lateral load. The p-y method solved using computers is used because of its simplicity. Four other methods available for the solution of a single laterally loaded pile include: The elastic method, curves and charts, static method (Broms Method), and non-dimensional curves (Reese, 1984). The elastic method and curves and charts method are not as widely used. The elastic method is thought to have limited applications, and a large number of curves and charts are needed for a simple case. The non-dimensional and Broms Method are a good way to check the computer output and response of the pile. The focus of this paper will be on the p-y method and its application to silty soils.

2.2 p-y Method

The p-y method models a laterally loaded pile as a soil-structure interaction problem because the lateral load applied results in lateral deflection of the pile, which causes reactions in the soil. Static equilibrium between the pile and soil must be obtained. The numerical solution of the problem requires a relationship between the pile deflections and the soil reactions. Matlock (1970) used the Winkler assumption that the soil reaction at a point is dependent only on the pile deflection at that point and not on pile deflections above and below. The soil can therefore be removed and replaced as shown in figure 2.1 by a set of mechanisms for the purpose of analysis.

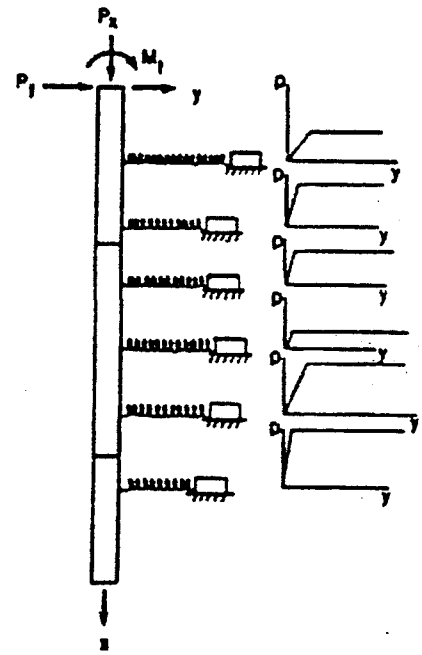

Figure 2.1

Model of a pile under lateral load (Reese, 1984)

The soil-response curves shown are simple models used to represent natural soils. A typical p-y curve for soil is shown in figure 2.2.

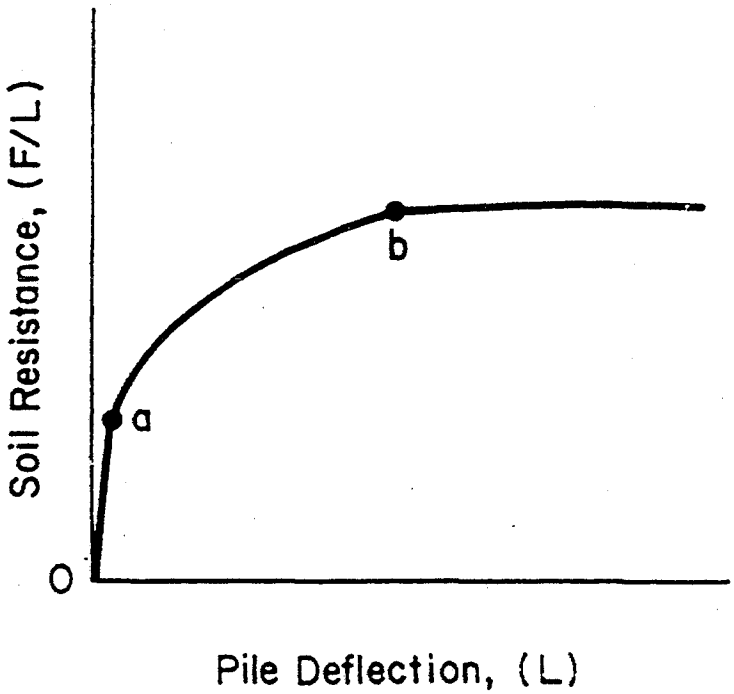

Figure 2.2

Conceptual p-y curve (Reese, 1984)

These curves present the force per unit length along the pile, p, versus pile deflection, y. The start of the curve 0-a is representative of the elastic action of the soil. The transition portion of the curve is shown by a-b. The ultimate soil resistance is reached at point b. Bending moment curves obtained from lateral load tests can be used to obtain values of p and y at points along the pile using the following equations:

$$y = \iint \frac{M(x)}{EI}$$

Eq. 2.1

$$p = \frac{d^2}{dx^2} M(x)$$

Eq. 2.2

If p-y curves can be predicted, equation 2.3 can be solved to yield pile deflection, pile rotation, bending moment, shear, and soil reaction for any load below failure.

$$EI\frac{d^4y}{dx^4} + P_x\frac{d^2y}{dx^2} - p - W = 0$$

Eq. 2.3

EI is the flexural rigidity of the pile, y is the lateral deflection of the pile at a point x along the length of the pile, x is the position along the pile, P_x is the axial load on the pile, p is the soil reaction per unit length, and W is the distributed load along the length of the pile (Reese, 1984). The equation can be solved using a finite difference equation 2.4

$$y_{m-2}R_{m-1} + y_{m-1}(-2R_{m-1} - 2R_m + P_x h^2) + y_m(R_{m-1} + 4R_m + R_{m+1} - 2P_x h^2 + k_m h^4) + y_{m+1}(-2R_m - 2R_{m+1} + P_x h^2) + y_{m+2}R_{m+1} - W_m = 0$$

Eq. 2.4

where y_m is the deflection at point m along the pile, R_m is the flexural rigidity at point m, P_x is the axial load, k_m is the soil modulus at point m, and W_m is the distributed load at point m. Once the deflections are obtained, the shear, moment, and slope can be found at all points along the pile. A computer program such as FHWA COM624 is a more widely used method of obtaining the deflections. The computer saves time and avoids human error. This method only applies for the solution of a general case using the p-y method. Application of the p-y method to real world problems and conditions is not as simple.

The p-y or nonlinear response method can be applied to a wide range of soil types. Presented methods include: p-y curves for soft clay (Matlock, 1970), p-y curves

for sand (Reese, Cox, and Koop, 1974), p-y curves for stiff clay above the water table (Reese and Welch, 1975), and p-y curves for stiff clay below the water table (Reese, Cox, and Koop, 1975). These four methods cover a wide area of soil profiles.

2.2.1 p-y curves for Soft Clay

Matlock (1970) proposed a method for the development of p-y curves in soft clay. The program was sponsored by a group of five oil companies for research on laterally loaded piles for offshore structures in soft normally consolidated marine clay. The test pile was 12.75 inches in diameter and embedded 42 feet. The pile was instrumented with 35 pairs of electric resistance strain gages to provide extremely accurate bending moment measurements. The pile was driven into clays near Lake Austin, Texas then recovered and retested in clays in Sabine Pass, Texas.

The structural analysis of this problem is equivalent to a complex beam-column on an inelastic foundation. The Winkler assumption allows for the separation of the soil into several independent layers providing soil resistance p and pile deflection y. Differentiation of the measured bending moments resulted in accurate curves of the distribution of soil reaction along the pile. The integration of the bending moment diagrams resulted in the deflection along the pile. Incremental loads were applied for selected depths and p was plotted as a function of y. The recommended design procedure was based on these experimental p-y curves.

The upper portions of the soils at Lake Austin had been subjected to desiccation and contained joints and fissures. The Sabine clay was more typical of a slightly overconsolidated marine deposit. Therefore the development of design criteria is based

primarily on the results of the Sabine tests. For short-term static loading, Matlock recommends the following:

1. Estimate the variation with depth of c (undrained shear strength) and γ' (submerged unit weight). Obtain the values of ε_{50}, the strain which corresponds to half the maximum stress. Typical values of ε_{50} are given in Table 2.1.

Consistency of Clay	ε_{50}
Soft	0.020
Medium	0.010
Stiff	0.005

Table 2.1

Values of ε_{50} for Soft Clays (Matlock, 1970)

2. Compute the ultimate soil resistance per unit length of pile, using the smallest value obtained from equations 2.5 and 2.6.

$$P_U = \left[3 + \frac{\gamma'}{c}x + \frac{J}{b}x\right]cb$$

Eq. 2.5

$$P_U = 9cb$$

Eq. 2.6

In these equations γ' and c have already been defined, x is the depth from the ground surface, b is the width of the pile, and J is an empirical parameter experimentally

determined to be 0.5 for soft clays and 0.25 for medium clays. Using these equations the value of P_U is calculated at each depth a p-y curve is needed.

3. Obtain y_{50}, the deflection at half the ultimate soil resistance using equation 2.7.

$$y_{50} = 2.5\varepsilon_{50}b$$

Eq. 2.7

4. Calculate the points for the p-y curve using equation 2.8. The value of p remains constant once the value of $y = 8y_{50}$ is reached.

$$\frac{P}{P_U} = 0.5\left(\frac{y}{y_{50}}\right)^{\frac{1}{3}}$$

Eq. 2.8

Matlock developed a procedure for obtaining p-y curves for cyclic loading, which will not be discussed. Figure 2.3 shows a p-y curve for short-term static loading using Matlock's procedure for soft clay below the water table.

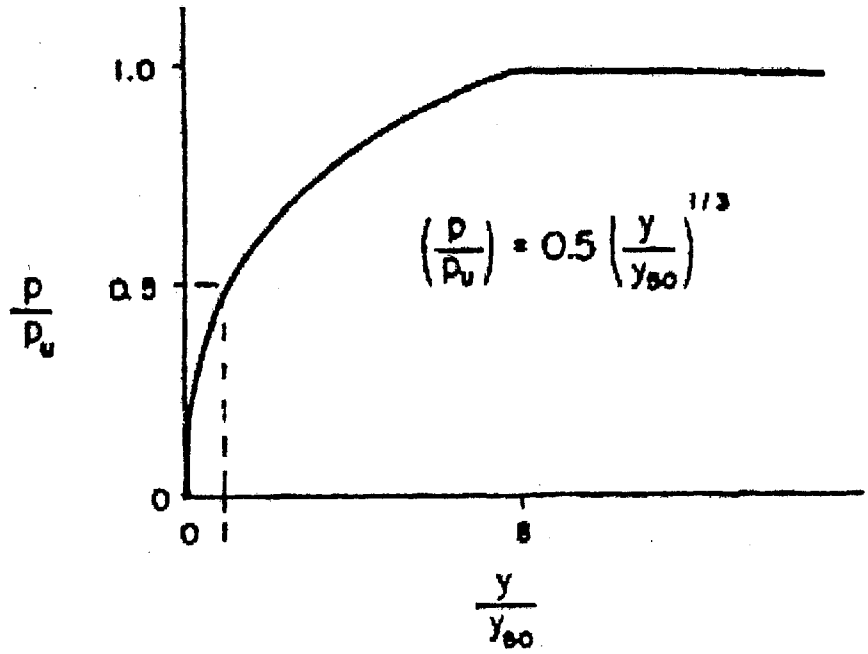

Figure 2.3

Characteristic shape of the p-y curve for soft clay below the water table for static loading (Matlock, 1970)

2.2.2 p-y Curves for Sand

Reese, Cox, and Grubbs (1974) performed a series of tests at a site on Mustang Island near Corpus Christi. The lateral loading tests were performed on two 24-inch steel pipe piles, which were embedded 69 feet. One pile was tested short term loading while the other was subjected to repeated loading. The soil condition at the site was fine sand, uniformly graded with an internal angle of friction of 39 degrees. The water level was kept a few inches above the ground surface throughout the tests to simulate offshore conditions. Reese, Cox, and Koop (1974) had a companion paper presented at the Sixth Annual Offshore Technology Conference. This paper presented the recommendations for

p-y curves in sand. Although the tests were performed in submerged sand, the tests are applied to sands above the water table by making appropriate unit weight adjustments depending on the position of the water table.

For both static and cyclic loading, a series of lateral loads were applied to the test piles. Using the proper instrumentation during testing, bending moment curves were obtained from each load applied to the piles. The bending moment curves obtained during testing, along with the proper boundary condition for each loading type, allows for the values of p and y to be calculated by solving equations 2.1 and 2.2. The solution of equation 2.1 can be obtained with accurate results unlike equation 2.2. Accurate moment measurements are required in order to solve equation 2.2 analytically.

The soil resistance curves in this study were obtained by assuming the soil modulus could be described as a function of depth by a nonlinear curve. The parameters for the nonlinear curve were calculated from the test data, which allowed the analytical solution to be obtained for the soil reaction curve. Although there was some basis for this method from theory, the empiricism involved in the recommendations was developed because the behavior of the sand did not yield a completely rational analysis.

The ultimate soil resistance was found using free body diagrams and assuming the Mohr-Coulomb failure theory was valid for sand. Equations 2.9 and 2.10 give the value of ultimate soil resistance near the ground surface and well below the ground surface, respectively.

$$P_{ct} = \gamma H\left[\begin{array}{l}\dfrac{K_o H\tan\phi\sin\beta}{\tan(\beta-\phi)\cos\alpha}+\dfrac{\tan\beta}{\tan(\beta-\phi)}(b+H\tan\beta\tan\alpha)\\ +K_o H\tan\beta(\tan\phi\sin\beta-\tan\alpha)-K_a b\end{array}\right]$$

Eq. 2.9

$$P_{cd} = K_a b\gamma H\left(\tan^8 \beta - 1\right) + K_o b\gamma H \tan\phi \tan^4 \beta$$

Eq. 2.10

In the above equations, γ is the unit weight of the sand, ϕ is the angle of internal friction, b is the pile diameter, H is the depth below the ground surface, K_a is the Rankine coefficient of minimum active earth pressure, β is equal to $45 + \phi/2$ and is obtained from Rankine's theory for passive pressure, α is equal to $\phi/2$, and K_o is the coefficient of earth pressure at rest. Equations 2.9 and 2.10 can be set equal to find a depth x_t, which defines the intersection where the ultimate soil resistance near the surface and well below the ground surface meets. Equation 2.9 should be used above this depth, and equation 2.10 below. P-y curves may be constructed at desired depths using these equations. A p-y curve developed using this method is shown in Figure 2.4. The curve contains three straight lines and a parabola. To yield a consistent shape between the experimental and recommended p-y curves, the parabola and second straight line were chosen empirically. The slope of the initial portion of the p-y curve is shown in Table 2.2.

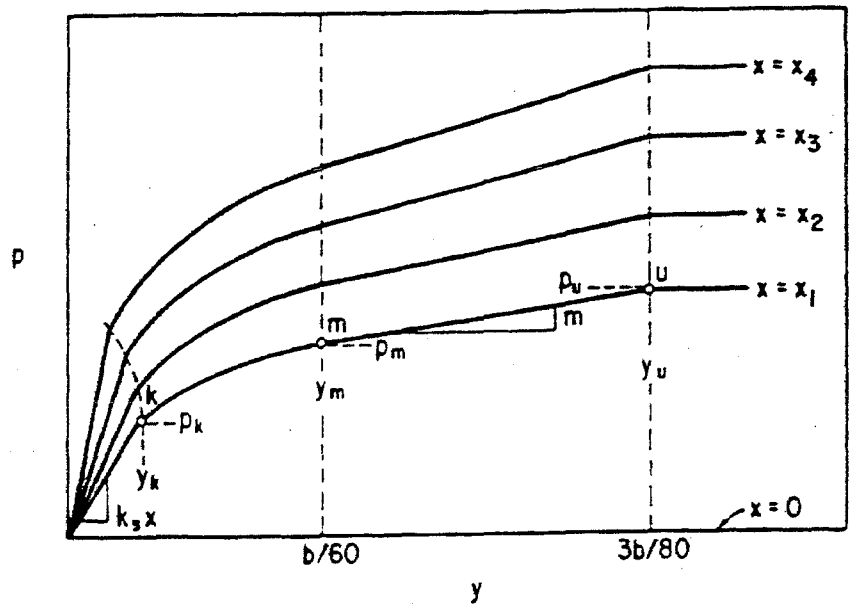

Figure 2.4

Characteristic shape of proposed p-y criteria for sand and static loading (Reese, Cox, and Koop, 1974)

Relative Density	Loose	Medium	Dense
Range of k (lbs/in^3)	2.6 – 7.7	7.7 – 26	26 – 51

Table 2.2

Terzaghi's Values of k for Submerged Sand (Reese, Cox, and Koop, 1974)

An empirical adjustment factor was needed to adjust the computed ultimate soil resistance values for agreement with the measured values. The factor was obtained by dividing the observed values by the computed values. The computed values were then adjusted by this factor to obtain P_U proposed in the method. The intermediate portion of the curve is defined by the points p and y corresponding to k, m, and u in Figure 2.4. The respective values of y_m and y_u were found to be b/60 and 3b/80. The value of p_m can be obtained by multiplying the ultimate soil resistance (Eq. 2.9 and 2.10) by an empirical, non-dimensional factor B shown in figure 2.5.

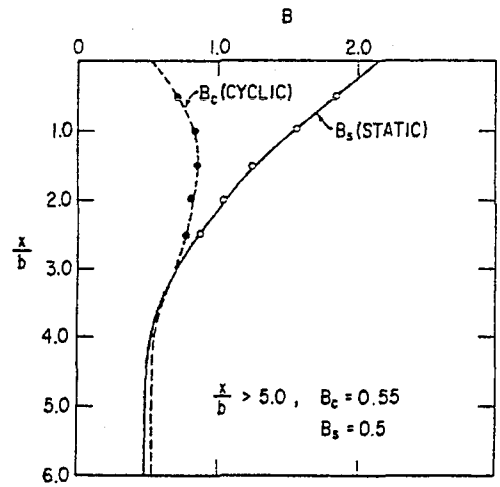

Figure 2.5

Non-dimensional coefficient B for soil resistance vs. depth (Reese, Cox, and Koop, 1974)

The p-y curve is constructed by a parabola between points k and m. The parabola intersects the origin and connects at point m with a slope equal to the slope of line from m to u. Point k is the intersection of the parabola with the initial straight line. Beyond u the line is horizontal. A step-by-step method to obtain the values for the parabola and lines is given in the recommendation, but will not be discussed.

2.2.3 p-y curves for Stiff Clay Above the Water Table

Welch and Reese (1972) laterally tested a drilled shaft 30 inches in diameter and 42 feet long. The site tested was located in Houston, Texas. The soil at the site consisted of 28 feet of stiff to very stiff clay red clay, 2 feet of silt and clay layers, and very stiff tan silty clay to a depth of 42 feet. The developed criteria are for laterally loaded drilled shafts, both static and cyclic loading, above the water table because the water table was located at a depth of 55 feet at the time of testing. A steel pipe 10 inches in diameter was used as the instrument pipe, which extended two feet above the ground for a total length of 44 feet. Strain gauges were then placed at strategic points along the pile to obtain the required measurements. Reese and Welch (1975) analyzed the data obtained to create p-y curves.

The goal in obtaining these experimental p-y curves was to solve equations 2.1 and 2.2 previously discussed. To ensure simple differentiation and integration, a polynomial describing a truncated power series was used to describe the data. A least squares curve-fitting technique was then employed to fit the function to the data. A polynomial of degree seven was found to fit the data without erratic behavior. This curve was then double integrated to obtain the deflection of the shaft as a function of depth. The shear was obtained by differentiating the polynomial and the soil reaction was obtained by differentiating the shear. The p-y curves were then obtained by plotting the soil reaction and deflection at selected depths for different loads. The recommendations were based on these p-y curves.

Using the value suggested by Skempton (1951) for a long strip footing, the deflection at half the ultimate load can be found using equation 2.7 referenced in Matlock's soft clay recommendations. Laboratory triaxial tests were run and ε_{50} was found to be .005 in/in and using equation 2.7, the average value of y_{50} was calculated to be 0.375 in. The ultimate soil reaction was not reached at all depths since this is a deep foundation problem, so the values of ultimate soil reaction were estimated using equation 2.11.

$$\frac{P}{P_U} = 0.5\left(\frac{y}{y_{50}}\right)^{\frac{1}{4}}$$

$$P = P_U \text{ for } y \succ 16y_{50}$$

Eq. 2.11

This equation was obtained from the curve formed by plotting the values of P/P_U and y/y_{50}. This equation is similar to the one proposed by Matlock, and the values when compared were in reasonable agreement near the ground surface. Since this is the most critical zone, Matlock's equations for ultimate soil resistance were adopted (Eq. 2.5 and 2.6). The only difference used in this method is that c is the average undrained shear strength from the ground surface to depth x, instead of the undrained shear strength at the depth x.

An assumption was made that the shape of the laboratory stress-strain curves and the experimental p-y curves would be similar. This correlation forms equation 2.12.

$$y = \left(\frac{2.5b}{\varepsilon_{50}}\right)\varepsilon^2$$

Eq. 2.12

With laboratory stress-strain curves, equations 2.5, 2.6, 2.7, 2.11, and 2.12 can be used to predict p-y curves for a deep foundation in stiff clay above the water table with a given diameter and short-term static loading. P-y curves for cyclic loading can be obtained with the addition of extra steps to account for the effects of repeated load.

2.2.4 p-y curves for Stiff Clay Below the Water Table

Reese, Cox, and Koop (1975) presented a design method for creating p-y curves to the Seventh Annual Offshore Technology Conference for laterally loaded piles in stiff clay. The criterion gives recommendations for p-y curves for stiff clay below the water table. Two-24 inch-diameter piles and one 6-inch pile 50 feet in length were driven into stiff clay and subjected to lateral loading near Austin, Texas. These piles were tested with short-term cyclic and static loads. The water table was maintained at a few inches above ground during testing to simulate clay below the water table (marine conditions). The soils at the sight consisted of stiff, preconsolidated, clays of marine origins. Some preliminary studies of experimental p-y curves were undertaken to establish if there was a diameter effect seen from the tests of the 6-inch and 24 inch diameter piles. The studies were unproductive and the recommendations were based only on the 24-inch diameter tests.

A characteristic p-y curve for short-term cyclic loading can be seen in Figure 2.6. The curve has an initial straight line from the origin to point 1; two parabolic sections, from point 1 to point 2 and from point 2 to point 3; two straight lines from point 3 to point 4 and a horizontal line beyond point 4. At low magnitudes of soil stress and strain,

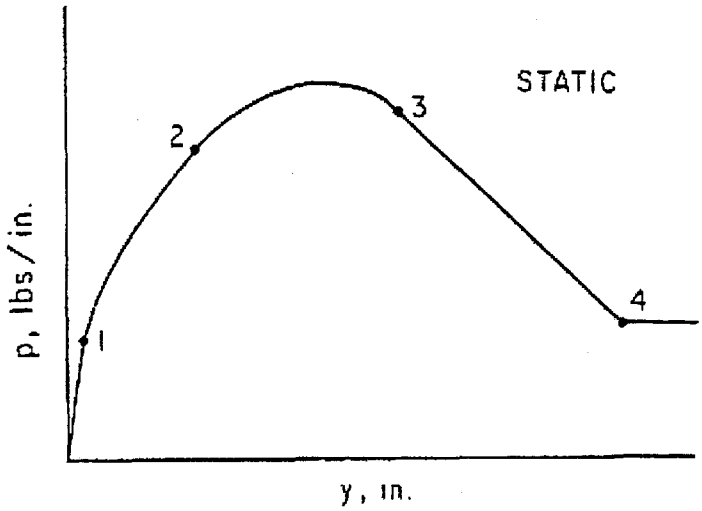

Figure 2.6

Characteristic shape of proposed p-y criteria for stiff clay (Reese, Cox, and Koop, 1975)

a straight-line relationship is often observed. The slopes of the initial straight lines were determined using equation 2.13.

$$E_s = \frac{p}{y}$$

Eq. 2.13

E_S is the initial soil modulus; p and y are the coordinates of the initial portion of the p-y curve.

The ultimate soil resistance, near the ground surface, uses the idea of a wedge of clay moving up and out from the pile. Several assumptions were made in order to obtain this equation including: the clay has a constant shear strength over the depth H, the wedge of soil moving up and out can be defined by three plane surfaces and a plane next to the pile, the undrained shear strength of the clay is fully developed along the sliding surfaces, the bottom surface of the wedge is at a 45° with the horizontal, and there is no

vertical force between the pile and upward-moving soil. Equation 2.14 was derived from this simplified failure model.

$$P_C = 2c_a b + \gamma' bH + 2.83c_a H$$

Eq. 2.14

P_C is the ultimate soil resistance at depth H, c_a is the average undrained shear strength from the surface to depth H, b is the diameter of the pile, and γ' is the submerged unit weight of soil. At a certain depth below the ground surface, the soil will fail by flowing horizontally around the pile. Assuming that blocks of soil around the pile have failed, equation 2.15 is developed.

$$P_C = 11cb$$

Eq. 2.15

In this equation, c is the undrained shear strength at the depth for the p-y curve. The smaller of these two values is used for the ultimate soil resistance. The ultimate soil resistances calculated were found to be larger than the values obtained experimentally. It was decided to adjust the ultimate soil resistance empirically by dividing the observed ultimate soil resistance by the computed ultimate soil resistance. The observed and computed values agree with the use of this empirical coefficient. The remainder of the p-y curve derivation uses the concept that a load deflection curve can be related to the stress-strain curve from a laboratory specimen, which has already been discussed.

Recommendations are given for the instance when there are no laboratory stress strain curves for the soil. Two parameters used are ε_C given in table 2.3 and y_C given by equation 2.16.

Average Undrained Shear Strength (ton/ft^2)	ε_C (in/in)
0.5 – 1.0	0.007
1.0 – 2.0	0.005
2.0 – 4.0	0.004

Table 2.3

Values of ε_C for Stiff Clays (Reese, Cox, and Koop, 1975)

$$y_C = \varepsilon_C b$$

Eq. 2.16

The equation of the parabola going through the origin of the p-y curve shown in figure 2.7 is

$$p = 0.5 p_C \left(\frac{y}{y_C} \right)^{0.5}$$

Eq. 2.17

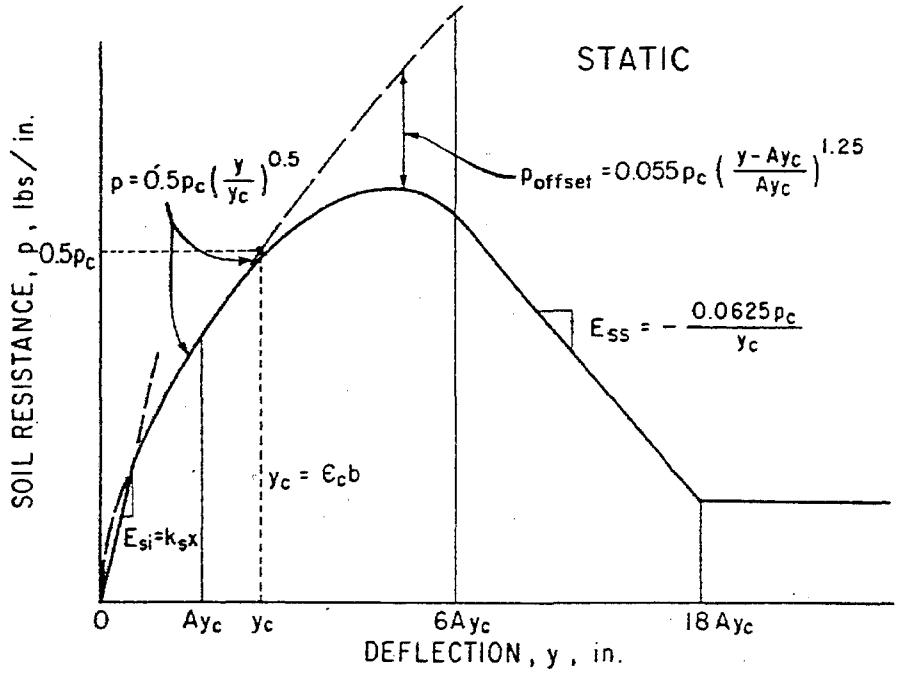

Figure 2.7

Characteristic shape of proposed p-y criteria for static loading in stiff clay (Reese, Cox, and Koop, 1975)

The parabolic shape of the p-y curve begins at the intersection the intersection of the straight line, which starts at the origin. The parabola continues until the point defined by the deflection Ay_C is reached. A is shown in figure 2.7 for the non-dimensional depth x/b at which the p-y curve is desired. At the deflection point Ay_C the parabola is offset by the value in equation 2.18.

$$p_{offset} = 0.055 p_C \left(\frac{y - Ay_C}{Ay_C} \right)^{1.25}$$

Eq. 2.18

At the deflection point $6Ay_C$, the offset stops and the p-y curve becomes a straight line with a slope given by equation 2.19.

$$E_{ss} = -\frac{0.0625 p_C}{y_C}$$

Eq. 2.19

The straight line will continue until the deflection point of $18Ay_C$ is reached, and then it will become a horizontal line beyond that point. This method also allows for the development of p-y curves for the cyclic case, which will not be discussed.

2.3 Piedmont Soils

The Piedmont consists of in-place weathered rock extending from Pennsylvania to Alabama. It is located between the Atlantic Coastal Plain on the east and the Appalachian Ridge on the west as shown in figure 2.8. The soil is underlain by the parent metamorphic rock, which is predominantly composed of gneisses and schists of early Paleozoic era or older. Intrusive deposits of granite and mafic rocks, such as gabbro can be found. The engineering behavior of piedmont residual soil is poorly understood (Vinson and Brown, 1997). The physical structure and engineering properties of these soils are different from those of sedimentary materials. Since residual soils retain much of the internal configuration (bedding and defects) of the parent rock, much of the knowledge from the study of sediments is not applied easily to residual soils (Sowers, 1963).

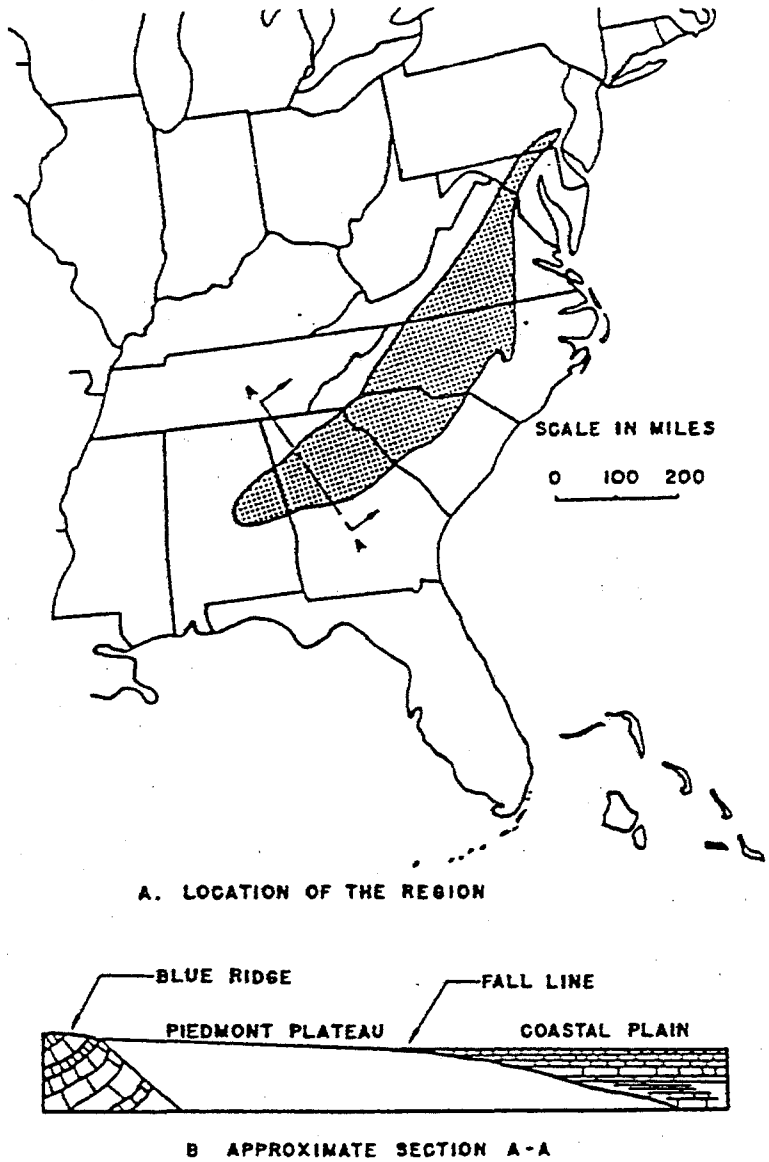

Figure 2.8

Location and idealized section of Piedmont and Blue Ridge (Sowers, 1983)

2.3.1 Residual Soil Formation

The parent rocks were crystallized after being subjected to intense heat and pressure. Once cooled, a complex fabric of interlocked mineral grains was formed. Many of the rocks exhibit evidence of their formation under heat and pressure by the segregation of their minerals into parallel bands or sheets (Sowers, 1963). The residual soils are formed by the chemical decomposition of the original rock forming clay minerals, hydrous micas, iron oxides, and semi-soluble carbonates and bicarbonates. Mechanical weathering is not a factor because the flat topography does not promote erosion, yet the humid climate causes rapid and deep weathering. The most important factors affecting the depth of weathering are the composition of the rock and the defects such as faults and fissures (Sowers, 1954). The depth of weathering and the thickness of the residual soil layer can be extremely variable. Due to the different degree of weathering with depth, soil zones are formed. The weathering is greatest at shallow depths and decreases with depth until the parent rock is reached. The typical weathering zones can be seen in figure 2.9.

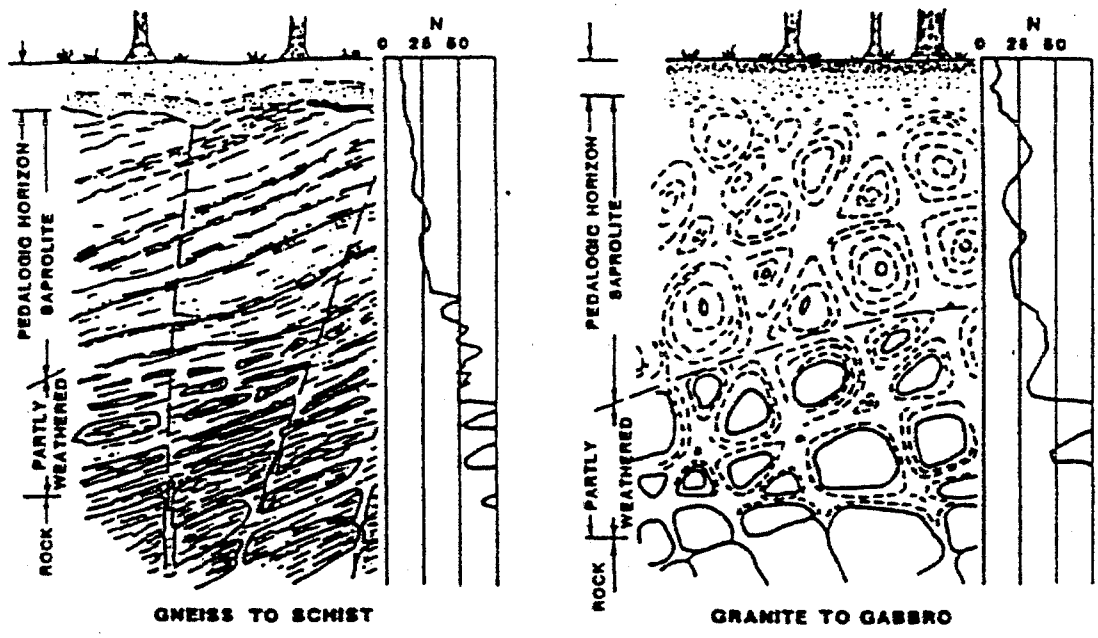

Figure 2.9

Typical weathering profile of Piedmont Soil (Sowers, 1963)

2.3.2 Residual Soil Profile

The residual soil profile can ordinarily be divided into three zones: the upper zone of stiff red sandy clays, the intermediate zone of loose to firm micaceous sandy silts, and the partially weathered zone of gravelly silty sands and some rock. These three zones are underlain by the unweathered parent rock. There is no perfectly defined boundary for these zones because they are defined by the degree of weathering which can be variable. There is normally a gradual transition from one zone to the other. Also, the boundaries are not horizontal because weathering is accelerated near fractures where water leaches. Several systems for defining the zones based on weathering have been proposed including: Sowers (1963), Deere and Patton (1971), Brecke (1975), and Law Engineering and Marta (1980). The major problem with any of these methods is to define the boundaries (Sowers, 1983).

The soil of the upper zone shows little evidence of the parent rock from which they were derived. This zone includes soil minerals such as angular quartz, small amounts of weathered mica, clay minerals of the kaolinite family, and iron oxides. The thickness ranges from 3 to 8 feet, but may exceed 10 feet in flat hilltops. The soils are homogeneous and usually stiff. There are two causes for the stiffness. First, the soils are desiccated. Since the clays are largely of the kaolinite family, they do not tend to absorb water and swell. Second, the leaching of the soluble minerals from the surface tends to cause the accumulation of these minerals in the deeper parts of the upper zone where they harden into weak cements (Sowers, 1963). Due to the degree of weathering, the upper zone contains a large amount of fines, which causes a large variability in the plasticity

characteristics. Liquid limits can range from 30 to 80, and plasticity indexes from 12 to 45. The soils are classified as CL or CL-ML by the Unified Soil Classification System (USCS).

The intermediate zone is often the most important from the foundation engineering point of view (Sowers, 1963). Most structural foundations will be founded in this zone because the upper zone is shallow while the intermediate zone is stronger and deeper in comparison. The soil retains much of the characteristics of the original rock because it is formed from the incomplete weathering of the parent rock. The soils are not homogeneous because of the segregation of the soil minerals into bands, which resembles the banding of the parent rock. These soils are termed saprolites because they are soil, yet they retain the appearance and structure of the parent rock. These similarities can include mineral alignment and defects.

The intermediate zone contains predominantly quartz, clay minerals, mica, and partially weathered feldspars. The soil also contains oxides of iron and manganese, which gives the soil a wide range of color. The sizes can be variable, but often are uniform in a given area or band. The saprolite contains typical mica contents of 5 to 25%. The mica comes from the crystalline rocks, which are not as easily weathered as the feldspars. Some soil bands may be all mica while others may contain none (Sowers, 1963). This creates a wide range of void ratios for the saprolites, because void ratios increase with mica content. A frequency distribution curve of void ratios, based over 1,000 undisturbed samples indicates that the average void ratio is about 1 (Sowers, 1963).

The intermediate zone usually shows a grain size curve with a uniform to well-graded curve in the sand sizes, representing the unweathered quartz and mica, and a long

flat curve for the silt and clay sizes, representing the kaolins. Atterberg limits are not easily obtained for the saprolite. The soil slides instead of flows in the liquid limit cup, and the soil is not easily rolled into threads in order to determine the plastic limit. The range of the liquid limit is approximately 25 to 60, and the plasticity indexes are much lower from 0 to 20. The soils are ML and MH, according to the USCS, and are described as micaceous silty sands and sandy silts.

The lower limit of the intermediate zone is not well defined. Weathering becomes less with depth, until unaltered parent rock is reached. The partially weathered zone consists of the transition between soil and rock. The zone is characterized by lenses or bands of relatively sound rock separated by seams of the same sandy silts and silty sands that are found in the intermediate zone (Sowers, 1963). The lesser weathering can be seen in grain size curves where gravel and boulder sizes are encountered. The soils are usually non-plastic, but can be slightly plastic when small percentages of fines are encountered. The USCS classifies the partially weathered zone as GW, GF, SW, and SF. Most can be described as slightly silty gravelly sands and silty sands (Sowers, 1954).

2.4 Engineering Properties

The engineering properties reflect the degree of weathering and the structure of the residual soil. The properties of the upper zone resemble properties similar to homogeneous clays. Desiccation has caused these soils to become preconsolidated and stiff. The soils of the upper zone do not usually create engineering problems, unlike the soils of the intermediate and partially weathered zones. These soils create engineering problems because they are non-homogeneous in nature. This creates much variability in

areas such as strength, compressibility, shrinkage and expansion, compaction, permeability, and groundwater, etc.

2.4.1 Strength

Many tests have been performed on the intermediate and partially weathered zones including unconfined compression, direct shear, triaxial shear, rotating vane, etc. While many tests have been made, the very complex nature of the soils makes it difficult to draw many generalized conclusions (Sowers, 1954). Testing consistently shows the soils exhibiting strength with no confining pressure and increasing strength with increasing confinement. The unconfined compression test would predict very low strength values based on this behavior. Direct shear tests are unreliable, because they tend to over predict the strength of the soils. The triaxial shear test is the most reliable method of testing the strength, but many samples and tests are needed to obtain accurate results.

Many stress conditions can be modeled using various confining pressures with the triaxial shear test. Undrained shear tests are not commonly performed for analysis of engineering problems because of the high permeabilities predicted. The most common test run on the samples is the consolidated-undrained (CU) triaxial shear test. The sample is sheared rapidly without drainage after the lateral confining pressure consolidates the sample. The effective stresses at failure can be obtained from this test by measuring the pore pressures in the sample. Consolidated-drained (CD) tests can be performed to obtain the effective stresses directly but are seldom performed due to the longer testing times.

The soils of the intermediate zone can be described using a two-part Mohr-Coulomb failure envelope. A straight line is observed for shearing strengths above 100 to 200 kPa, and a concave downward curve is observed at pressures below. Bonding between the soil grains (true cohesion) can be observed. All of the physical bonds between particles in the original rock were not broken during weathering. While soils containing large amounts of quartz and feldspars exhibit little cohesion, soils containing large amounts of mica exhibit much more cohesion. Part of the cohesion appears to be the result of capillary tension since varying the moisture content (without a change in void ratio) will change the cohesion (Sowers, 1954).

The internal friction appears to result from interlocking of angular quartz and mica flakes plus the true friction. The increase of weathering and void ratio causes decreases of the internal friction. Saprolites containing large amounts of mica have much lower angles of internal friction resulting from higher void ratios.

The shear strength varies because it is anisotropic in nature. Tests with the flaky minerals oriented parallel to the potential shear plane exhibit about two-thirds to three-fourths the strength perpendicular to it (Sowers, 1983). The strength of banded soils vary greatly from band to band, and resemble stratified soils.

2.4.2 Compressibility

Materials of the saprolite and the partly weathered zone consolidate similar to other soils when subjected to vertical pressures with lateral confinement. The materials become denser with increasing confining stress. A plot of the time rate of consolidation of a partly saturated saprolite exhibits significant initial and primary consolidation, and

usually significant secondary consolidation (Sowers, 1983). Higher permeabilities and anisotropic effects of the structure of the soil on drainage causes much more rapid primary consolidation than for clays. Secondary consolidation is often related to structural settlement and can continue for years. More secondary consolidation can be observed when there is a significant mica content present. The amount of secondary settlement is relatively large, similar to that in organic soils (Sowers, 1963).

Stress-void ratio curves for saprolites resemble those for undisturbed preconsolidated clays. Predicted preconsolidation loads using Casagrande's empirical method, shows no correlation between depth and preconsolidation stresses. The preconsolidation present is probably related to the residual mineral bonds of the parent rock. When the rock cooled, the differential contraction of the various minerals caused high stresses to develop between the grains (Sowers, 1963).

2.4.3 Shrinkage and Expansion

Most saprolite soils have very low plasticities, yet the volume changes caused by drying and absorption of moisture sometimes resemble those of highly plastic clays. Shrinkage and expansion appear to be mechanical processes. Shrinkage occurs when capillary tension on the pore water compresses the soil. The soils often expand when dried beyond the shrinkage limit caused by the loss of capillary tension in the dry voids, which permits the quartz-mica framework to return to its original volume. Likewise, the expansion of the soil from wetting reduces the capillary tension resulting in an increase in void ratio. Unequal expansion of the soil can break the remaining mineral bonds (Sowers, 1963).

2.4.4 Compaction

The clays, micaceous silts, and micaceous silty-sands of the upper and intermediate zones are not easily compacted. The soils of the partly weathered zone are good construction materials, yet they are not easily obtainable. The Standard Proctor test (ASTMD 698-58T) shows maximum dry densities for compacted soils of the intermediate and partially weathered zones that are lower than satisfactory for the best fills. The optimum moisture contents vary from 12 to 35 percent. The higher values correspond to the highly micaceous soils with lower densities. Strengths of these soils are not as poor as expected from the low maximum densities if the compaction percentages exceed about 95 percent of the Standard Proctor maximum (Sowers, 1963).

2.4.5 Permeability

As seen in Table 2.4, the permeability varies greatly from one zone to another.

Soil Description	Permeability (cm/sec)	Type of flow
Upper zone	$10^{-3} - 10^{-7}$	isotropic
Saprolite	$10^{-4} - 10^{-6}$	isotropic
Partly weathered rock	$10^{-1} - 10^{-5}$	anisotropic
Rock	Impervious	none

Table 2.4

Typical permeability values for residual soils (Sowers, 1983)

The permeability is a function of the degree of weathering, the size of weather resistant particles, and the fracture patterns. Generally, flow in the upper zone and intermediate zone is isotropic, while flow in the partly weathered zone is anisotropic. The permeability of the soil mass may differ greatly from the above values because of dikes and similar intrusions of unweathered rock or seams which weather into true clays that obstruct seepage (Sowers, 1963). The permeability is much larger parallel to foliation than perpendicular to it.

2.4.6 Groundwater

The water levels are often complex and irregular. The normal gravity water table is usually established in the pervious saprolite of humid regions. Within the partially weathered zone and the rock, joints and seams form the aquifers (Sowers, 1985). Artesian water can be found in the rock and partially weathered rock. Typically the phreatic surface parallels the topography, but irregularities do occur from the anisotropic permeability of the lower layers. Seasonal rainfall causes fluctuations of several meters during the year.

CHAPTER 3

FIELD TEST PROGRAM

3.1 Introduction

The Auburn University Geotechnical Site provides a facility for research on foundation behavior in the residual soils of the Piedmont Plateau. The method of achieving the goal of this research project was to analyze the data from full-scale lateral load tests. Static lateral loads were applied one foot from the ground surface to six drilled shafts. The six statically loaded piles were 36 inches in diameter, and were embedded 36 feet into the residual soil formation. The drilled shafts in a test pair were spaced approximately 24 feet on center. One of the shafts was purposely defected during construction. The remaining five shafts with no defects will be discussed in this report.

3.2 Site Description

The Spring Villa Test Site lies in the Southern Piedmont Province. Specifically, the site is located in Lee County, Alabama. The soil at the site is micaceous sandy or clayey silt. Sand seams are also prevalent which formed from the intrusion of igneous quartz into the metamorphic parent rock. The upper zone is approximately two to three meters from the ground surface, underlain by the saprolite zone.

Many lab tests have been performed on the residual soils at this test site. Vinson and Brown (1997) describe water contents at varying depth shown in figure 3.1. The percent fines and percent sand with depth at the site are shown in figure 3.2, and the percent silt and percent clay are shown in figure 3.6. A variety of in-situ tests including the dilatometer test (DMT), standard penetration test (SPT), cone penetration test (CPT), and Menard-type pressuremeter test (PMT) have been performed at the test site.

The upper zone exhibits a larger plasticity index than the saprolite zone as seen in the top two meters of figure 3.1. This larger plasticity index is indicative of the larger clay content in the upper zone, which can be seen in figure 3.2. The larger clay content creates a stiff layer in the upper zone compared to the soil below. The in-situ tests performed at the site show this behavior of a stiff layer of soil near the surface with a softer layer beneath. Figures 3.3 – 3.5 show the depth of the upper zone ranging from 2 – 3 meters.

The percent fines, percent sand, and percent silt vary greatly at each depth, but no increasing or decreasing trend can be observed with depth. This pattern is indicative of the variable nature of these soils. More discussion on the site geology and stratigraphy is discussed in Site Characterization of the Spring Villa Geotechnical Test Site and a Comparison of Strength and Stiffness Parameters for a Piedmont Residual Soil (Vinson and Brown, 1997).

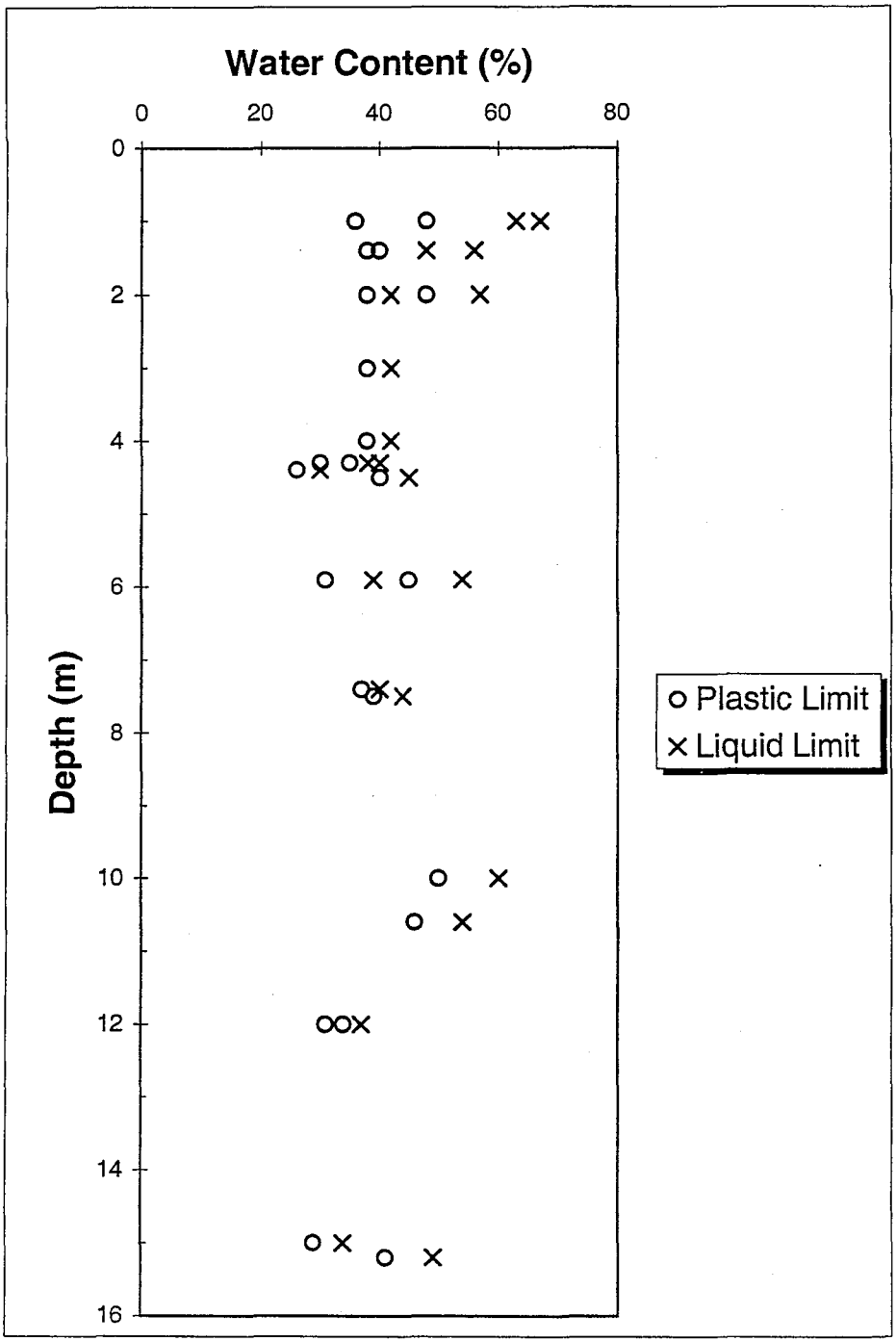

Figure 3.1

Auburn University Test Site Plasticity Summary (Vinson and Brown, 1997)

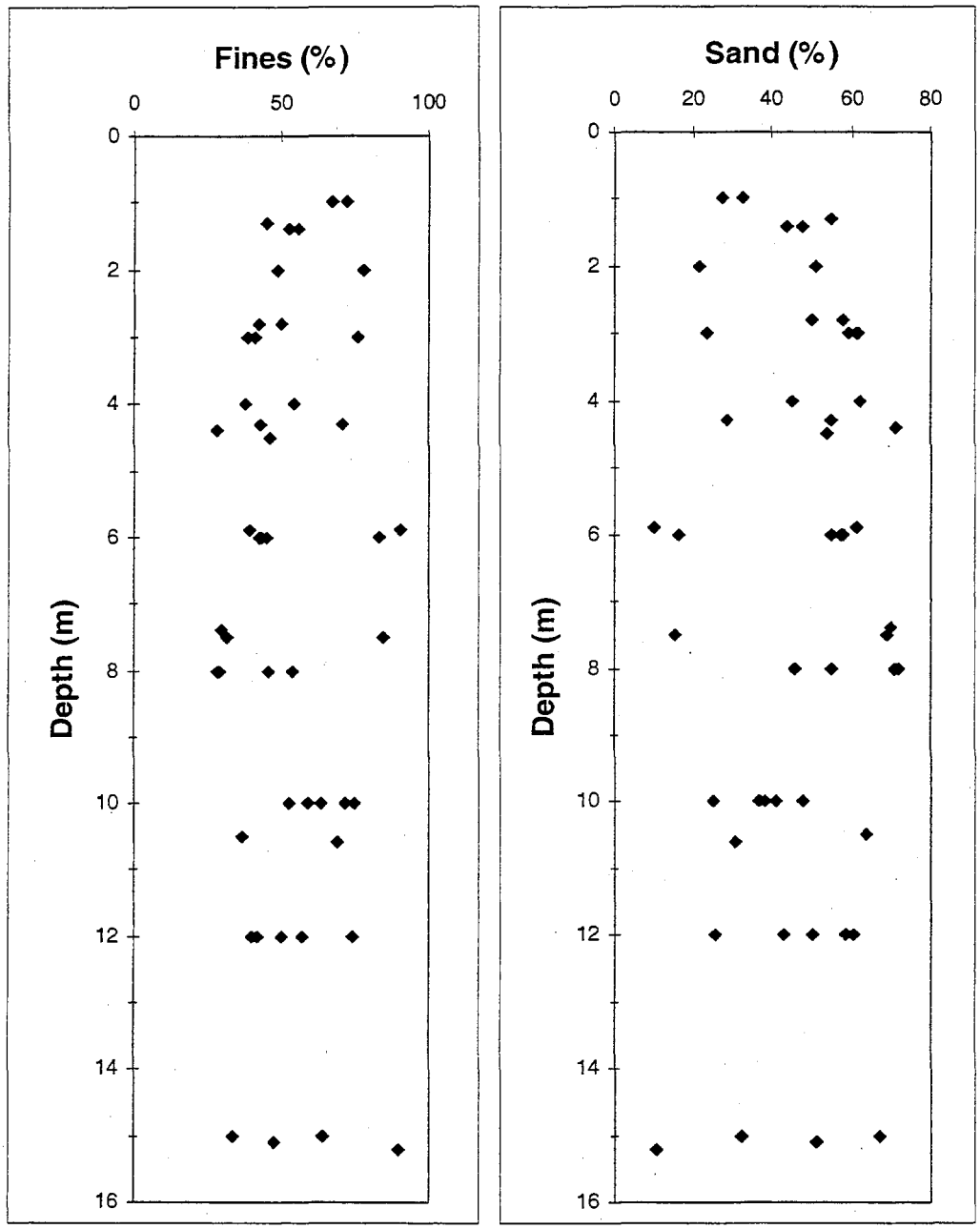

Figure 3.2

Particle Size Distribution (Vinson and Brown, 1997)

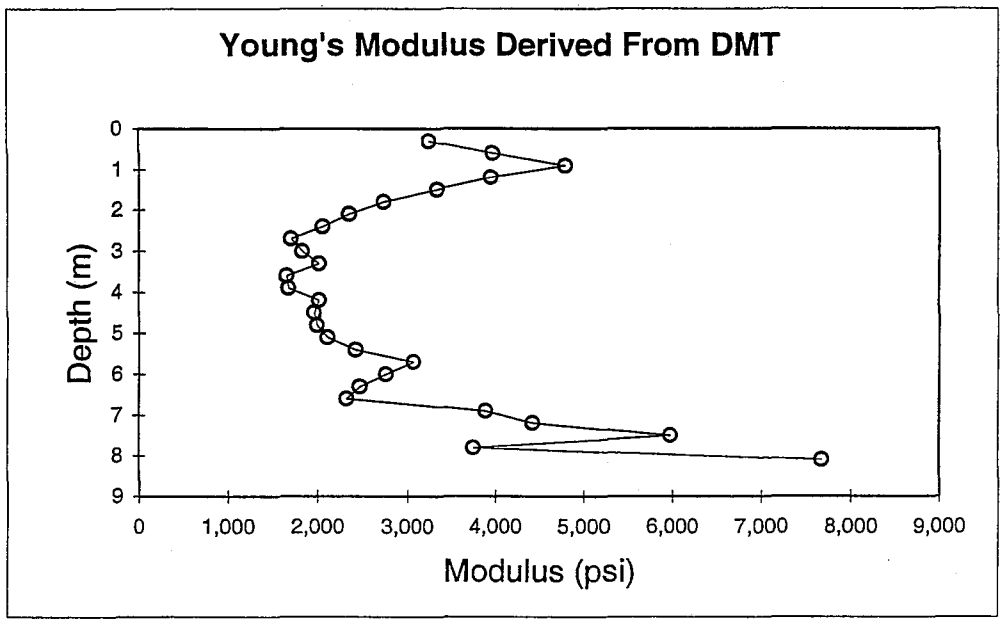

Figure 3.3

Young's Modulus from DMT (Vinson and Brown, 1997)

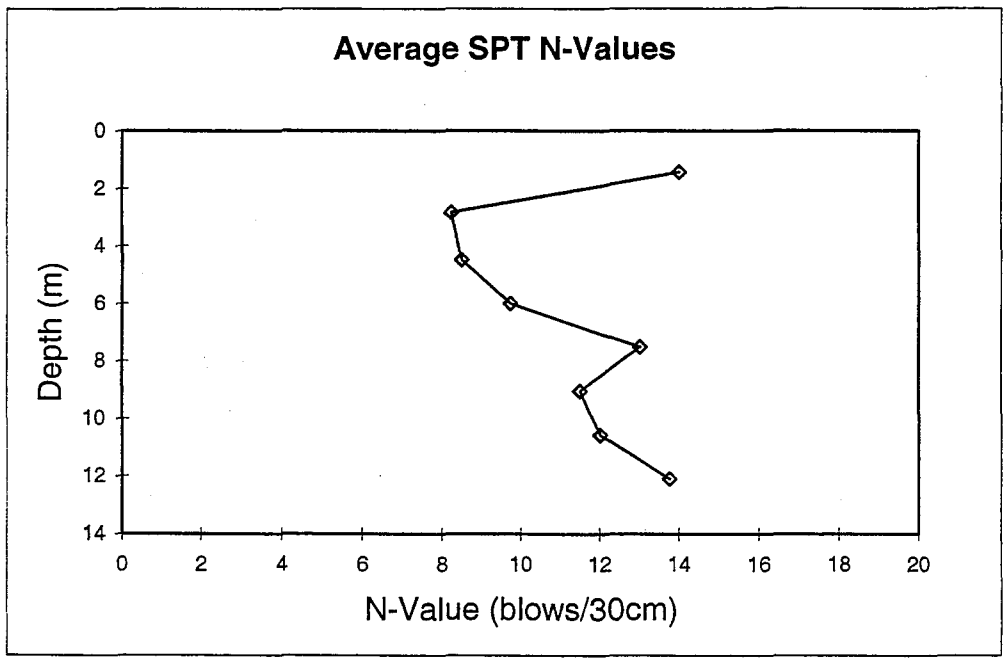

Figure 3.4

SPT Blow Count (Vinson and Brown, 1997)

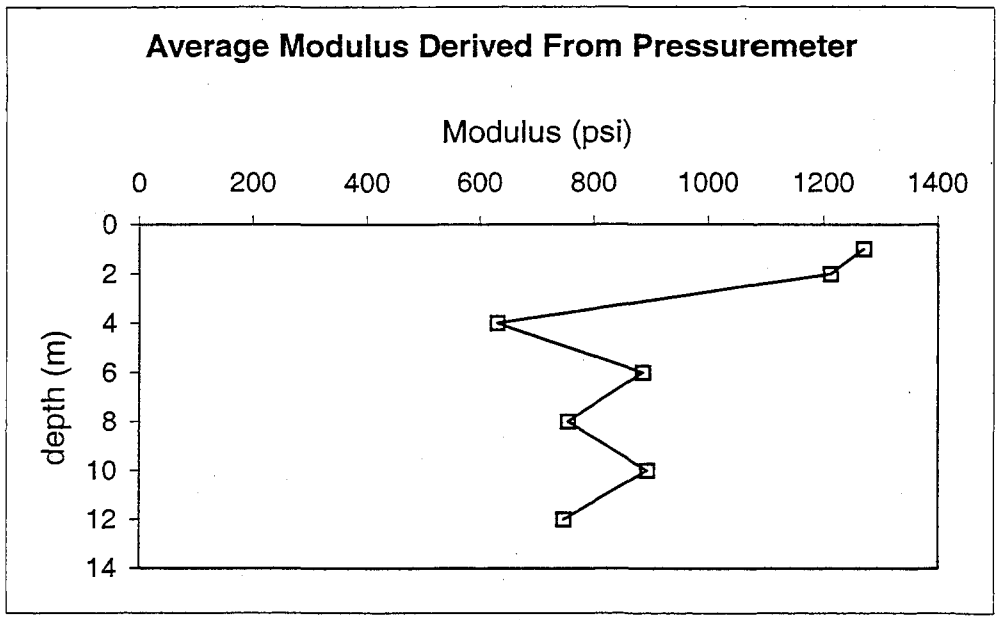

Figure 3.5

PMT Modulus (Vinson and Brown, 1997)

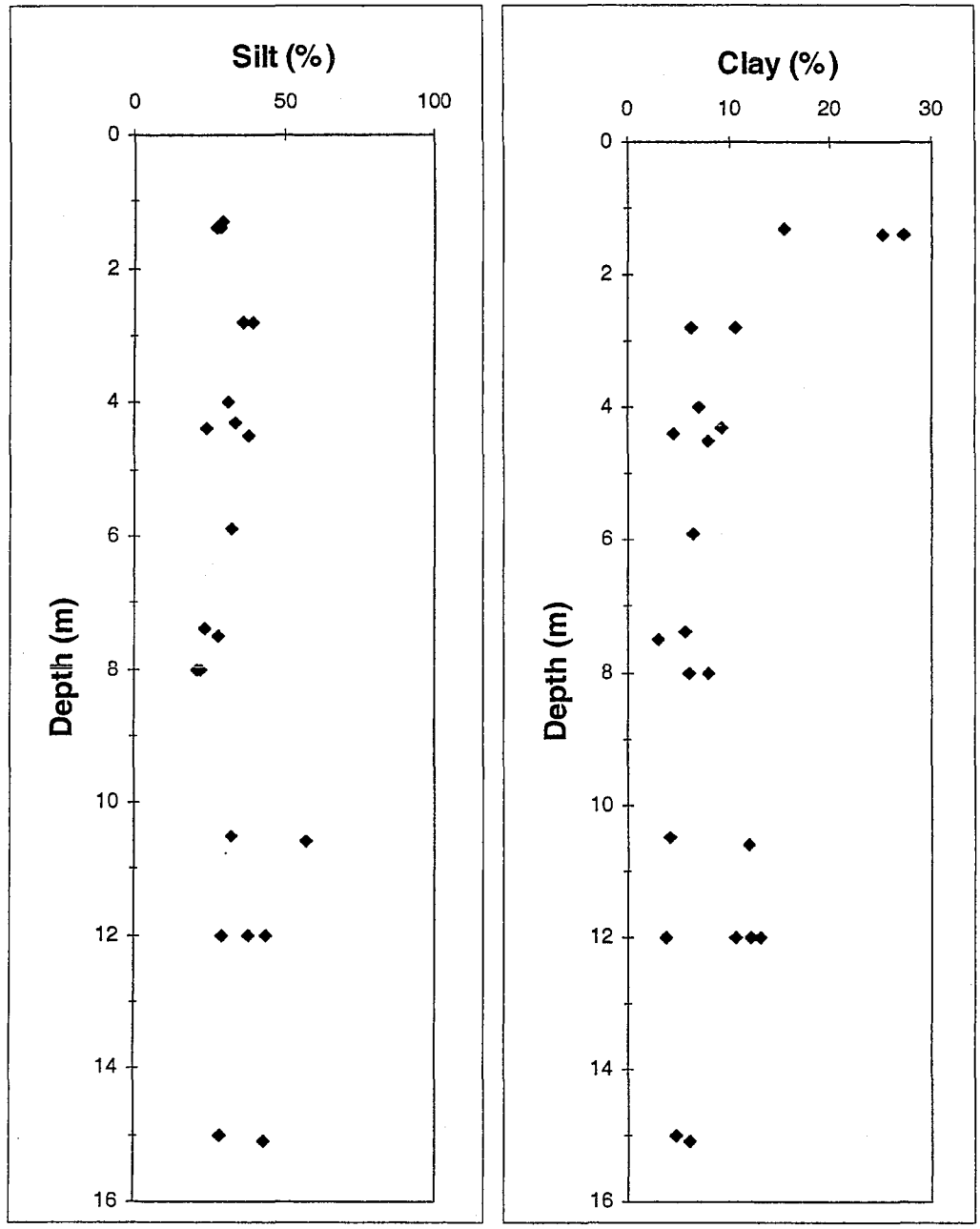

Figure 3.6

Particle Size Distribution (Vinson and Brown, 1997)

3.3 Site Layout and Pile Properties

The drilled shafts tested at the site were reinforced with 10 #11 bars. The steel was 60 ksi. The concrete had an assumed modulus of 4,400 ksi and a concrete strength of 4500 psi. The shafts were embedded 36 feet below the ground surface and were loaded 1 foot above the ground surface. The drilled shafts were spaced 16 and 24 feet on center in a grid. The shafts in a static test pair were spaced 24 feet on center, while the test pairs were spaced 16 feet on center. Figure 3.7 shows the location of each test shaft at the test site. The static test pairs consisted of shafts 1-6, 2-3, and 4-5. The other shafts shown in the site layout were not tested statically. This project is concerned only with the static tests performed on shafts 1, 2, 3, 5, and 6.

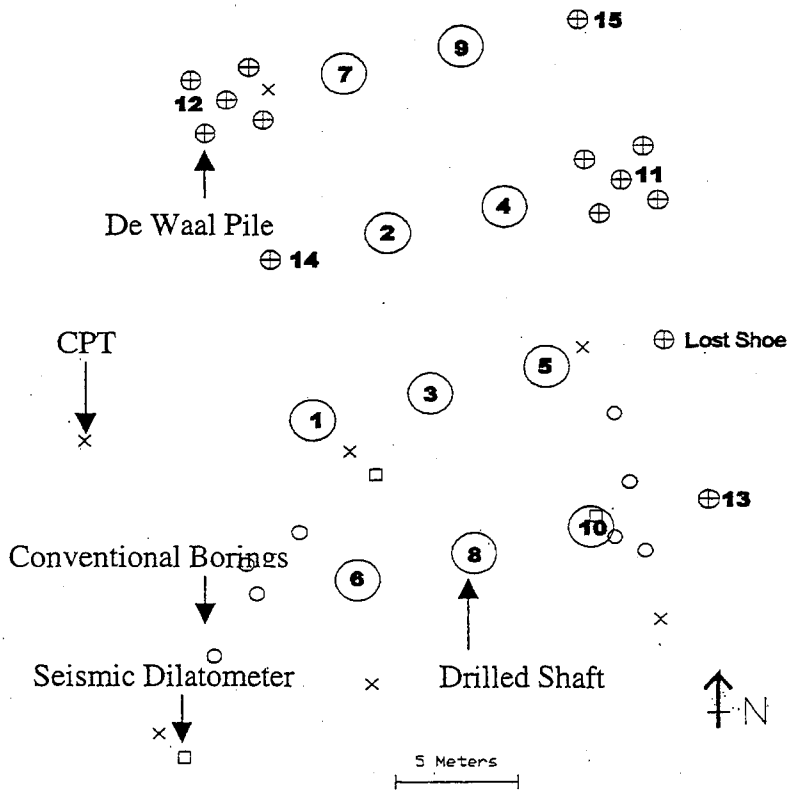

Figure 3.7

Auburn University Geotechnical Research Site Layout

3.4 Test Setup

The instrumentation used in the test setup for this research project allows for accurate measurements of the shaft deflections. An inclinometer tube was placed into each shaft during construction. During testing, an inclinometer probe was lowered into this tube to measure the deflection along the shaft. Strain gages were attached to the reinforcement cage during construction. Gages were placed on two sides of the shaft that correspond to the compressive and tensile zones during lateral loading. Bending moments were monitored by placing the gages at strategic points along the pile. Between the two shafts were located two stable reference beams, which were used in the measurement of pile head deflections. The measurements were taken by two Linear Variable Differential Transformers (LVDT), which were attached to these beams. Two tension bars were connected to two beams with bolts on the outside of the test shafts. The purpose of the tension bars was to pull the test shafts together when a load from a jack was applied. A jack, load cell, and bearing plate were placed between one of the shafts and the beam located on the outside of that shaft. Figure 3.8 shows the location of the instruments. The jack was located between the load cell and the beam. The bearing plate would be located against the shaft, and the load cell in the middle of the two. The load cell was used to record the load being applied by the jack. The bearing plate was used to keep the loading only in a lateral direction and relieve any twisting or torsion caused by the loading method.

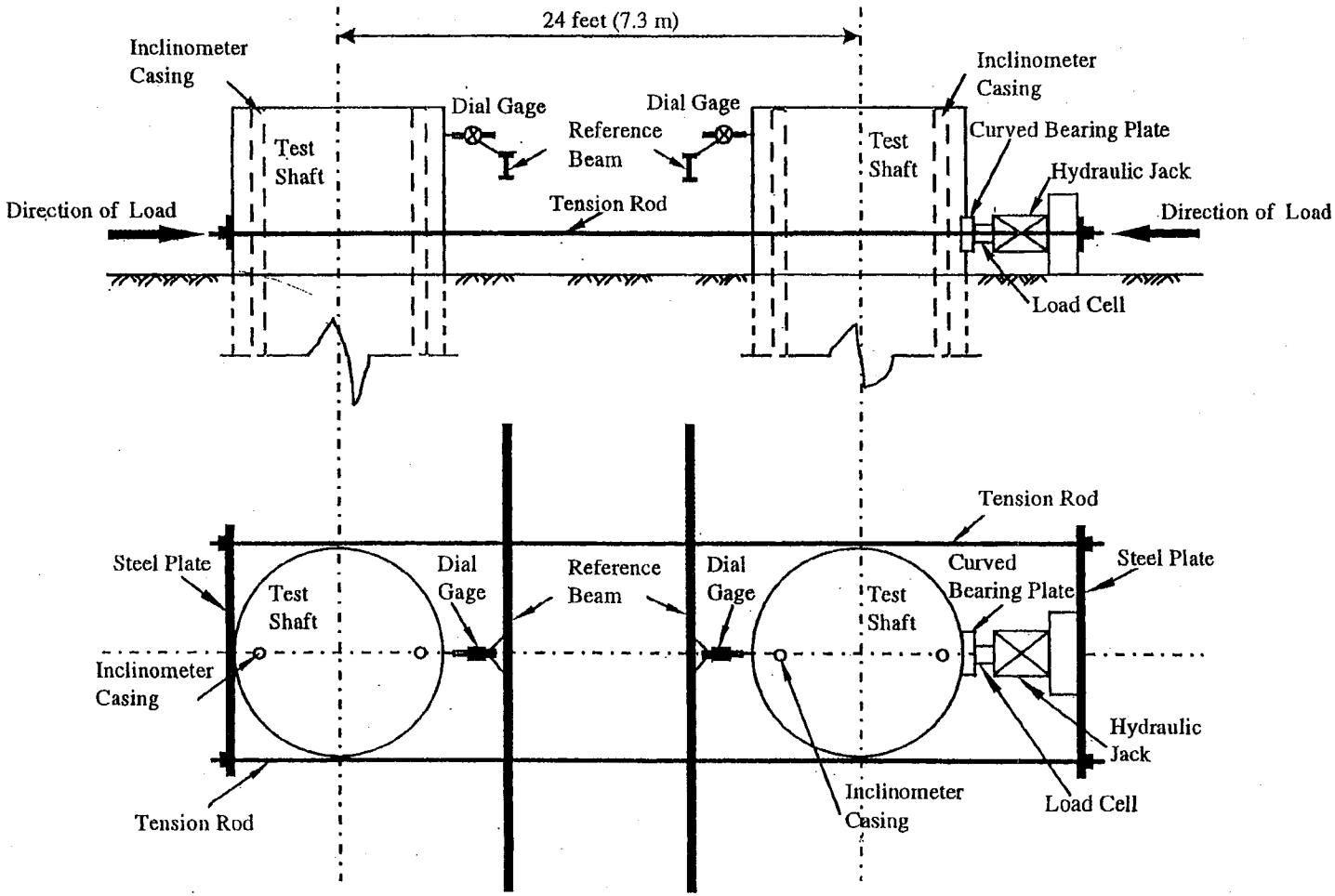

Figure 3.8

Static Test Setup

3.5 Testing Procedure

Four of the six shafts were loaded similarly. One of the non-defective shafts was loaded differently because higher loads were needed to fail the defective shaft, which was being tested against it. More data was recorded for the head deflection because less time was needed in the testing procedure.

More LVDT measurements were taken than any other measurements during the tests. The tests only required approximately 5 minutes for each loading. After a load was applied, the pile was observed. The LVDT measurements were taken after the pile came to a constant displacement. Once the measurement was taken, the next load would be applied. Table 3.1 shows the loads applied to each shaft.

Shaft Number	Load (kN)
1, 2, 3, 6	87, 174, 261, 348, 435, 522, 609, 695, 782
5	162, 334, 506, 589, 67, 757, 870, 924

Table 3.1

Loads Applied for LVDT Measurements

Obtaining inclinometer data required more time. The process was very similar as for the LVDT measurements. A load was applied, and the measurements were taken

once the constant deflection was observed. The inclinometer device had to be lowered the length of the shaft to record all the needed data. Inclinometer data was recorded every 0.5 m along the shaft, starting 0.5 m below the ground surface. Approximately 30 minutes was needed for the collection of data at each load interval. Due to the time involved, not as many loadings were observed for each shaft. Table 3.2 shows the loadings for each shaft.

Shaft Number	Load (kN)
1, 6	174, 348, 522, 695
2, 3	348, 435, 522, 609, 695, 782
5	162, 334, 506, 589, 670, 757, 870, 924

Table 3.2

Loads Applied for Inclinometer Measurements

Strain data were continuously monitored for each pile to determine the depth at which the maximum bending moment occurred. The strain measurements were taken at approximately 1.5m, 2.5 m, 3.5 m, 4.5 m, and 10m. The upper portion of the drilled shaft is where the largest strain will occur, so this is the area observed. The strain will decrease greatly with depth. From the strain data, the point when the concrete begins cracking can be observed. This is the point when the compressive strains become less than the tensile strains. The strains can be monitored to observe the location of the maximum bending moment also. The maximum bending moment ocurrs at the location of maximum strain.

CHAPTER 4

TEST RESULTS

4.1 Introduction

The results from the static load tests of the five non-defective shafts are presented in this chapter. The pile head deflections caused by each load were measured using a LVDT. Inclinometer data was used to calculate the deflection along the pile for each loading. Strain measurements were taken to observe where the maximum bending moment occurred in each pile, and the load when the concrete begins cracking.

4.2 Inclinometer Data

Inclinometer data from the load tests was used in Microsoft Excel to obtain calculated deflections along the pile. Inclinometer data was taken for each shaft before any loading was applied. These data were compared to the data taken while loads were applied. The comparison of this data was used to obtain a plot of the deflected shape of the pile. Inclinometer data was obtained every 0.5 meters along the pile, starting at 0.5 meters below the top of the shaft. LVDT measurements were taken to determine the deflections at the pile head. Figures 4.1 – 4.5 shows the deflected shape of each pile for all loads applied and recorded.

Test pair 1 – 6 had similar deflections around 35 mm for the highest load of 695 kN. The test pair displayed much different deflections for the lower loadings. Shaft 1 displayed larger deflections than shaft 6 for all other loads applied as shown in figures 4.1 and 4.5. Test pair 2 – 3 displayed a large difference in the deflections calculated for each load. Shaft 3 experienced a deflection of approximately 42 mm near the ground surface with an applied load of 782 kN. Shaft 2 only experienced about 29mm of deflection for the same depth and load. Shaft 5 had a blockage in the tube and the inclinometer data collected was incomplete; therefore a comparison of the deflections is not discussed. The inclinometer instrument was unable to lower into the tube past a depth of around 5.5 m below the ground surface, resulting in incomplete data. The problem may have been caused by an intrusion of concrete during the casting of the shaft.

4.3 LVDT Data

The LVDT's were used to directly measure the pile head deflection for each pile and load. Not all the shafts were exposed to the same loadings because of the nature of loading in pairs, discussed earlier in chapter 3. Figure 4.6 shows the results of the measurements taken.

As expected the increase in loading causes an increase in the head deflection of the pile. The non-linear relationship between the load and head deflection is shown in figure 4.6. Shafts 1, 3, 5, and 6 reached a maximum head deflection of approximately 40 mm. Shaft 2 only reached a maximum head deflection of about 30 mm. The data exhibit a range of behavior reflecting the variability of the response of Piedmont soils, as the shafts were all of similar diameter and stiffness.

4.4 Strain Data

Strain data were continuously monitored for each pile to determine the depth at which the maximum bending moment occurred. The strain measurements were taken at approximately 1.5m, 2.5 m, 3.5 m, 4.5 m, and 10m. The maximum bending moment will occur at the point along the shaft where the maximum strain occurs. This is important in understanding where a shaft will fail.

The positive values are strains measured in the compressive zone of the loaded pile, and the negative strains are located in the tension zone of the pile. When the tensile strains become large the concrete will begin cracking. Once the concrete begins to crack, the flexural rigidity (EI) will decrease significantly. Figures 4.7, 4.8, 4.9, and 4.10 show the strain measurements at low loads for shaft 1, 2, 3, and 6. Figures 4.11, 4.12, 4.13, 4.14, and 4.15 show the strain measurements at higher loads for shafts 1, 2, 3, 5, and 6 respectively.

According to the data, the maximum bending moment occurs in the top 1/3 of each pile, with the strain decreasing greatly with increasing depth below the ground surface. Shafts 1 and 6 exhibit no cracking of the concrete at lower loads. The compressive strains are similar to the tensile strains. Measurements of strains at low loads for shaft 2 and 3 do not exhibit normal strain behavior. The compressive and tensile strains should peak at the same depth. Therefore an error occurred in the measurement of these values.

Shafts 1, 2, 5, and 6 clearly indicate at higher loads that the concrete is cracking. This is indicated by large tensile strains and low compressive strains. Shaft 3 again exhibited irregular strain behavior caused by measurement error.

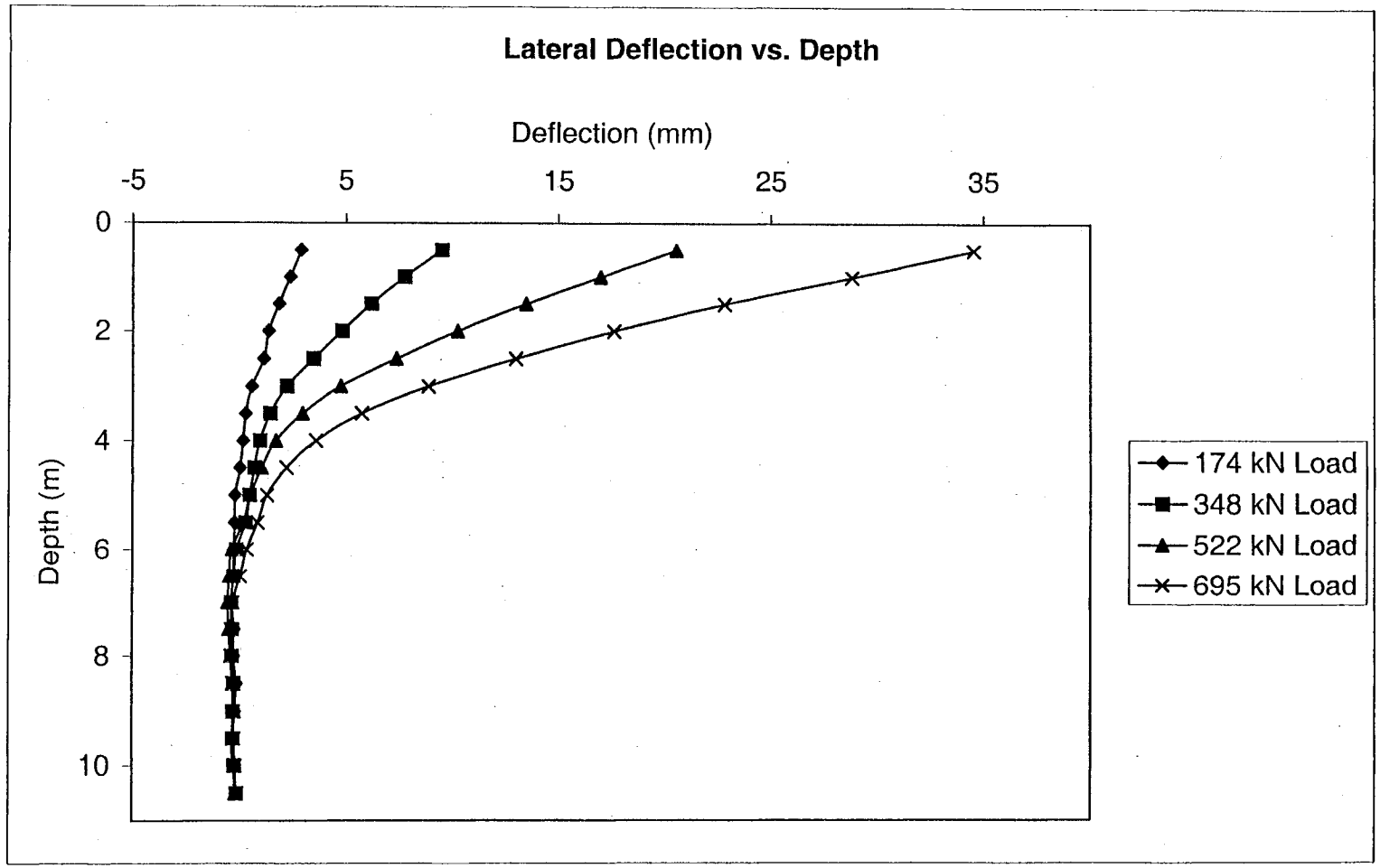

Figure 4.1

Shaft 1 Lateral Deflection vs. Depth from Inclinometer Data

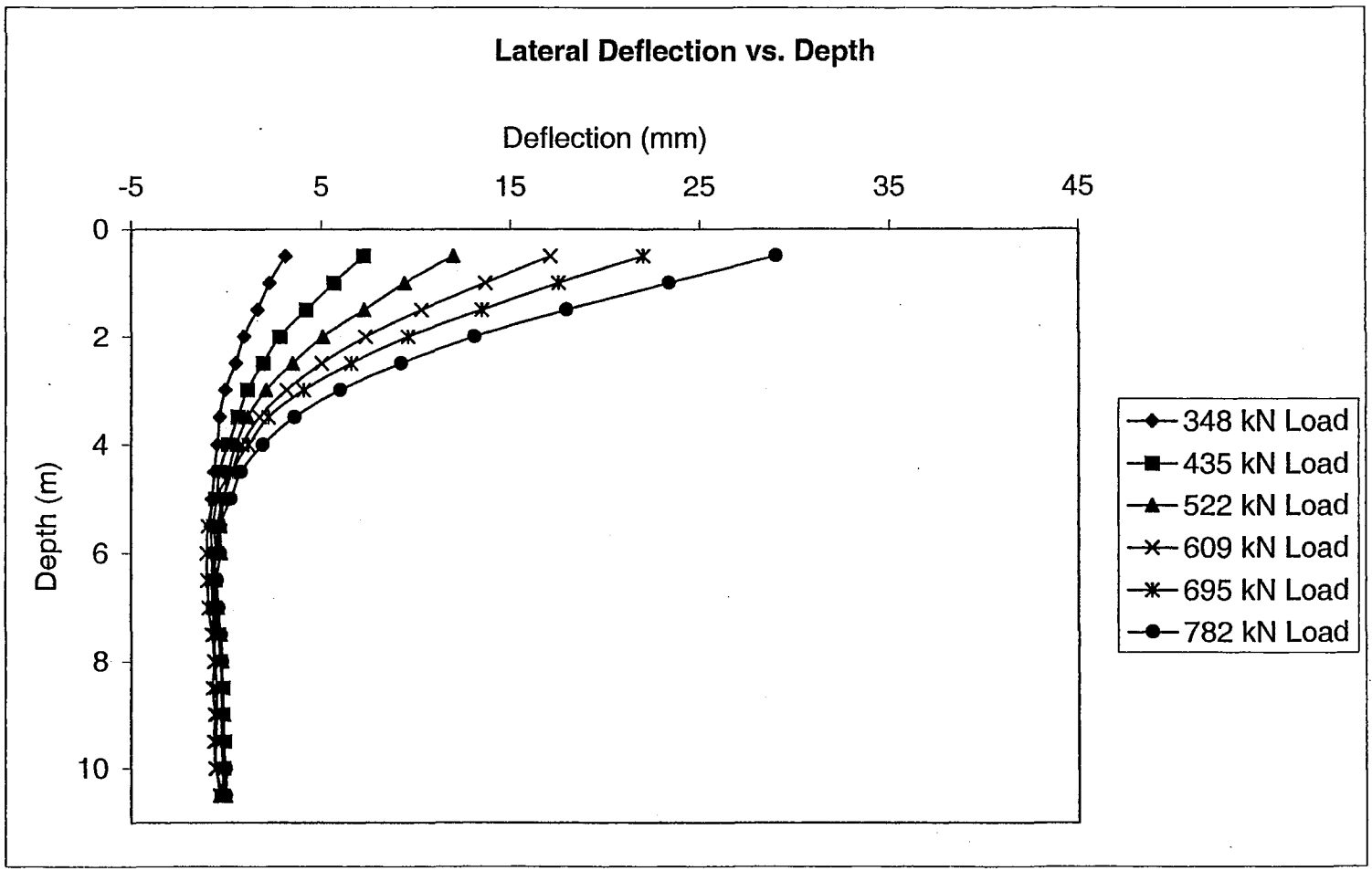

Figure 4.2

Shaft 2 Lateral Deflection vs. Depth from Inclinometer Data

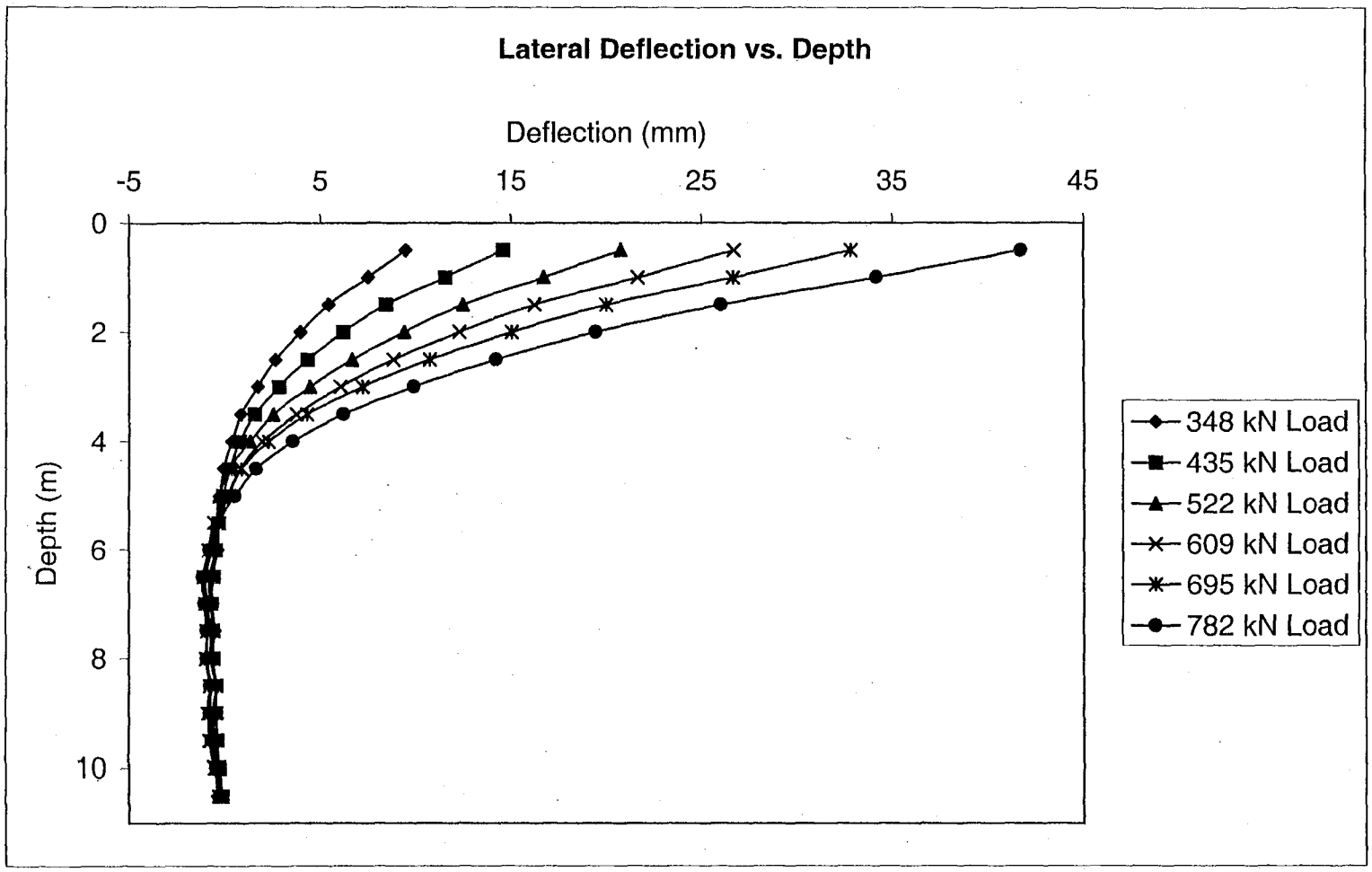

Figure 4.3

Shaft 3 Lateral Deflection vs. Depth from Inclinometer Data

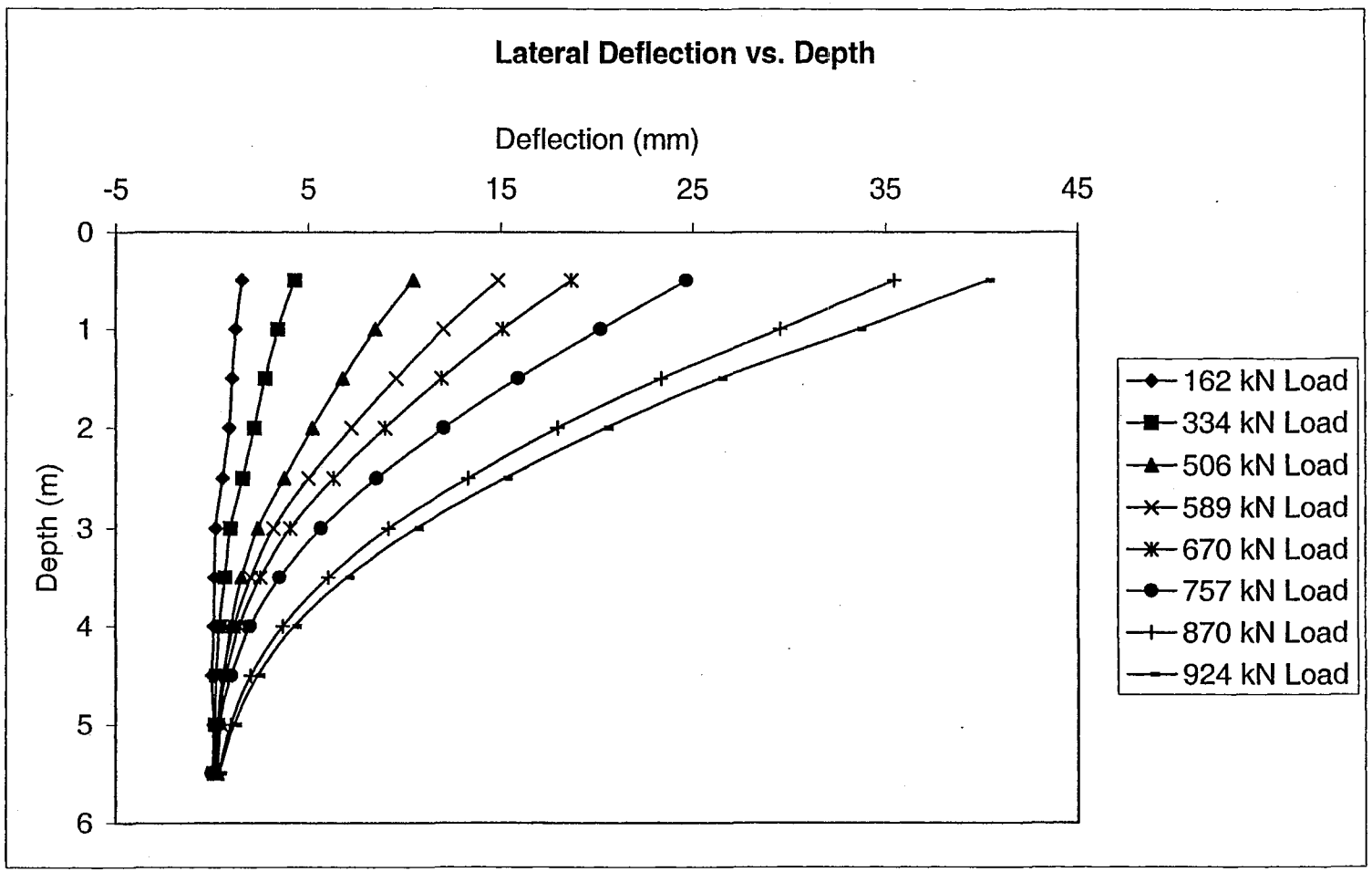

Figure 4.4

Shaft 5 Lateral Deflection vs. Depth from Inclinometer Data

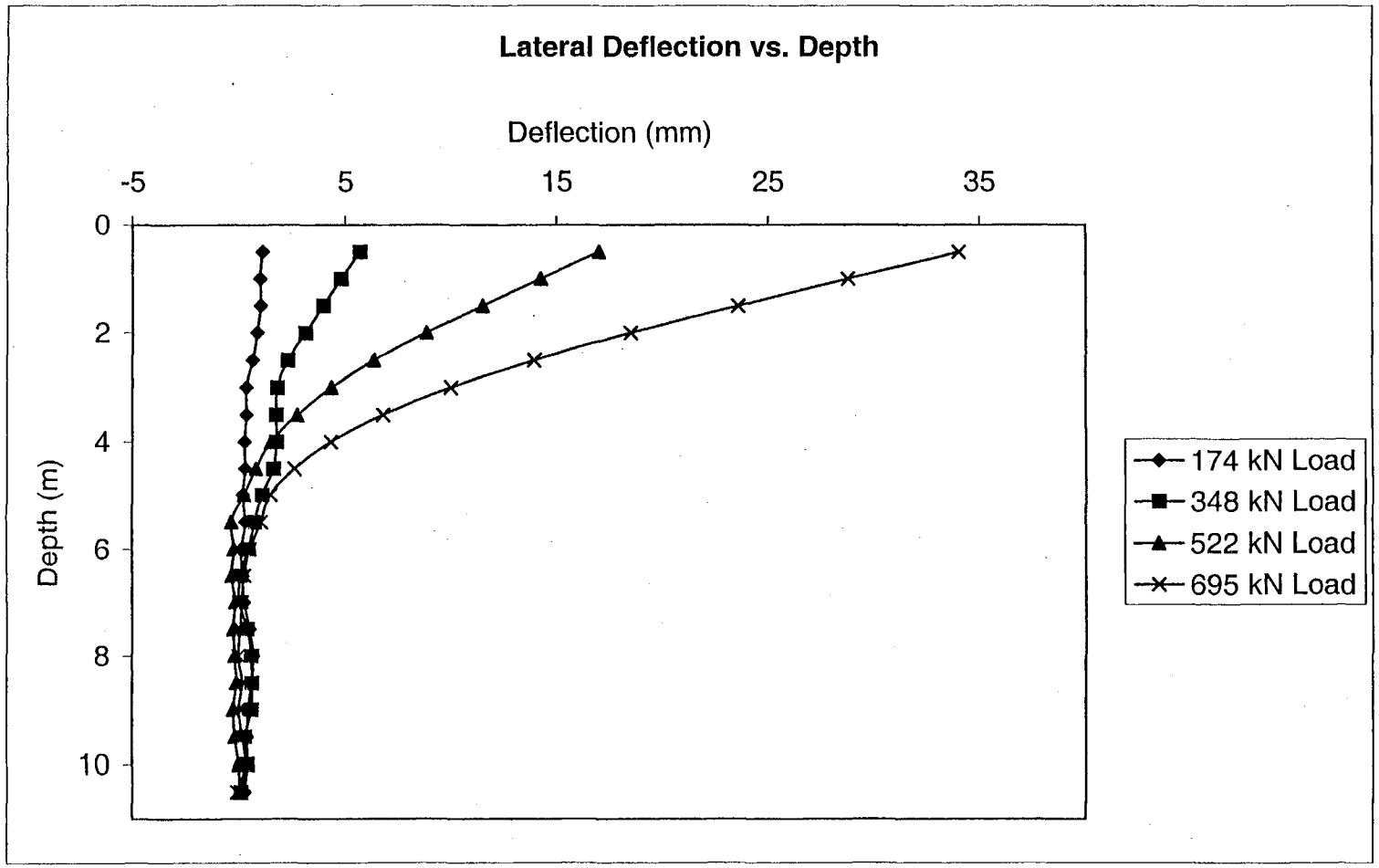

Figure 4.5

Shaft 6 Lateral Deflection vs. Depth from Inclinometer Data

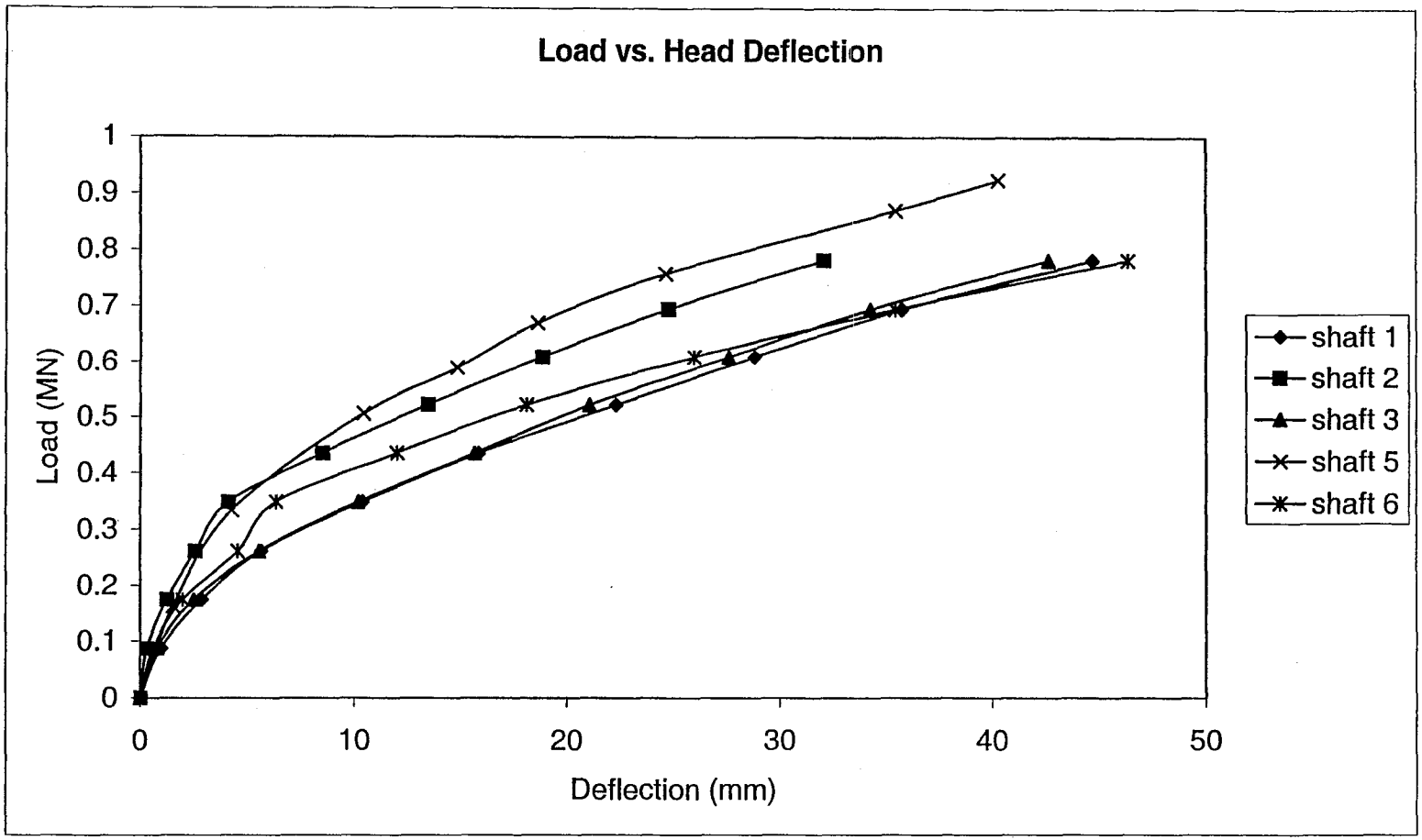

Figure 4.6

Load vs. Deflection from LVDT Data

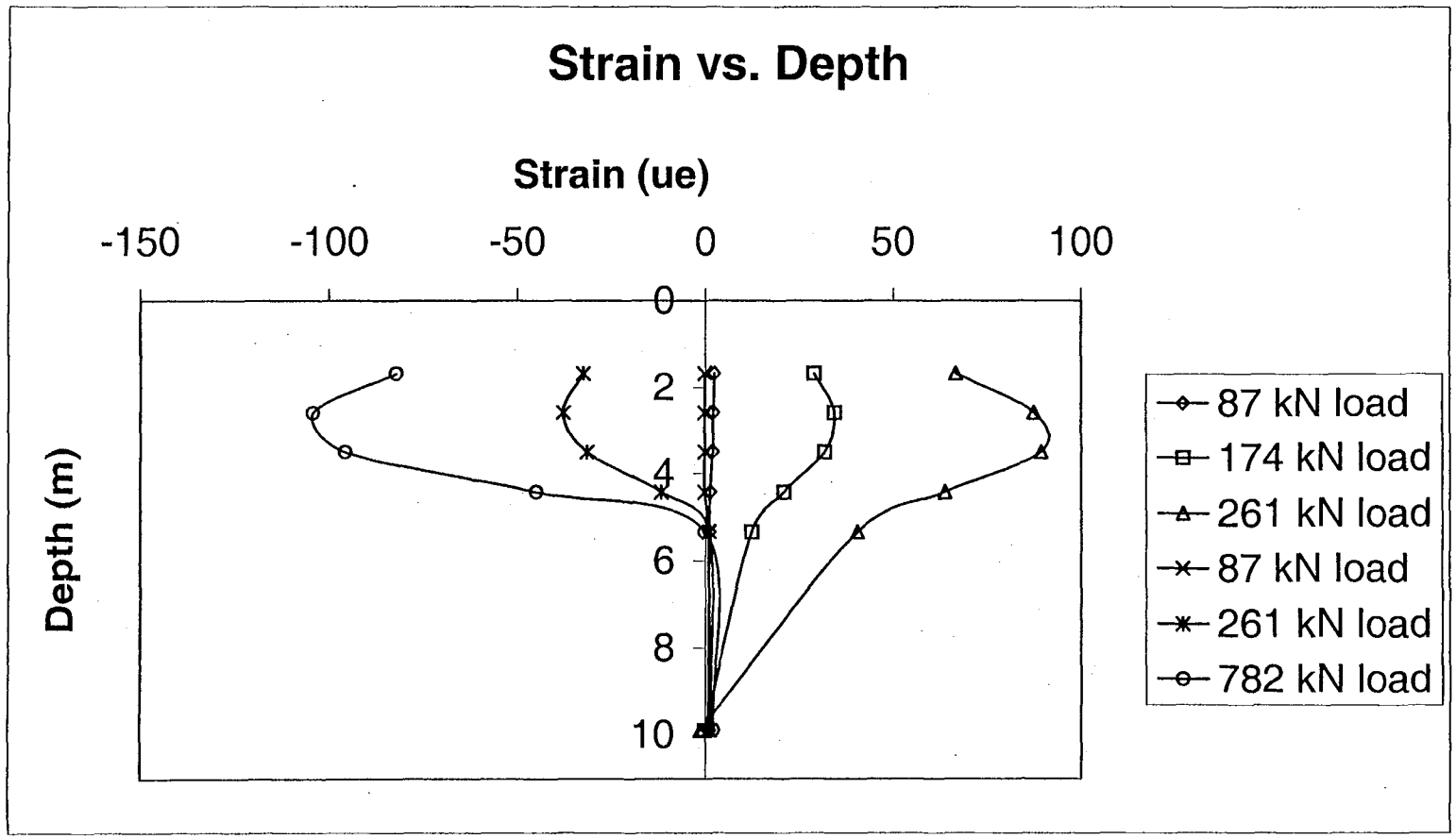

Figure 4.7

Shaft 1 Strain Measurements at Low Loads

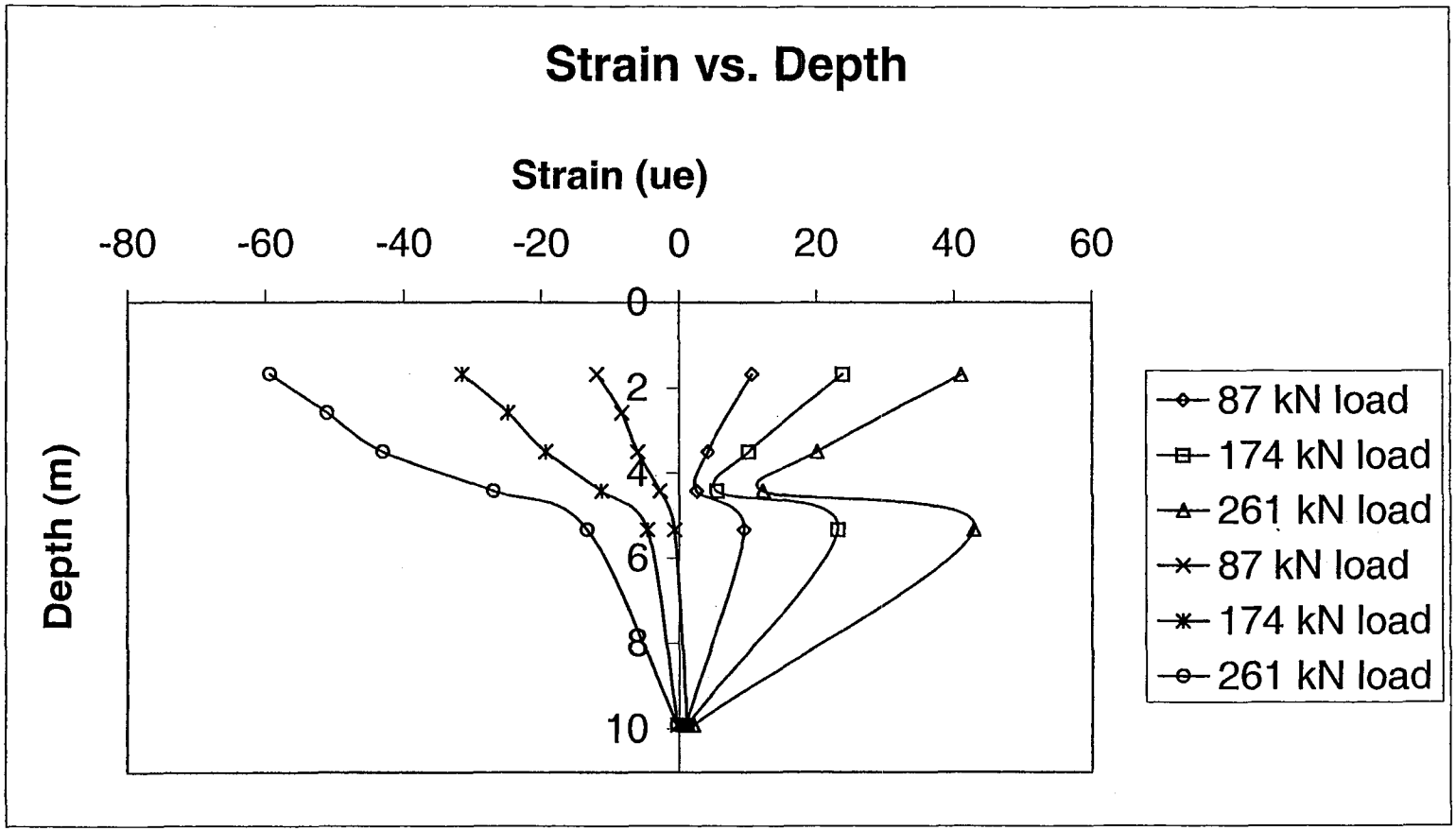

Figure 4.8

Shaft 2 Strain Measurements at Low Loads

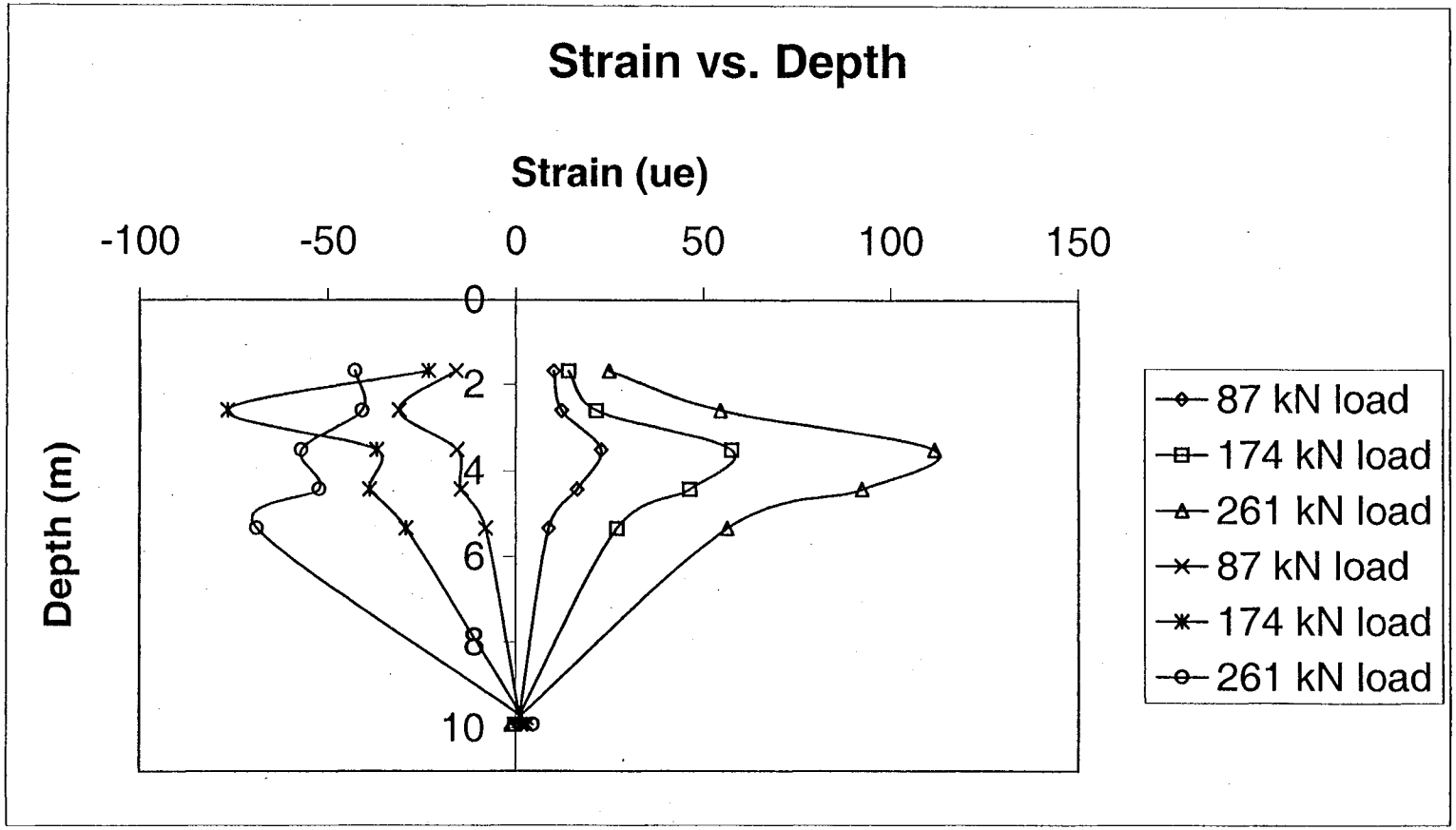

Figure 4.9

Shaft 3 Strain Measurements at Low Loads

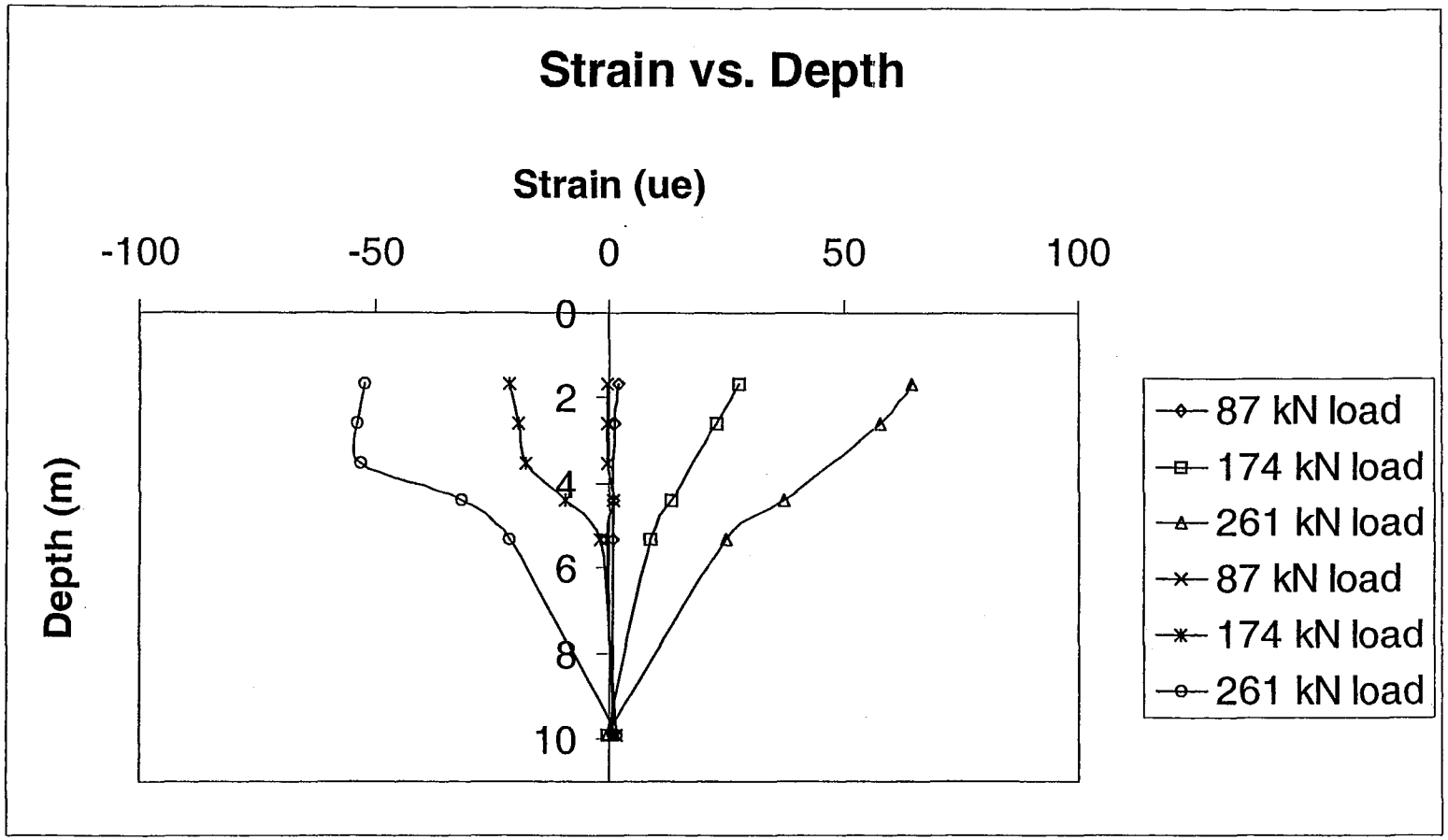

Figure 4.10

Shaft 6 Strain Measurements at Low Loads

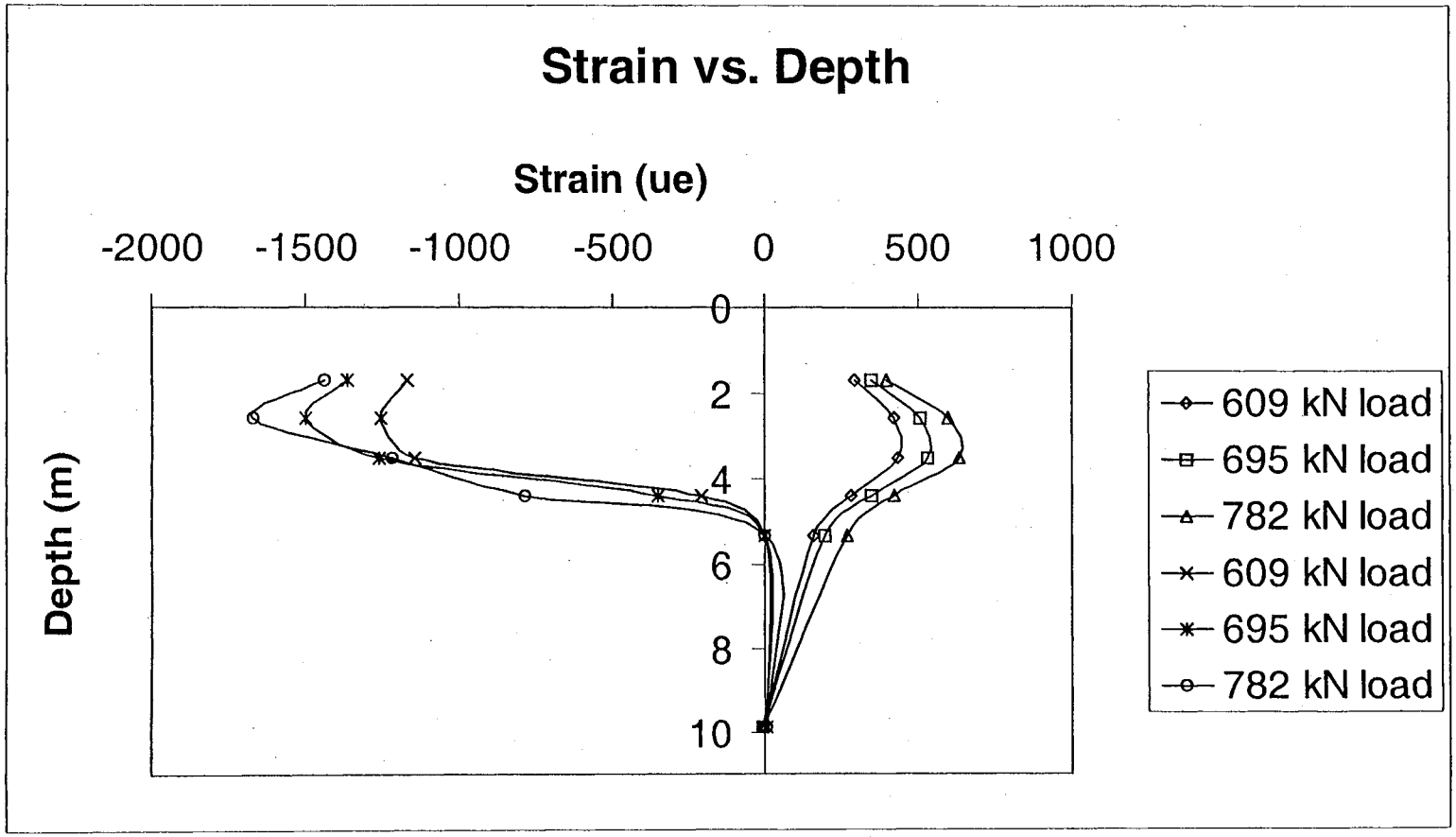

Figure 4.11

Shaft 1 Strain Measurements at Increased Loads

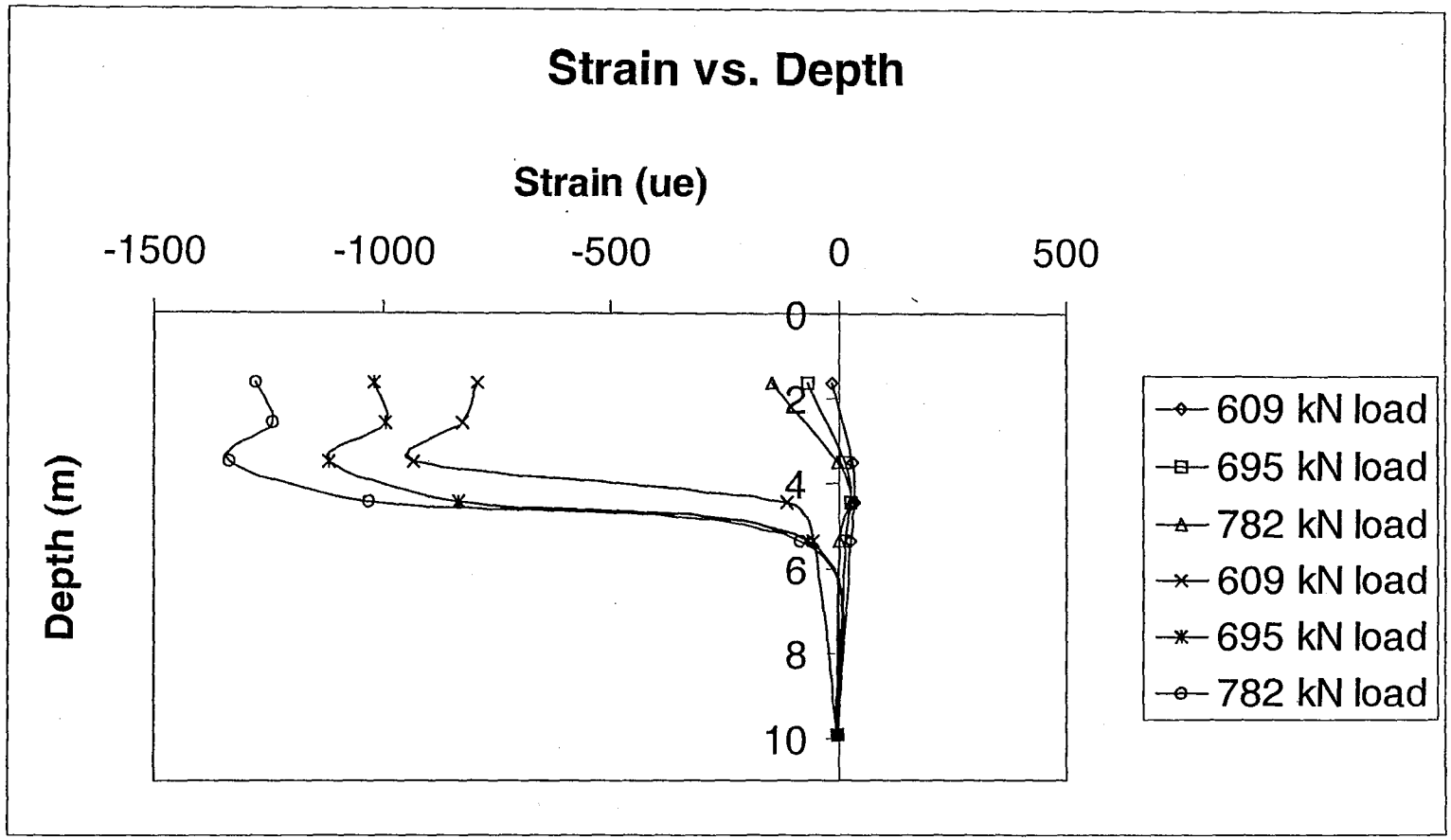

Figure 4.12

Shaft 2 Strain Measurements at Increased Loads

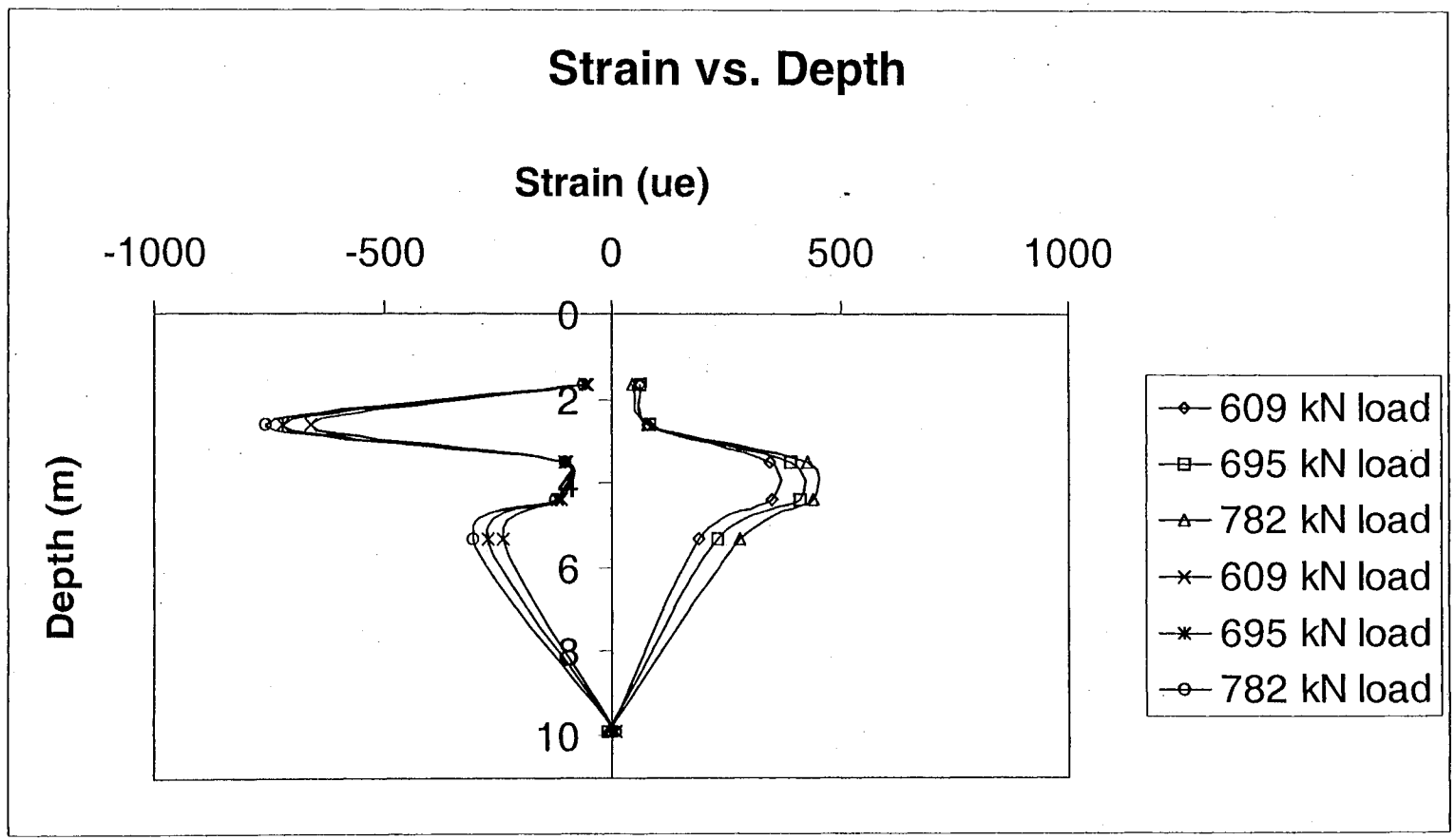

Figure 4.13

Shaft 3 Strain Measurements at Increased Loads

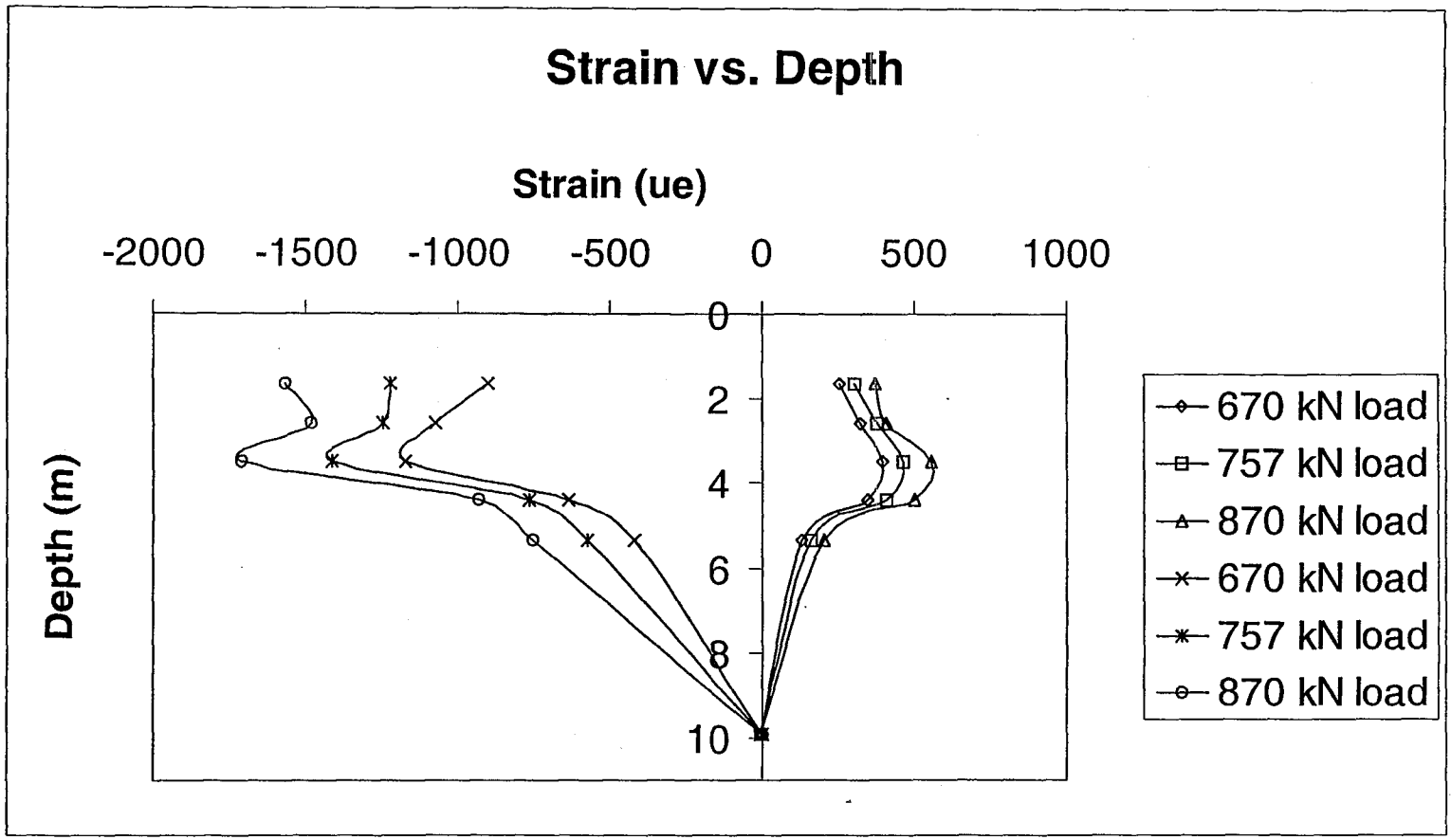

Figure 4.14

Shaft 5 Strain Measurements at Increased Loads

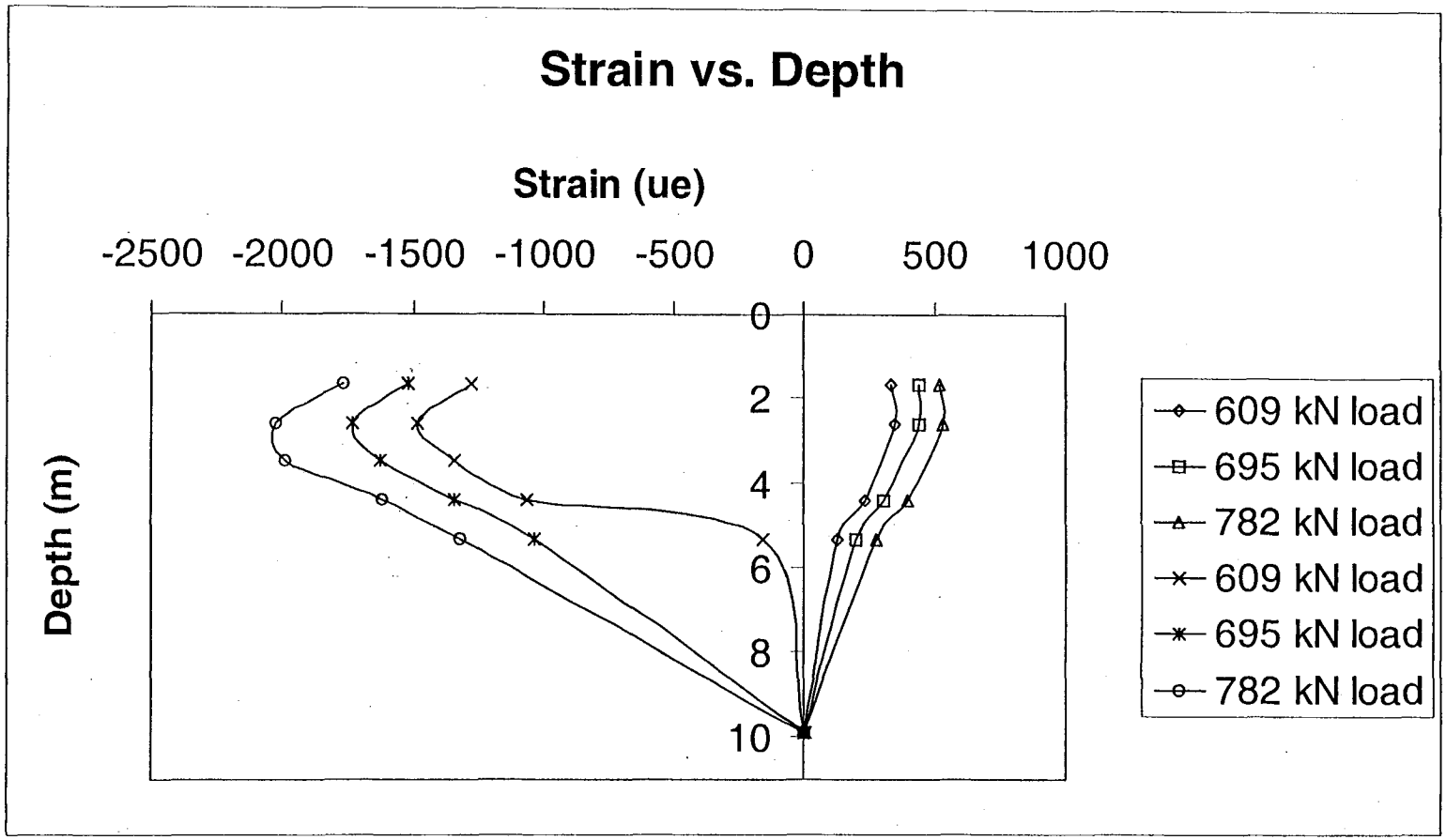

Figure 4.15

Shaft 6 Strain Measurements at Increased Loads

CHAPTER 5

ANALYSIS OF TEST RESULTS

5.1 Introduction

The main objective of this research project was to give recommendations for developing p-y curves for laterally loaded shafts founded in Piedmont soils. Equations for the development of p-y curves are presented in this chapter. The equations presented are based on any one of the following in-situ tests in the residual soil:

1. A Dilatometer Test (DMT) with the corresponding modulus (E_{DMT}) in psi.
2. A Cone Penetration Test (CPT) with the corresponding tip resistance (q_c) in Kpa.
3. A Standard Penetration Test (SPT) with the uncorrected blow count (N) for 30 cm.
4. A Pressuremeter Test (PMT) with the corresponding modulus (E_{PMT}) in psi.

Using the equations presented in this chapter, p-y curves can be derived to determine moments and deflections along the pile. This is easily accomplished using a computer program such as COM624.

5.2 Computational Model

The traditional approach to developing p-y curves using integration and differentiation of moments was not used in this research. Presented criteria in the past have used equations 5.1 and 5.2 in the development of p-y curves.

$$y = \iint \frac{M(x)}{EI}$$

Eq. 5.1

$$p = \frac{d^2}{dx^2} M(x)$$

Eq. 5.2

Extremely accurate measurements of the moments along a pile must be obtained in order to get use these equations. Many strain gages are required in the effort of obtaining accurate measurements. Also, an accurate measurement of the flexural rigidity (EI) of a pile is required in obtaining useful results. This has previously been accomplished using a steel pipe pile in which the Young's modulus (E) of 29,000 kips and the inertia (I) remains constant throughout testing. Therefore previous criteria were created using this method with steel piles under lateral loading.

This research involved reinforced concrete piles, which have a varying EI with an applied moment. The value of E varies because of the non-linearity in stress-strain relationships. The value of I is reduced due to the cracking of concrete. The concrete in the tensile zone below the neutral axis become ineffective after cracking. The pile parameters, discussed previously, were input to COM624. The program calculated the moments and corresponding EI based on an analysis of the cracked section. Figure 5.1

shows the variation of EI with moment. A p-y analysis for a reinforced concrete pile will have some computational error resulting from the assumption of a constant EI.

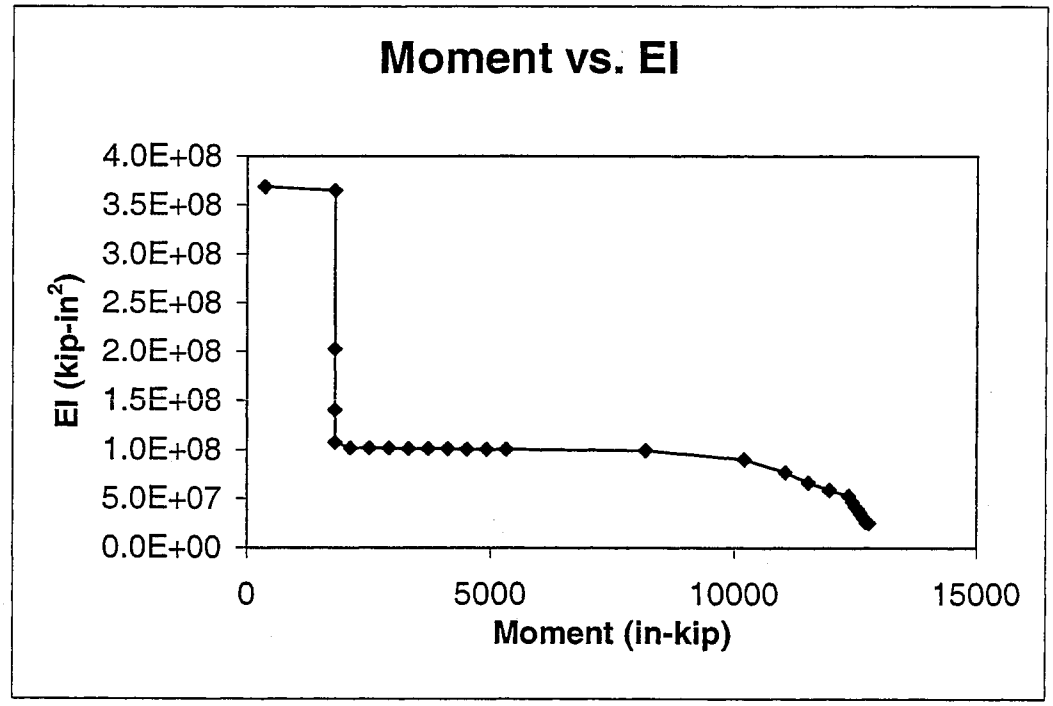

Figure 5.1

Moment vs. EI from COM624

5.3 COM624 p-y Criteria

COM624 has p-y criteria built into the program, which are used to internally generate p-y curves and allows the user to simply input soil strength parameters. These criteria include soft clay, stiff clay below the water table, stiff clay above the water table, sand, and vuggy limestone. The stiff clay and sand criteria were used to try and match the deflections measured in the field. The results show that these p-y criteria lack the capability to predict pile response in residual soils.

Three loads of 397 kN (69,000 lbs), 569 kN (128,000 lbs), and 747 kN (168,000 lbs) were input into the program. For the stiff clay criteria, the undrained shear strength of 92 kPa (1922 psf) observed from field measurements was input and run. The results were an extreme over prediction of head deflection; therefore these plots are not shown. The undrained shear strength and stiffness parameters were adjusted until the head deflection caused by the 569 kN load matched those measured in the field. The 397 kN load predicted a pile head deflection lower than those from field tests, shown in figure 5.2. The 747 kN load caused an error to occur in the program from an excessive head deflection. Although the 569 kN load did match the head deflection, the shape of the deflected pile was not matched, which can be observed in figure 5.3. These results suggest that the p-y response of the soil at this site is not well represented by curves produced using the stiff clay criteria.

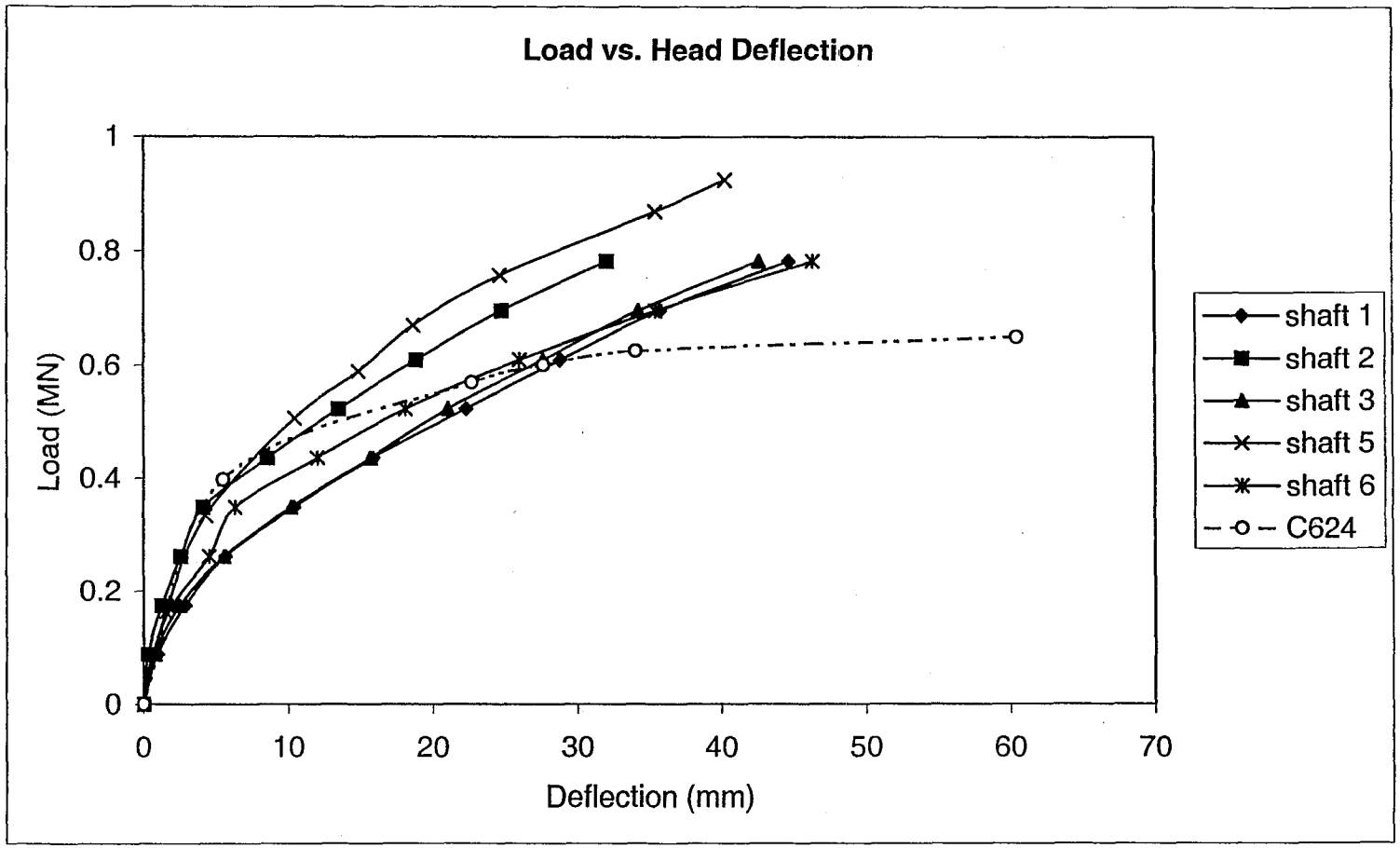

Figure 5.2

Load vs. Pile Head Deflection for Stiff Clay

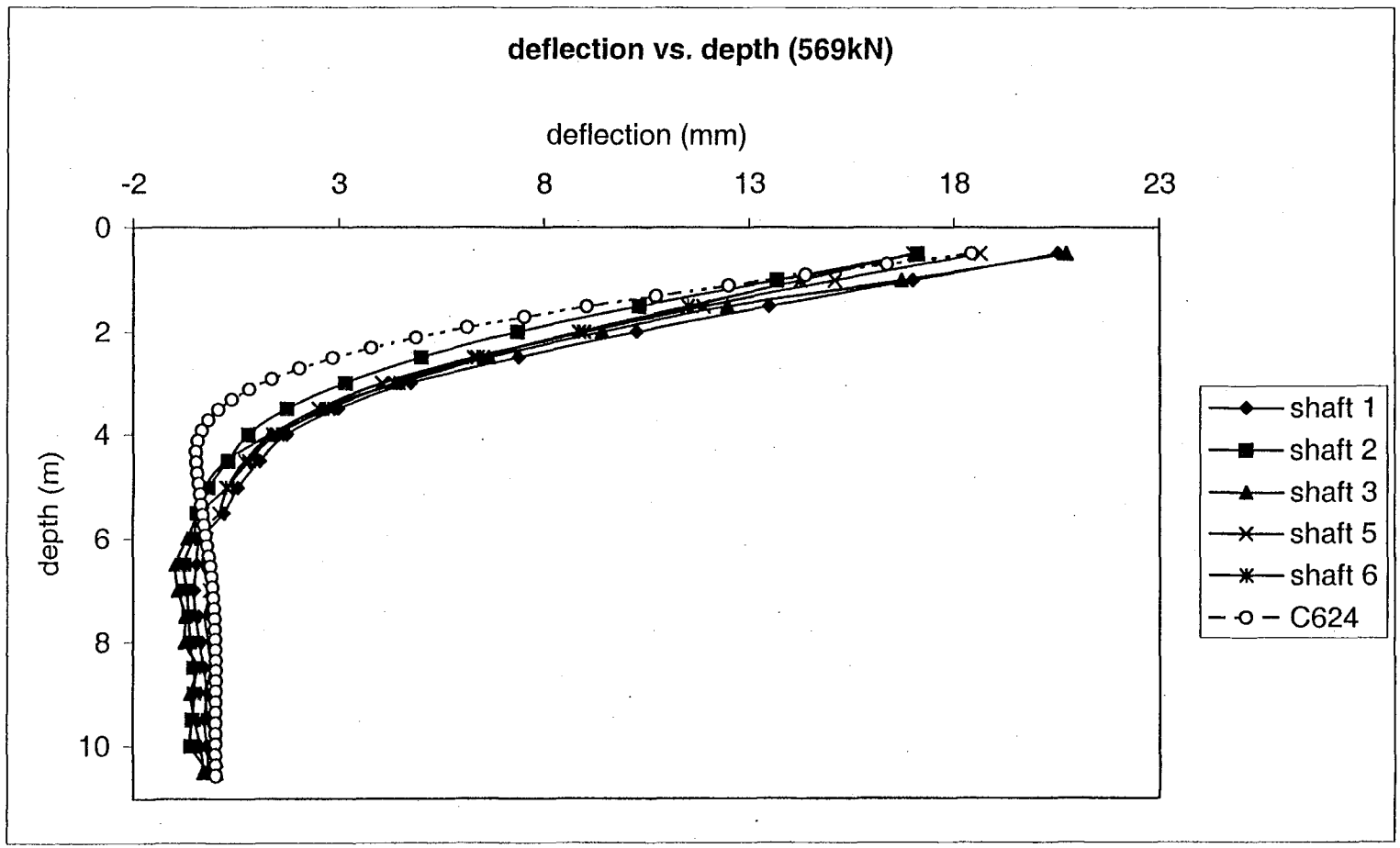

Figure 5.3

Stiff Clay Deflection vs. Depth for 569 kN Load

The angle of internal friction measured at the site (32°) was input to COM624 using sand criteria to try and predict pile response similar to that measured in the field. Again the pile head deflections were over predicted with a large amount of error. The angle and k were then adjusted similarly to the undrained shear strength for stiff clay until the head deflections from the 569 kN load matched those from the field tests. Figure 5.4 shows the similarity in pile head deflection with the field measurements for several loadings. The 397 kN load had a similar head deflection and deflected shape. The 569 kN and 747 kN loads resulted in head deflections similar to those measured, but the shape of the deflected piles were different. Figure 5.5 and 5.6 shows how the shape of the deflected piles were affected by larger lateral loads.

The clay criteria over predicted head deflections at large loads, and resulted in different deflected shapes of the piles compared to field measurements. The sand criteria showed similar head deflections for all observed loads, but the shape of the deflected piles from field tests was not duplicated.

This effort indicates that residual soils cannot be modeled effectively with existing p-y criteria for stiff clay or sand. The residual soil profile at this site (which is thought to be typical) has a stiff layer at shallow depths (discussed in chapter 2), which was not accounted for by these other criteria. The deflected shape of the pile was not captured very well by either criterion, which is a result of the composition of these soils. The soils are the result of in place weathering of parent rock. Depending on the parent rock present, different behavior can be observed. The soil does not behave exactly like a stiff clay or sand, but more as a combination of the two.

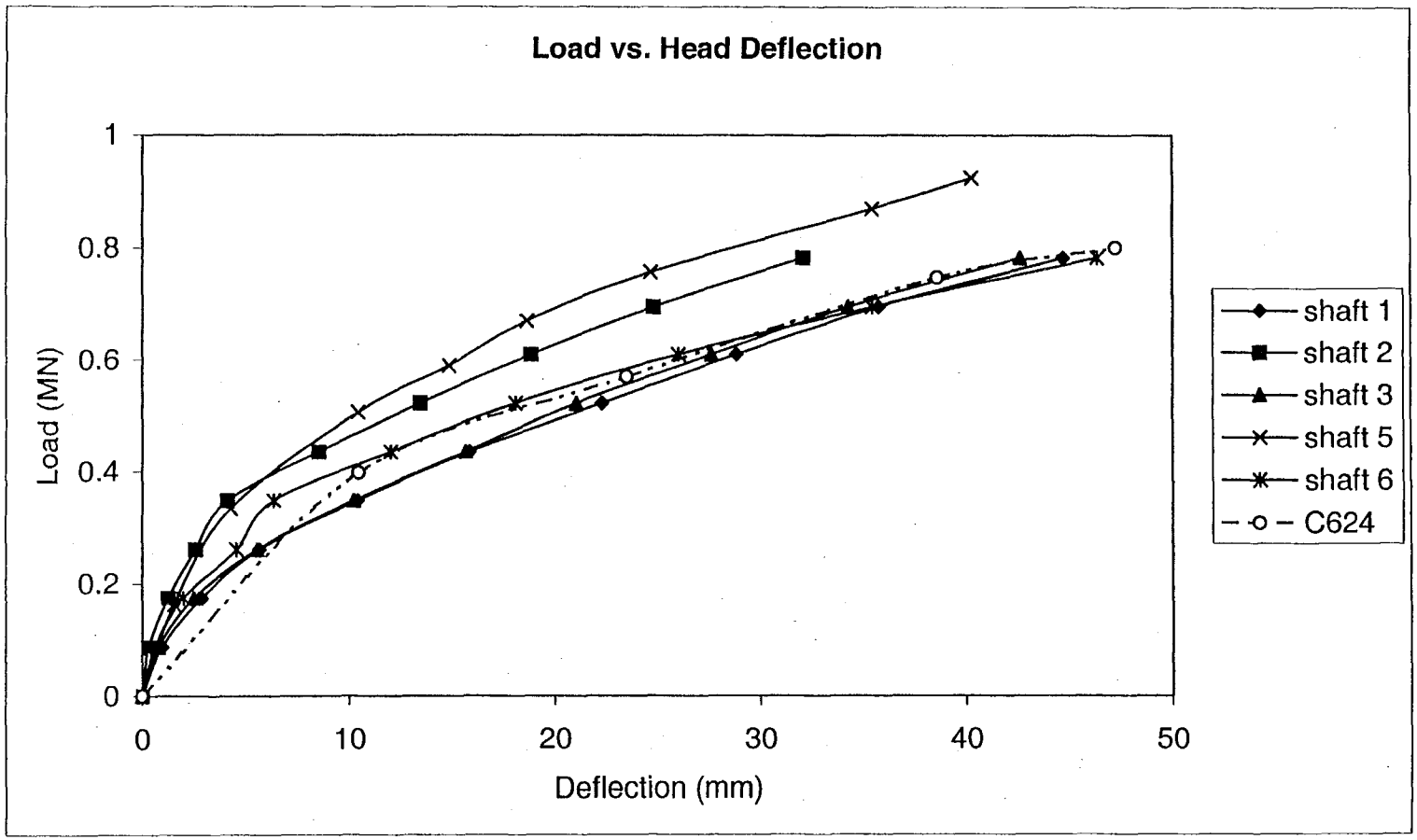

Figure 5.4

Load vs. Pile Head Deflection for Sand

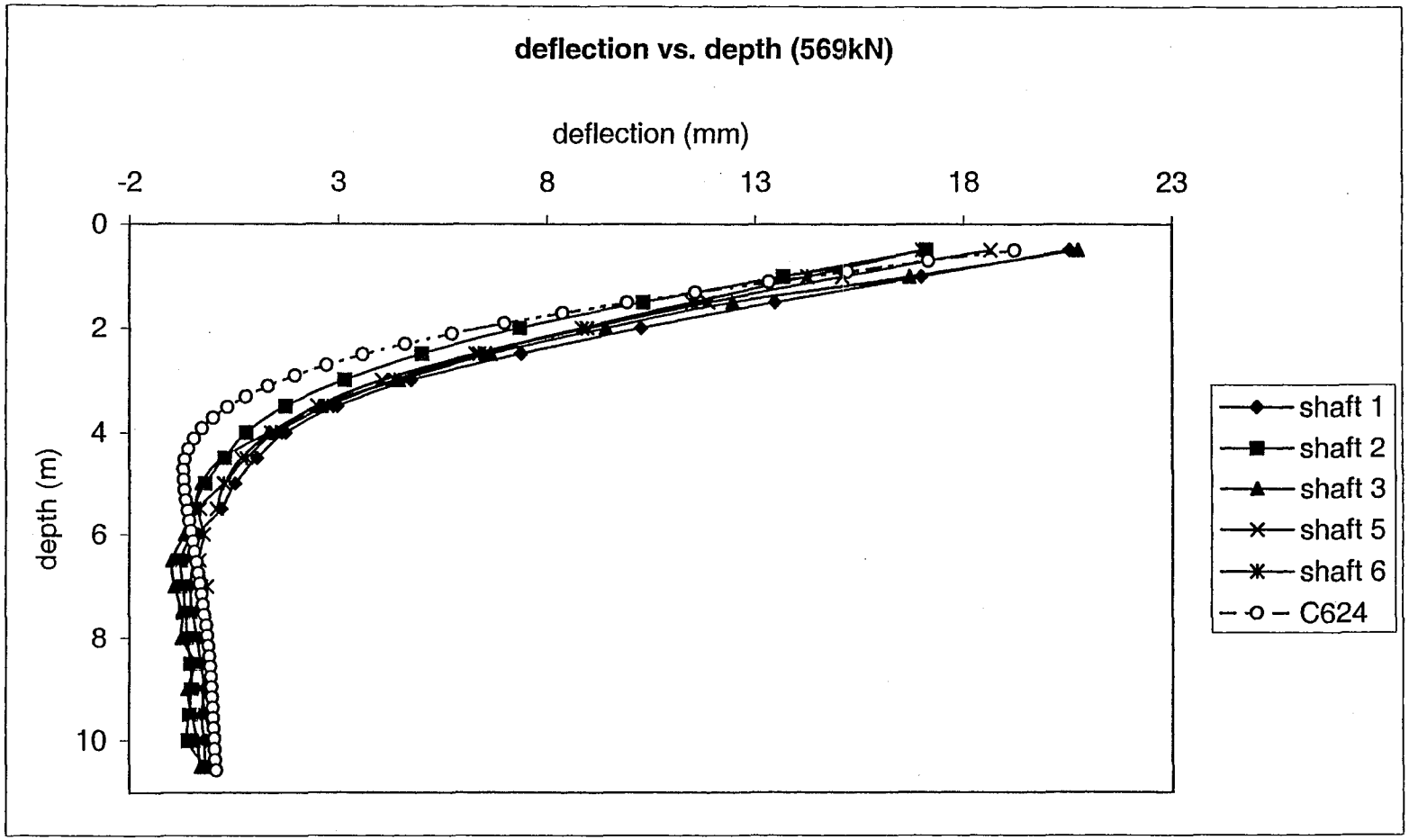

Figure 5.5

Sand Deflection vs. Depth for 569 kN Load

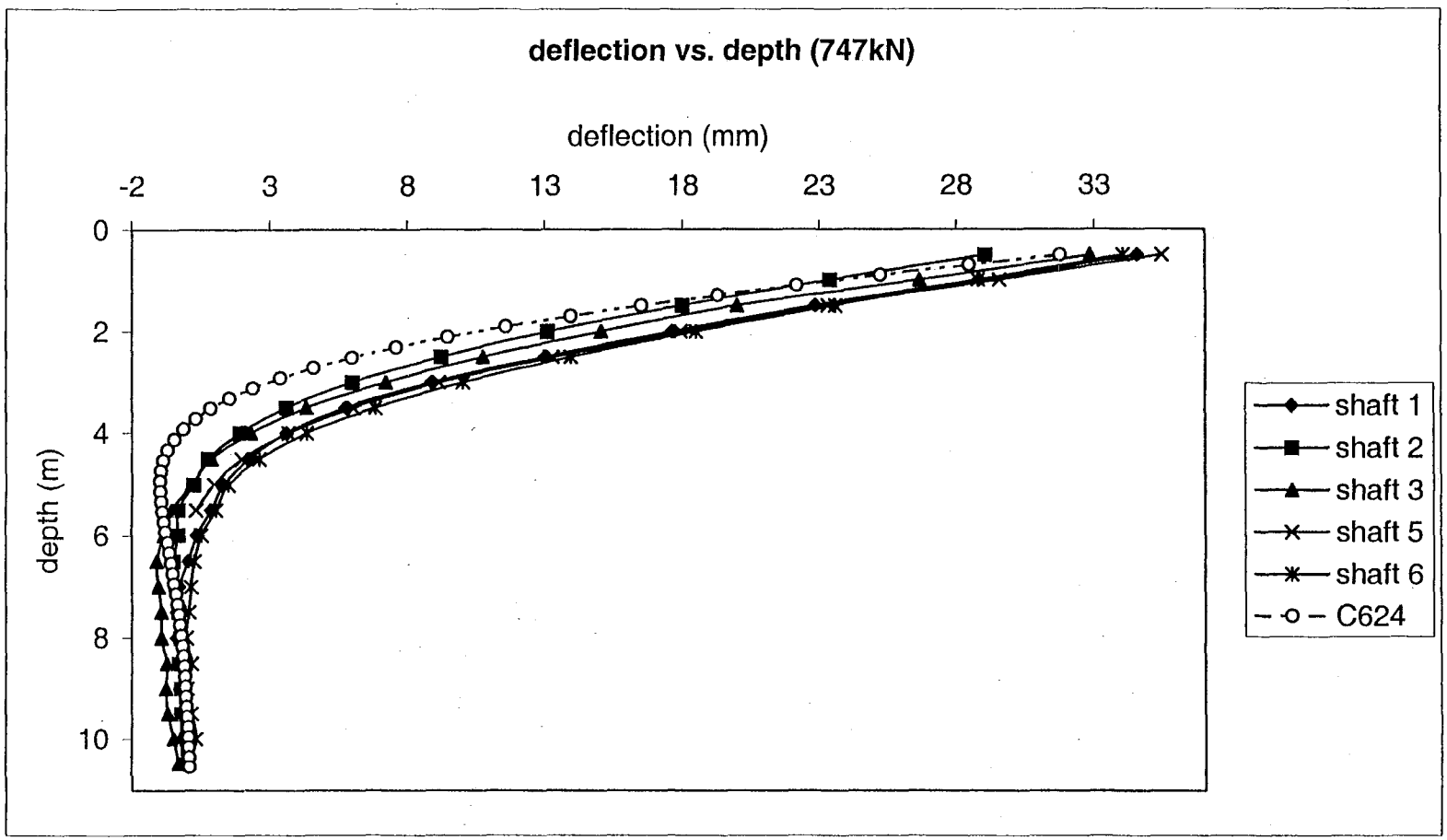

Figure 5.6

Sand Deflection vs. Depth for 747 kN Load

5.4.1 Development of p-y curves

In order to develop a form for p-y curves that adequately represent the Piedmont residual soils, a simple trial and error approach was used to back fit the computer solution to match the field measurements. Linear p-y curves were entered into COM624, which resulted in output of deflection data along the length of the pile for each given load. The slope of the linear p-y curves (k) was varied with depth for each load. The calculated deflection data were compared to the data from the tested shafts, and the p-y moduli (k) adjusted trying to match the shape of the two deflected piles.

The resulting pattern in soil stiffness is illustrated on figure 5.7. E_S is defined as k/b to establish a criterion independent of shaft diameter. The p-y relationship is therefore:

$$p = (E_s)(b)(y)$$

Eq. 5.3

In-situ data from the site were also observed and similar patterns were present, as indicated on the plots of DMT, SPT, and PMT test data versus depth, provided on figures 5.8 – 5.10. A strong correlation is observed between the lateral soil resistance on the test shafts and the measurements of soil stiffness and strength from the in-situ tests.

The lateral soil response is softer at larger lateral displacements because the load versus deflection showed a strong non-linearity in the lateral load versus deflection behavior of the test shafts. This can be observed in the test shafts load versus deflection plot shown in figure 5.11. This non-linear lateral load versus deflection is consistent with that of other types of p-y relationships used for sands and clays. The non-linear decrease

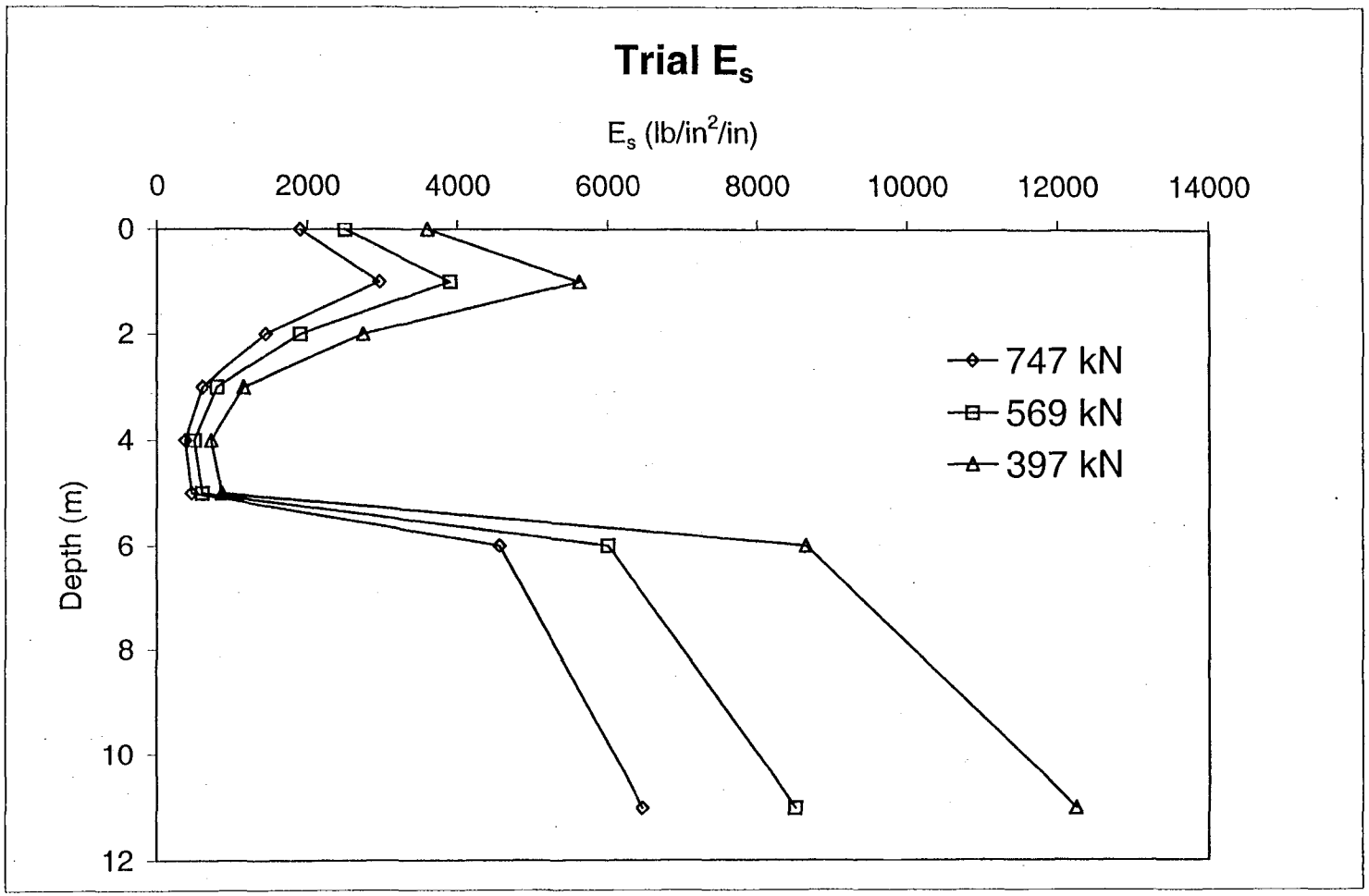

Figure 5.7

E_S from Back Fit Attempt

in soil stiffness with increased deflection derived from this back fit process is shown in figure 5.12. The same data are plotted on a log scale in figure 5.13.

E_S must be a nonlinear function of y to account for decreasing stiffness with increasing deflection. In order to model the non-linear response of the Piedmont residual soil, as shown on figure 5.14, the following equations are used:

$$E_S = E_{Si} \text{ ; for y/b} < 0.001$$

$$E_S = E_{Si}\left[1 - \lambda \ln\left(\frac{y/b}{0.001}\right)\right] \text{ ; for } 0.001 < \text{y/b} < 0.0375$$

$$p = p_{ult} \text{ ; for y/b} > 0.0375$$

Eq. 5.4

$$p_{ult} = (b)(y)[1 - 3.624\lambda]$$

Eq. 5.5

P_{ult} is defined as p at a value of y equal to 0.0375(b). E_{Si} was the in-situ test data multiplied by a constant in order to increase or decrease the soil response. The field test data were matched by adjusting E_{Si} and λ.

Some assumptions were made in forming this criterion. At large displacement magnitudes, the soil response was taken to be constant. The test data do not actually provide measurements at such large displacements, but this assumption follows the procedure used in the existing p-y criterion for sand. Also, this criterion was back matched to the test data beginning at 1 diameter below the ground surface. The p-y curves for the top 1 diameter are taken to decrease linearly to ½ this value at the ground surface. The initial linear portion of the curve is set at a displacement up to 0.001(b)

(0.1% of the shaft diameter). This cutoff is somewhat arbitrary, but it seemed to match the test data quite well.

Using the presented recommendations, p-y curves can be constructed for Piedmont residual soils. These p-y curves are based on in-situ test data. A constructed p-y curve in general from is shown in figure 5.15.

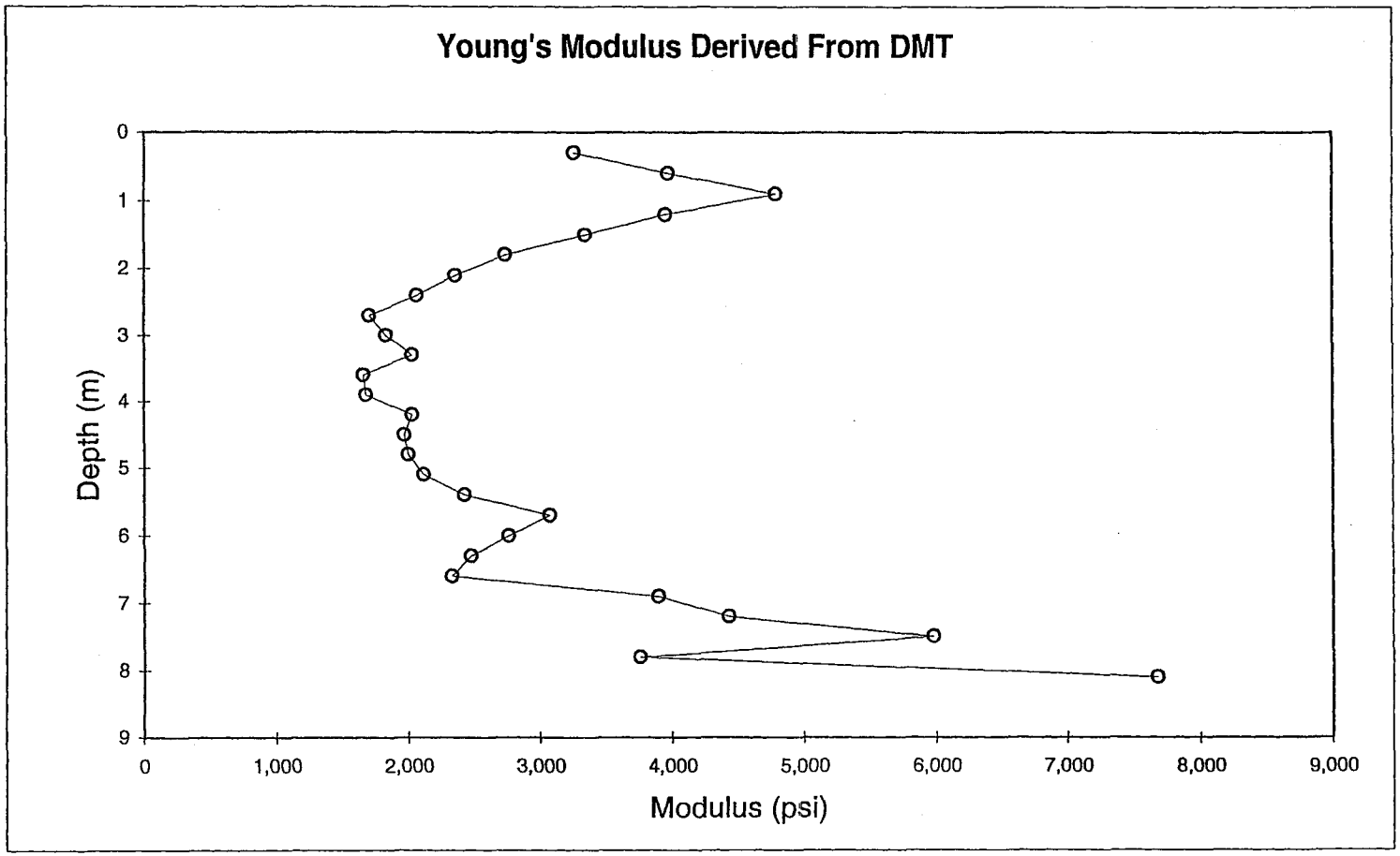

Figure 5.8

Young's Modulus from DMT (Vinson and Brown, 1997)

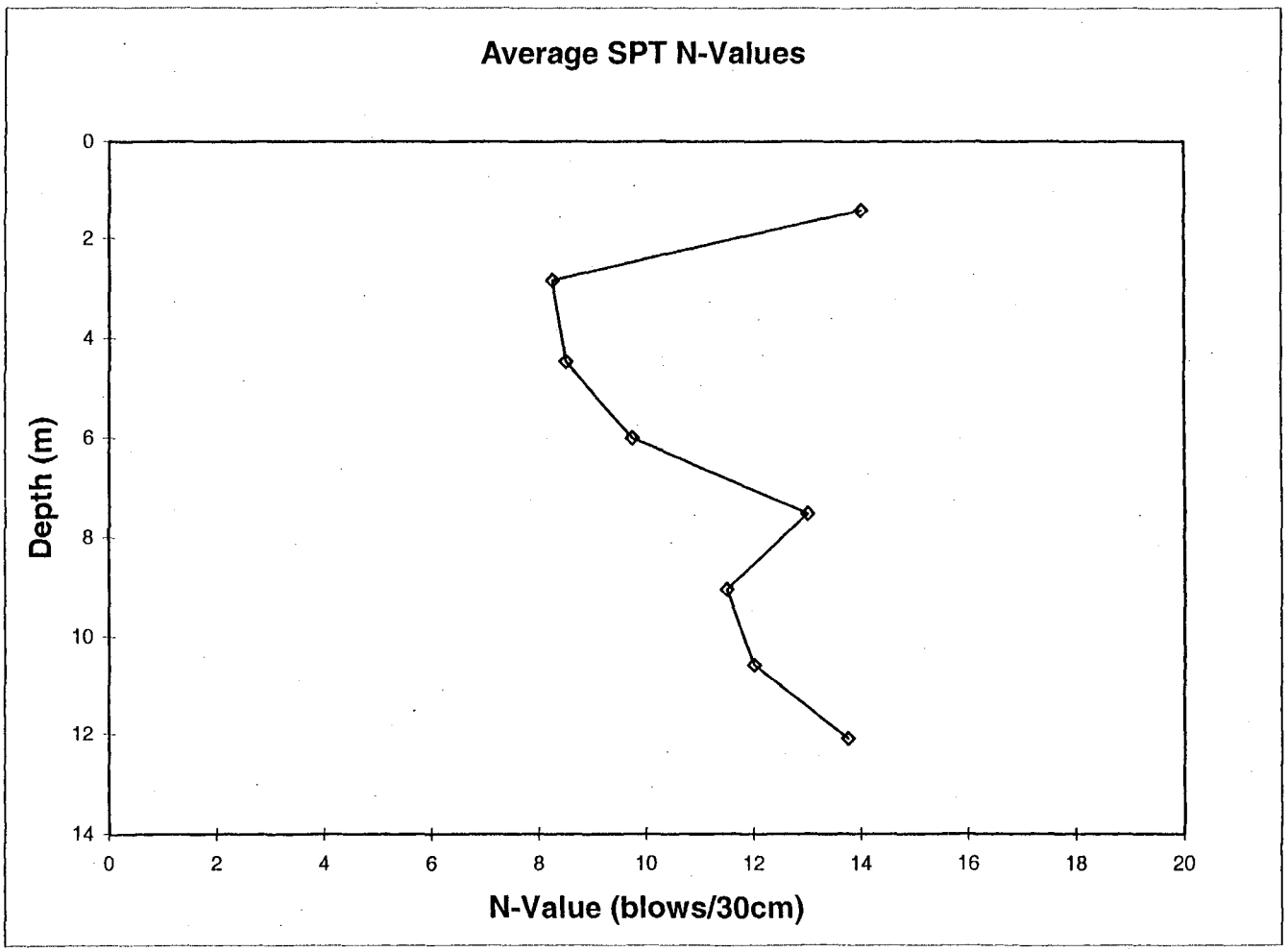

Figure 5.9

SPT Blow Count (Vinson and Brown, 1997)

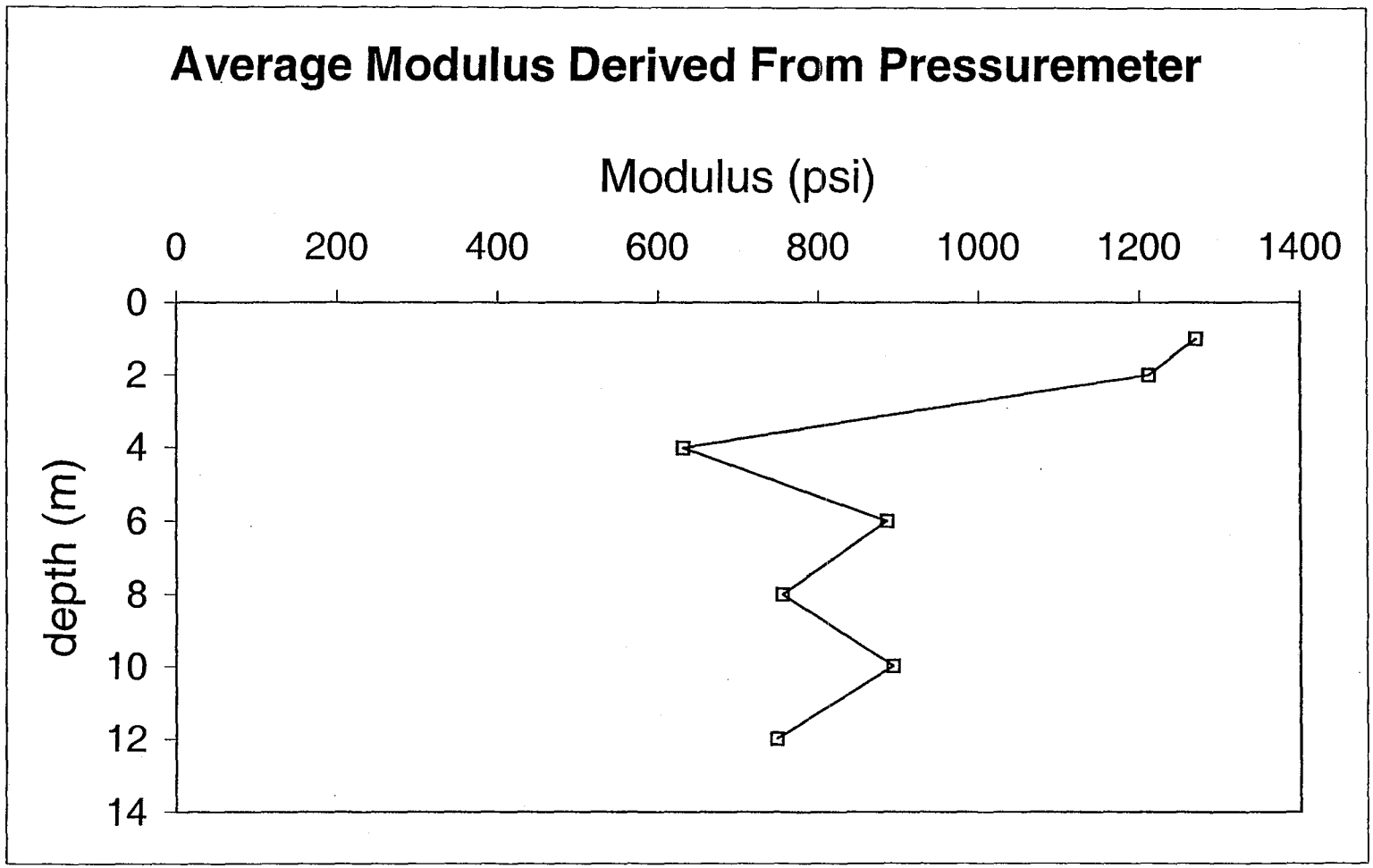

Figure 5.10

PMT Modulus (Vinson and Brown, 1997)

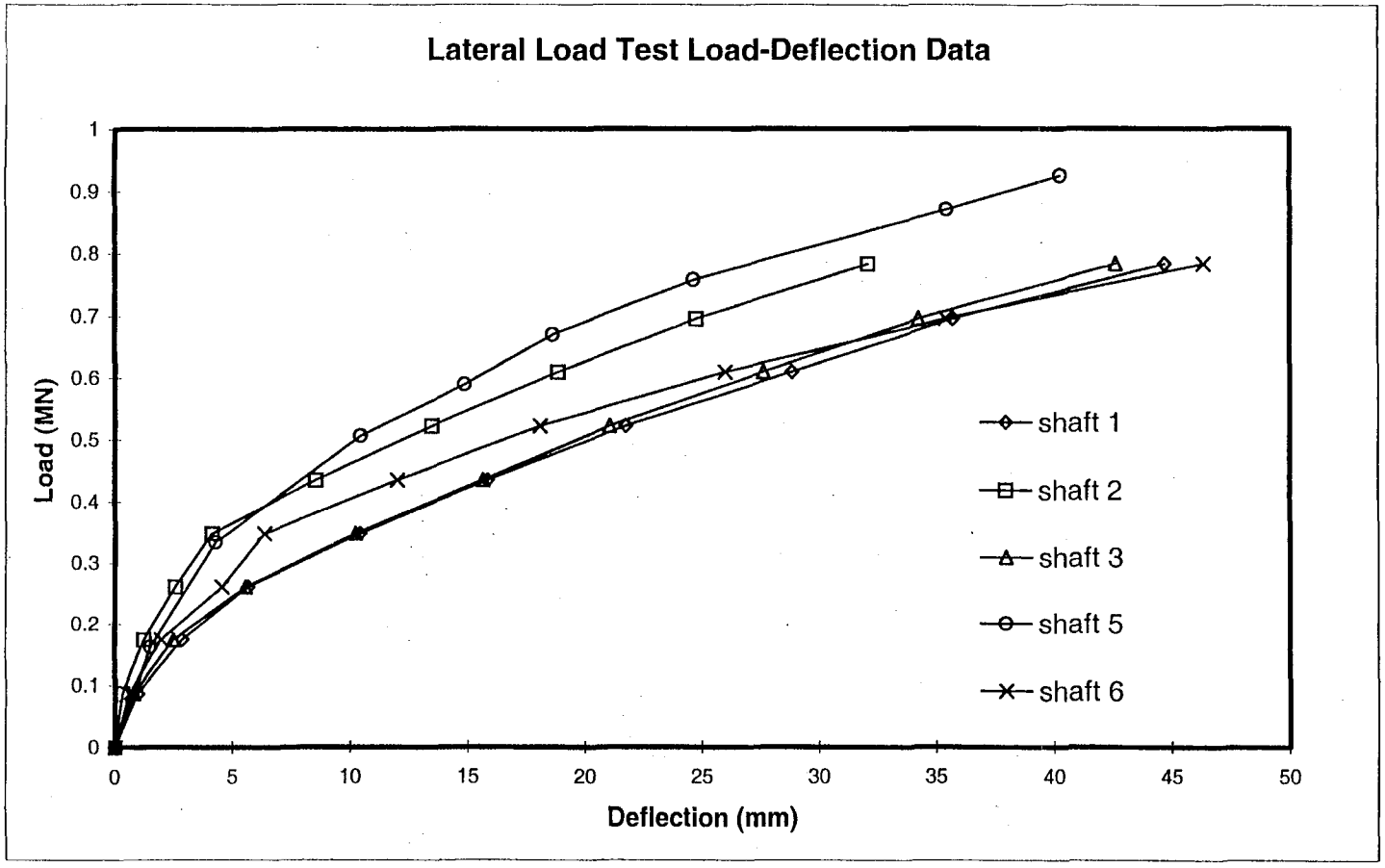

Figure 5.11

Load vs. Deflection from Field Load Tests

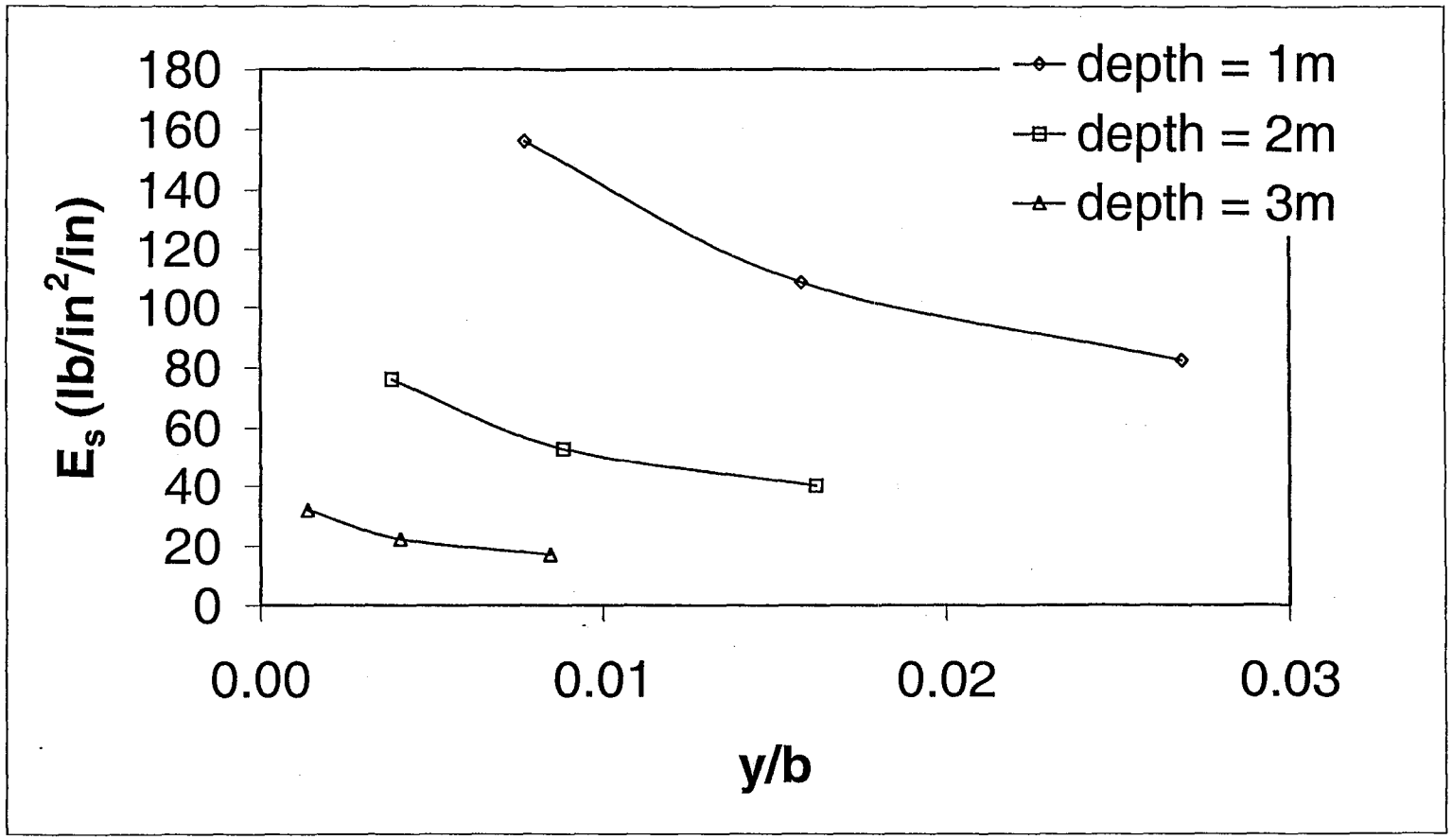

Figure 5.12

Non-linear Decrease in Soil Stiffness with Increased Deflection

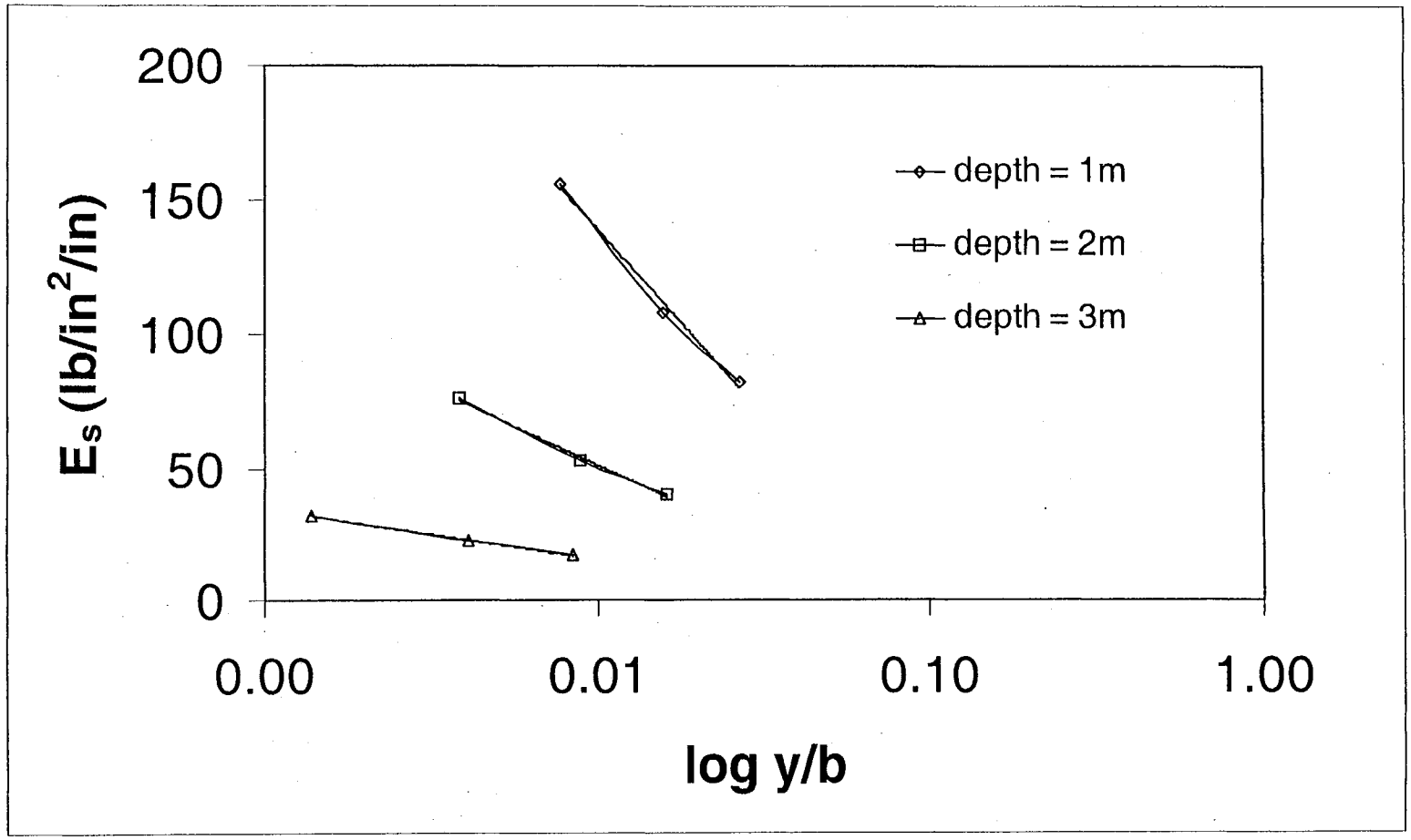

Figure 5.13

E_S vs. log y/b

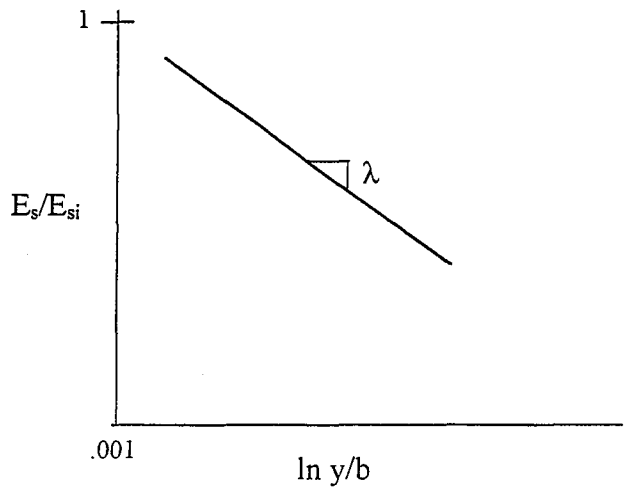

Figure5.14

Degradation Plot for E_S

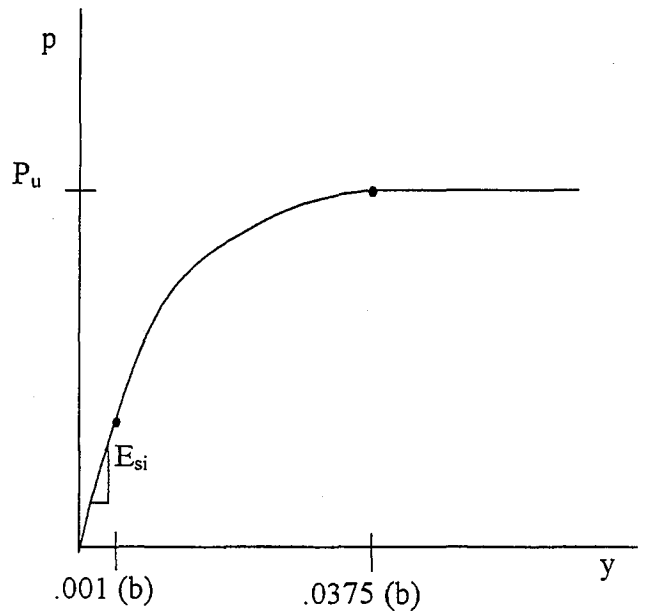

Figure 5.15

p-y Curve for Piedmont Residual Soil

5.4.2 Summary of Proposed Model

The proposed model was developed for Piedmont residual soils. The curve begins as a straight line with a slope of E_{Si} until a deflection of 0.001(b) is reached. Between a deflection of 0.001(b) and 0.0375(b) the curve is calculated using equations 5.3 and 5.4.

$$p = (E_s)(b)(y)$$

Eq. 5.3

$$E_s = E_{Si}\left[1 - \lambda \ln\left(\frac{y/b}{0.001}\right)\right] \text{ ; for } 0.001 < y/b < 0.0375$$

Eq. 5.4

The curve becomes constant after a deflection of 0.0375(b) is reached. The soil response at this point is defined as P_{ult}. The value of p at this point can be calculated using equation 5.5.

$$p_{ult} = (b)(y)[1 - 3.624\lambda]$$

Eq. 5.5

Following this model a p-y curve similar in shape to figure 5.15 can be constructed.

5.5 p-y Curve Results

Equations were developed using 4 in-situ test methods. The data from the DMT, CPT, SPT, and PMT were used to give recommendations for developing p-y curves. These in-situ tests were chosen because of the available data their widespread use in geotechnical engineering.

In developing the criterion, the data from each test method was taken and multiplied by a constant to obtain E_{Si}. Also, a single value of λ for the degradation of E_S was chosen to be used with all correlations. These two parameters were adjusted for each set of data until the head calculated matched those observed in the field.

Adjusting λ affected how quickly the soil response decreased with increasing deflection. For the Piedmont residual soil at the Auburn University Geotechnical Test Site, a λ of -0.23 was found to match the data. The constant α for each in-situ test was easily obtained by increasing or decreasing until the correct soil stiffness was obtained.

The general form of the p-y relationship shown in equation 5.3 was used to develop these curves. The diameter b and deflection y are known. E_S can be calculated using equation 5.4. The only variable not known is E_{Si}. E_{Si} can be found using equation 5.6.

$$E_{Si} = (\alpha)(E)$$

Eq. 5.6

E is the data obtained from an in-situ soil test. The constant α was found empirically by adjusting for each in-situ test method. E_{Si} can be calculated using the following relationships:

Dilatometer modulus in psi

$$(0.076)(E_{DMT})$$

Cone Penetration tip resistance in Kpa

$$(0.118)(q_c)$$

Standard Penetration blow count in blows/30cm

$$(22)(N_{SPT})$$

Menard Pressuremeter modulus in psi

$$(0.235)(E_{PMT})$$

The data obtained from the DMT, SPT, and PMT were shown in figures 5.8, 5.9, and 5.10 respectively. The CPT test data versus depth is shown in figure 5.16. The CPT tip resistance was used in development of the criterion because it is a better indicator of soil strength than the other measurements. However note that the trend of higher stiffness at shallow depth is less evident in these measurements.

Using the presented equations, p-y curves were developed to predict pile deflections using COM624. Figures 5.17 – 5.32 provide the measured and computed deflection data from the DMT, CPT, SPT, and PMT correlations cited above.

. All four equations produced reasonably good agreement with the measured deflections. The non-linear pile head deflections are predicted, and the deflected shapes of the piles from the field tests were captured quite well. Shaft 2 and 5 produced lower head deflections than the other three shafts at similar loads during testing. The equations presented compare with the head deflections similar to shafts 1, 3, and 6. The design equations thus fall on the conservative side with respect to the measurements.

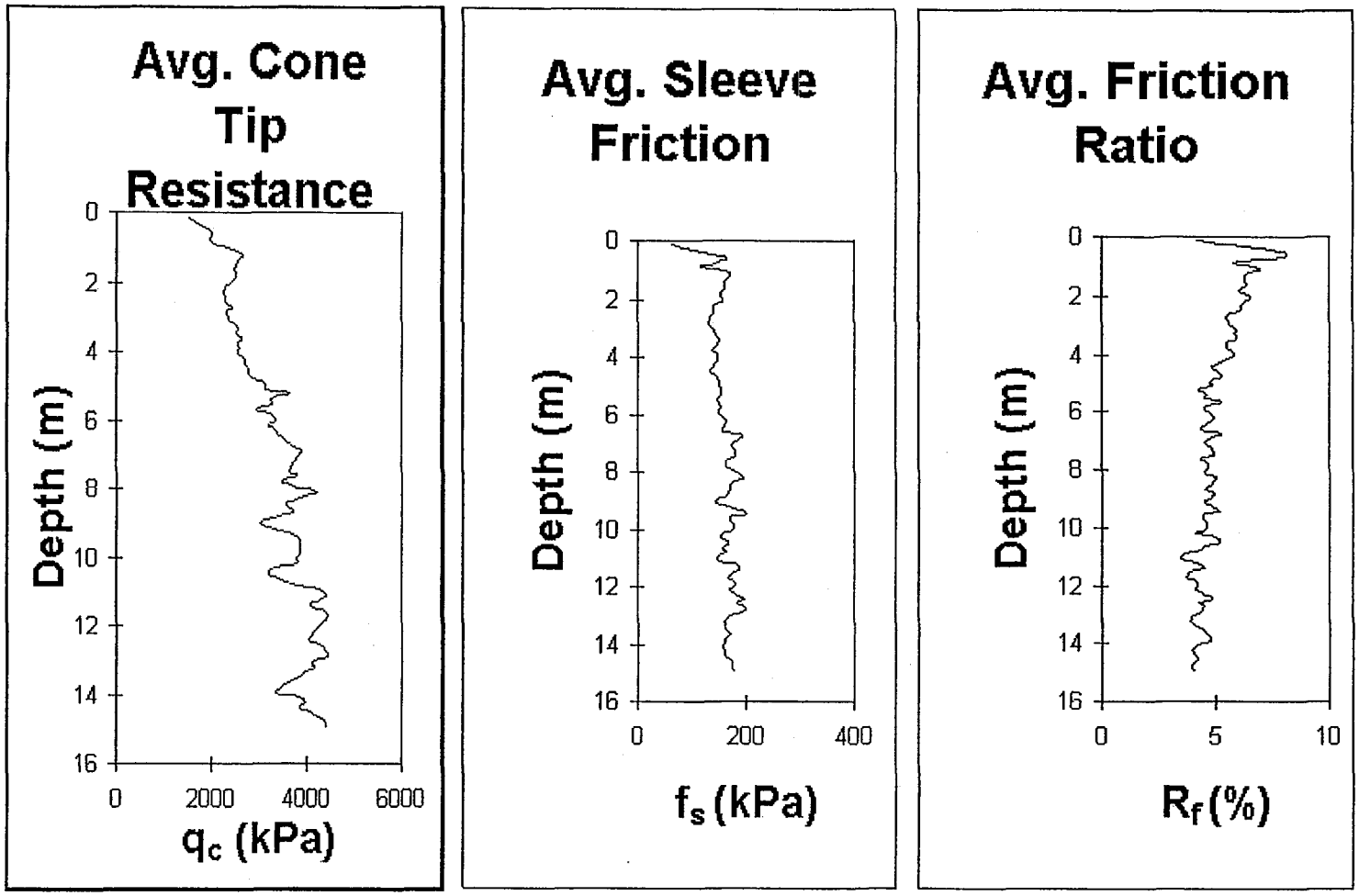

Figure 5.16

CPT Results (Vinson and Brown, 1997)

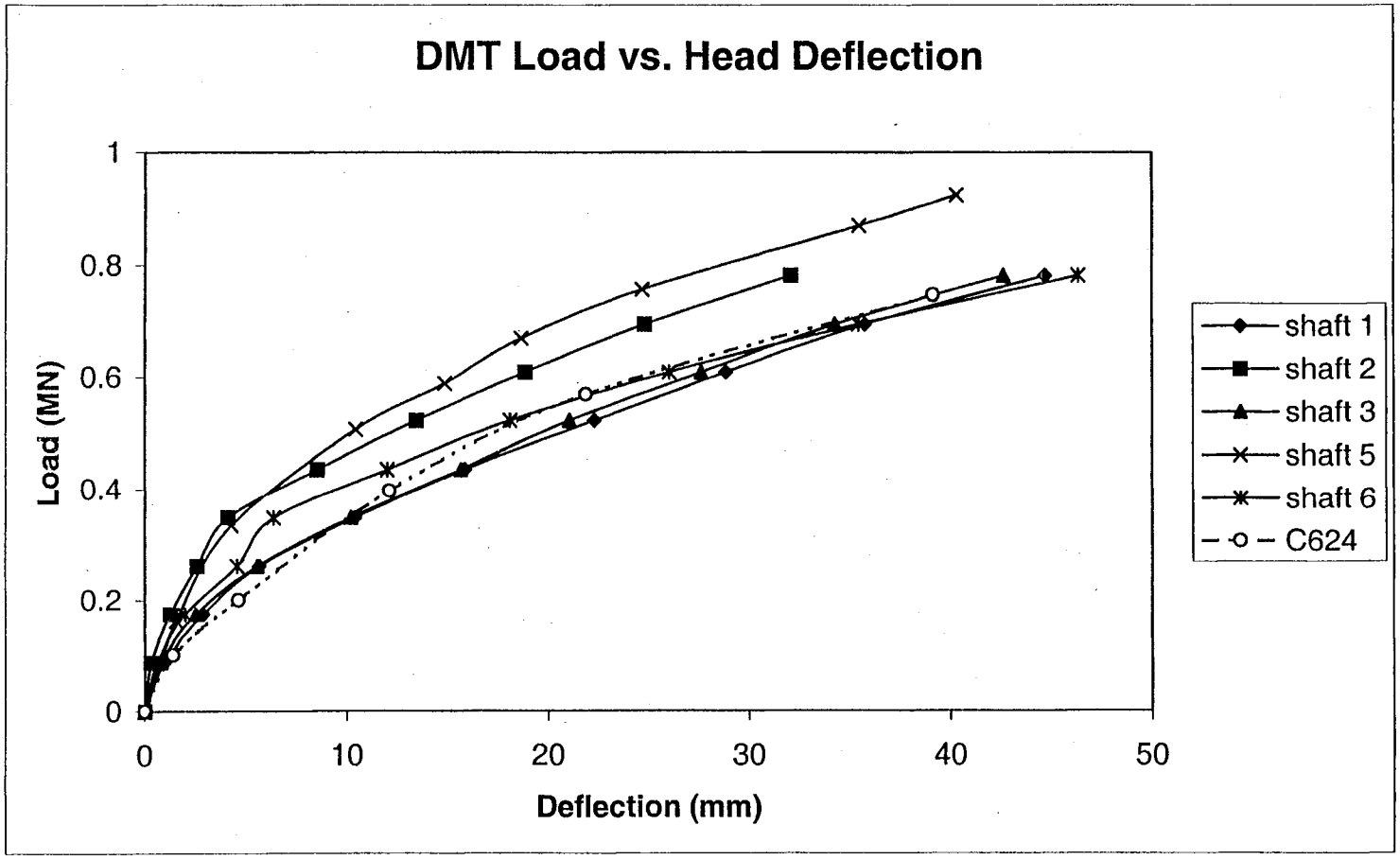

Figure 5.17

DMT Load vs. Head Deflection

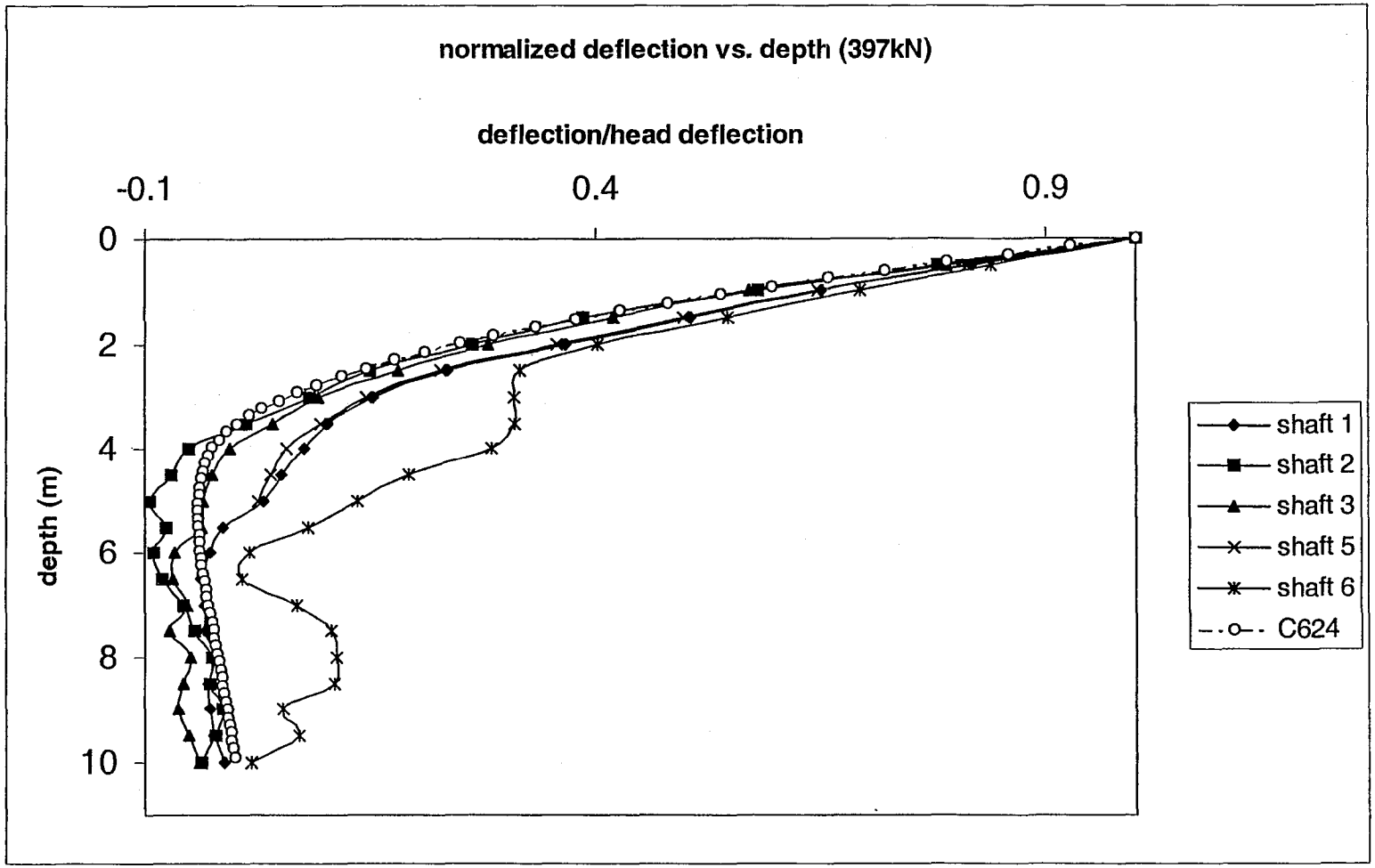

Figure 5.18

DMT Normalized Deflection vs. Depth for 397 kN Load

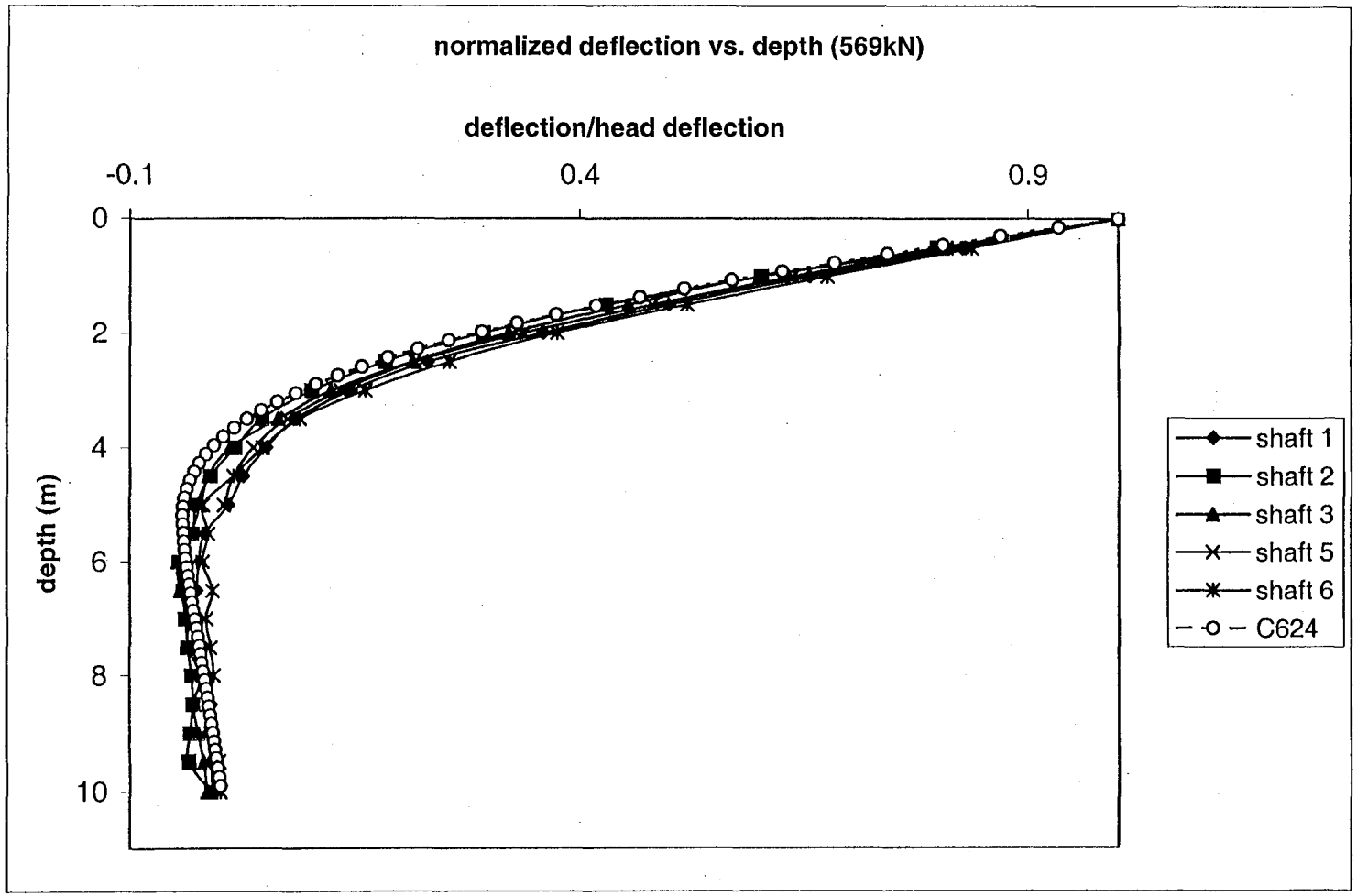

Figure 5.19

DMT Normalized Deflection vs. Depth for 569 kN Load

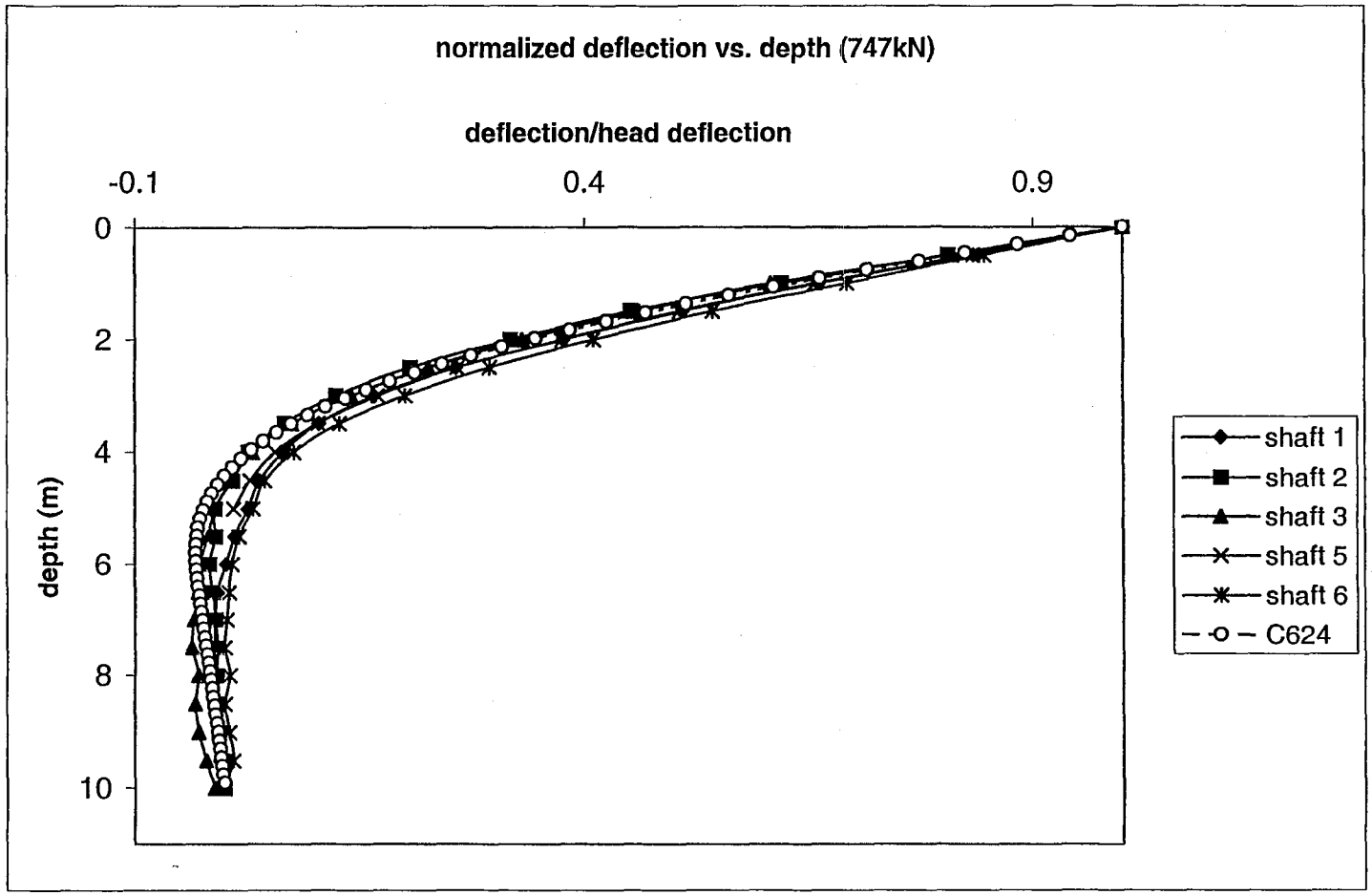

Figure 5.20

DMT Normalized Deflection vs. Depth for 747 kN Load

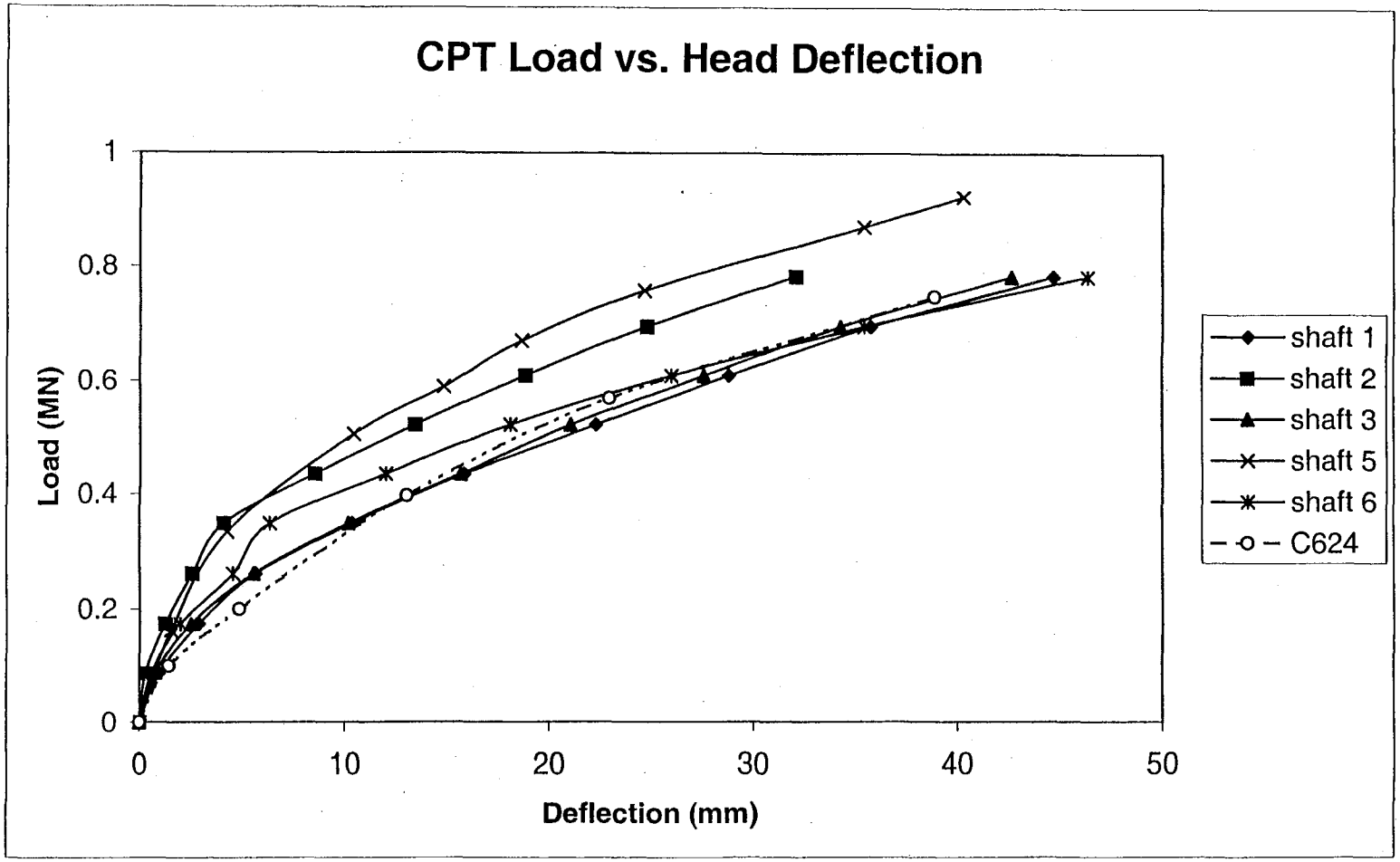

Figure 5.21

CPT Load vs. Head Deflection

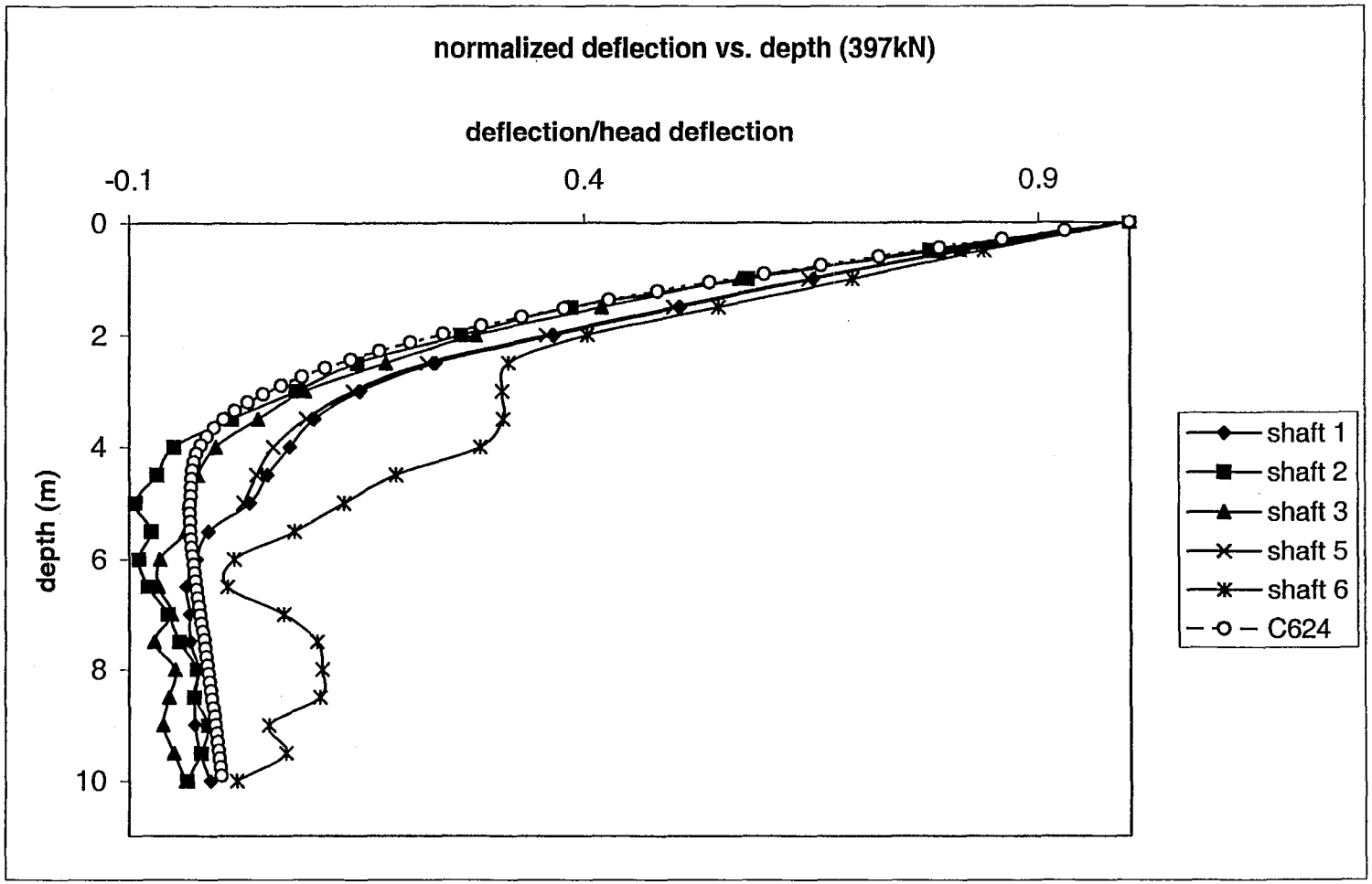

Figure 5.22

CPT Normalized Deflection vs. Depth for 397 kN Load

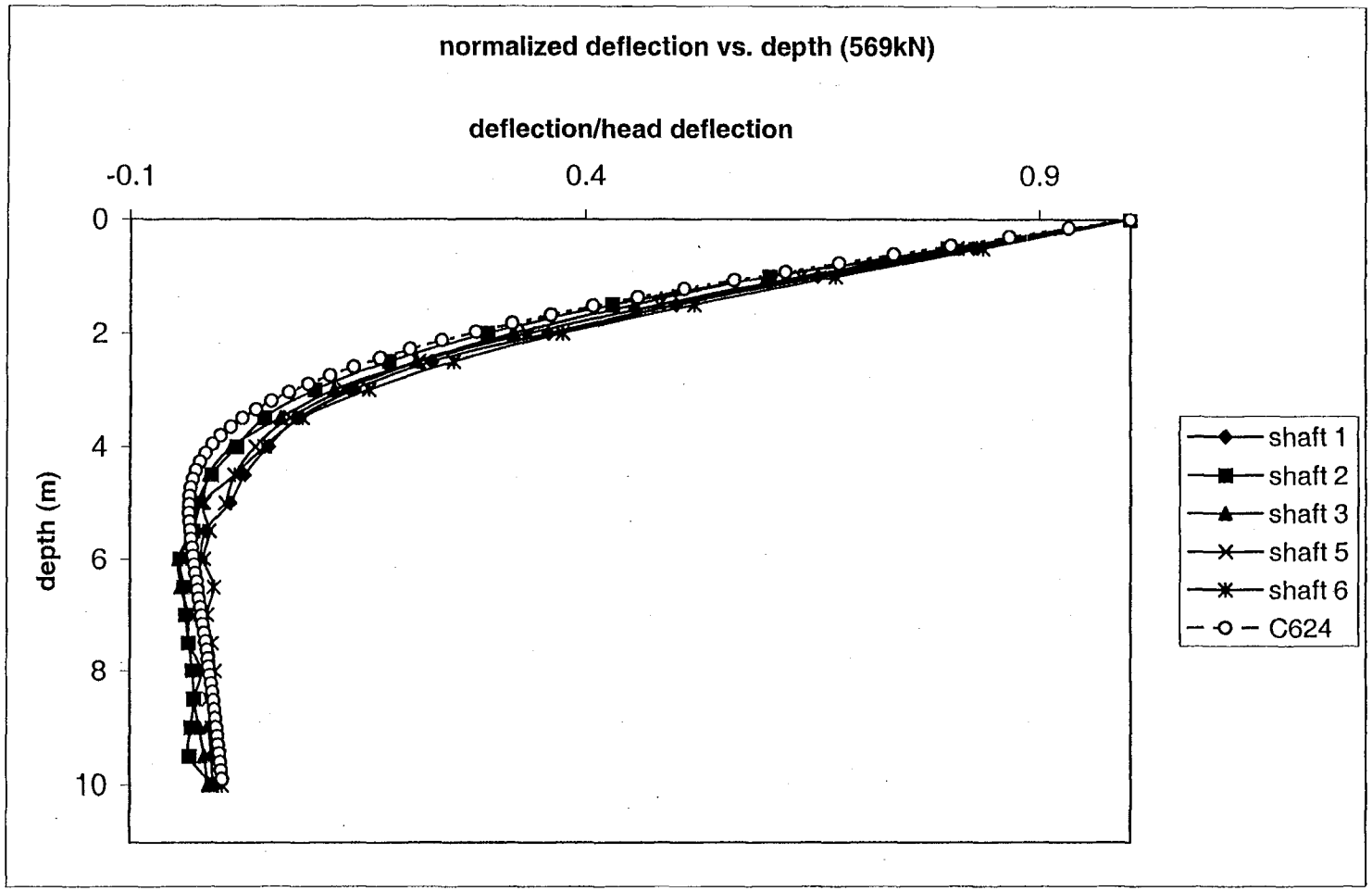

Figure 5.23

CPT Normalized Deflection vs. Depth for 569 kN Load

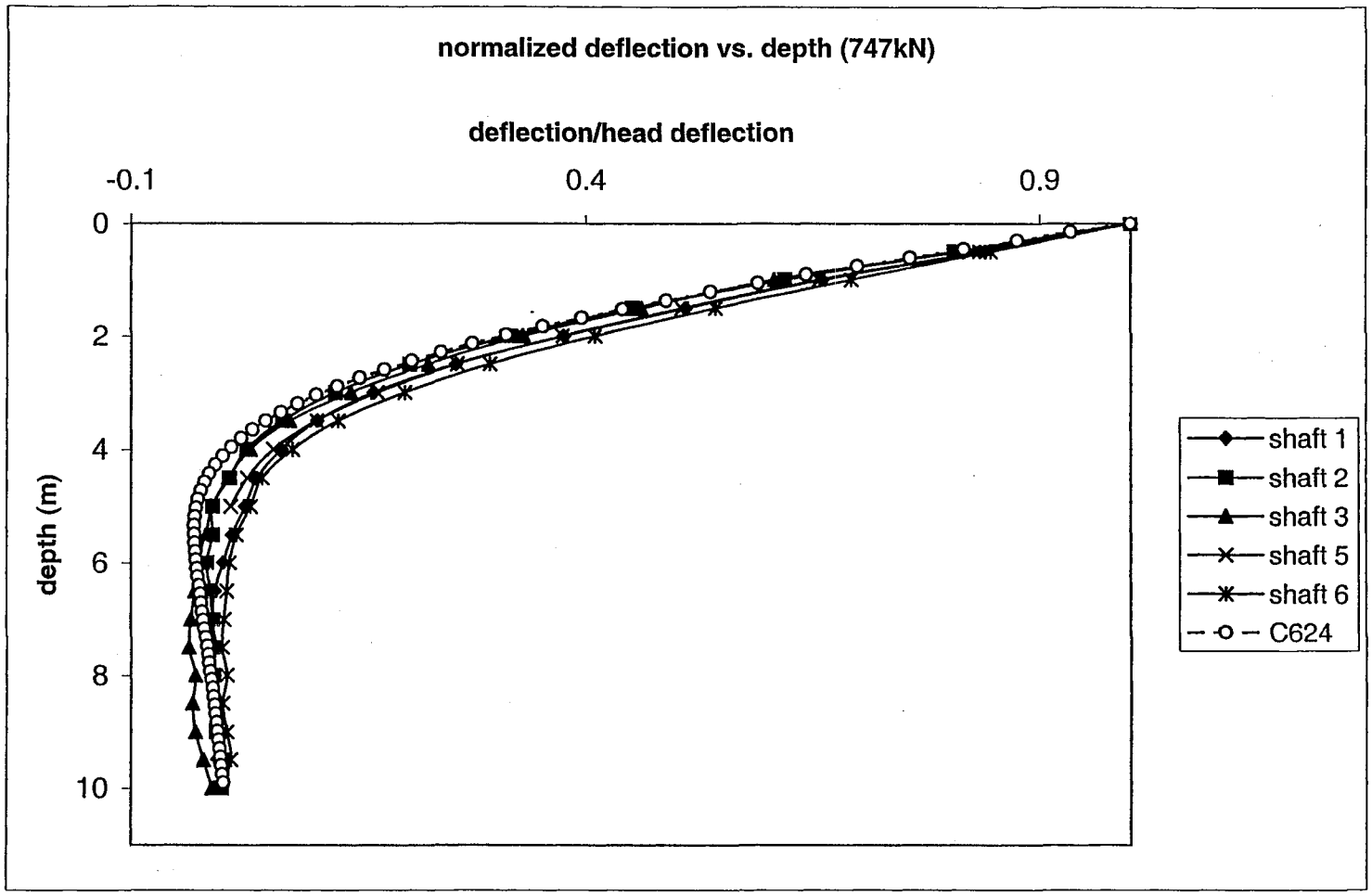

Figure 5.24

CPT Normalized Deflection vs. Depth for 747 kN Load

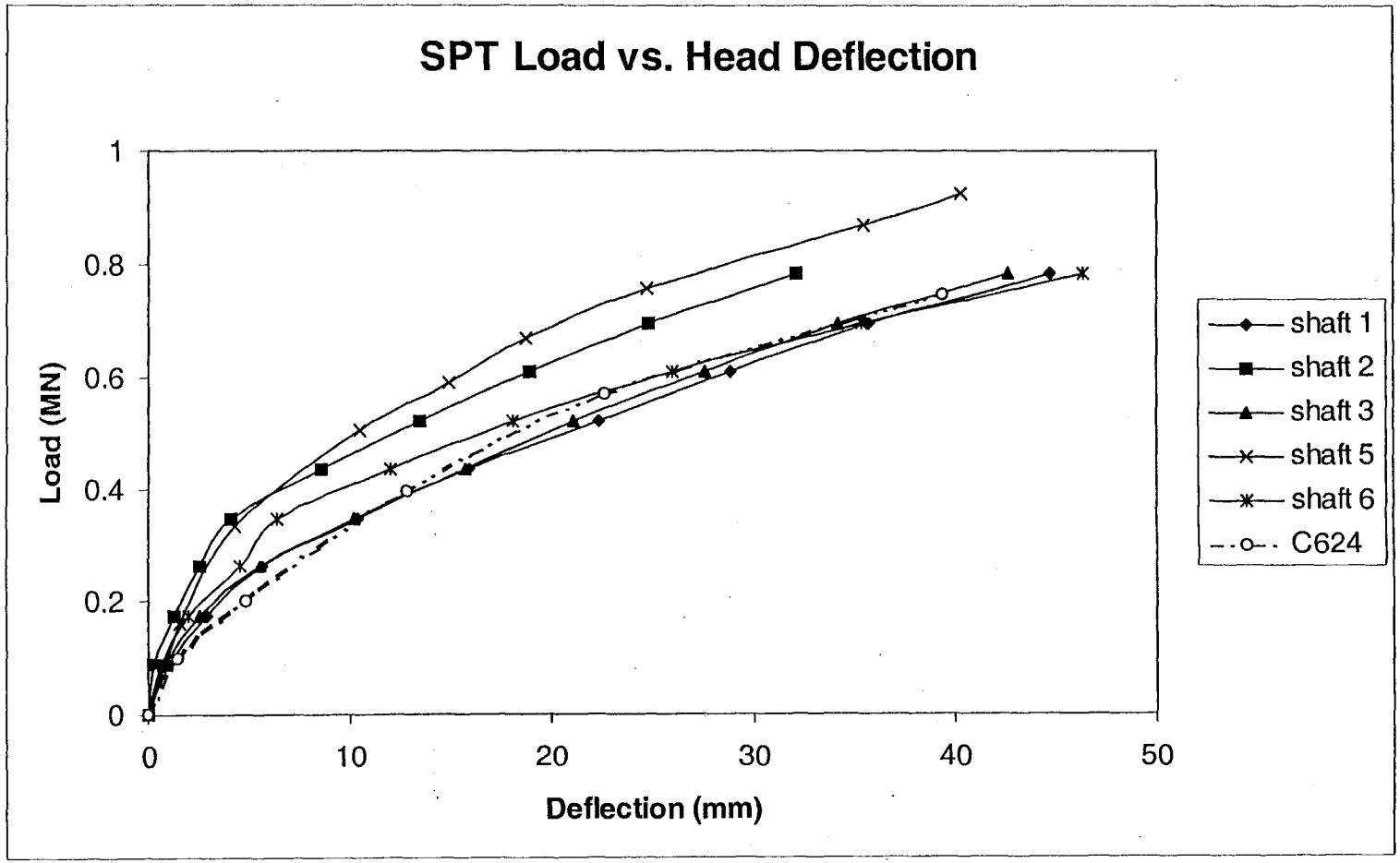

Figure 5.25

SPT Load vs. Head Deflection

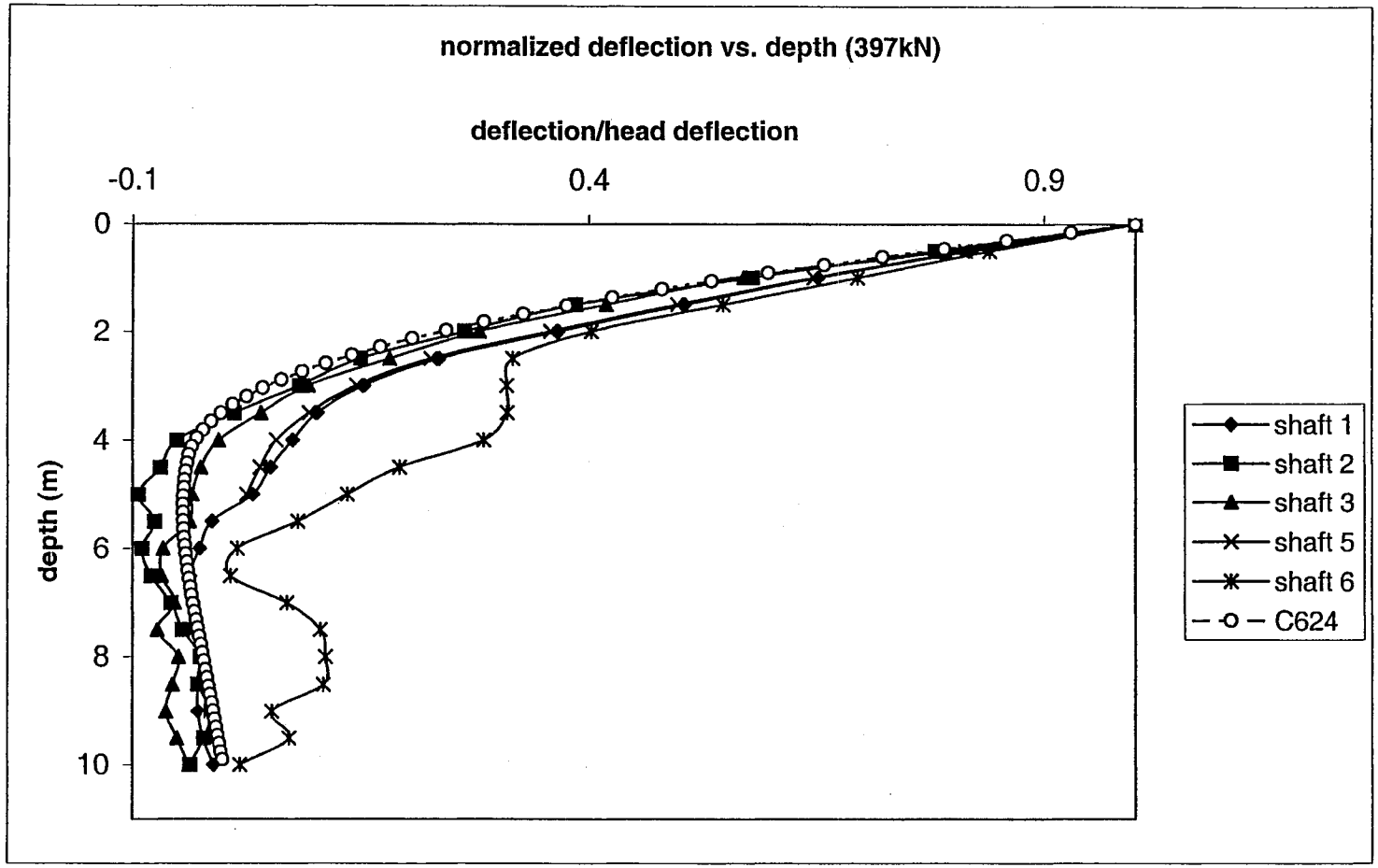

Figure 5.26

SPT Normalized Deflection vs. Depth for 397 kN Load

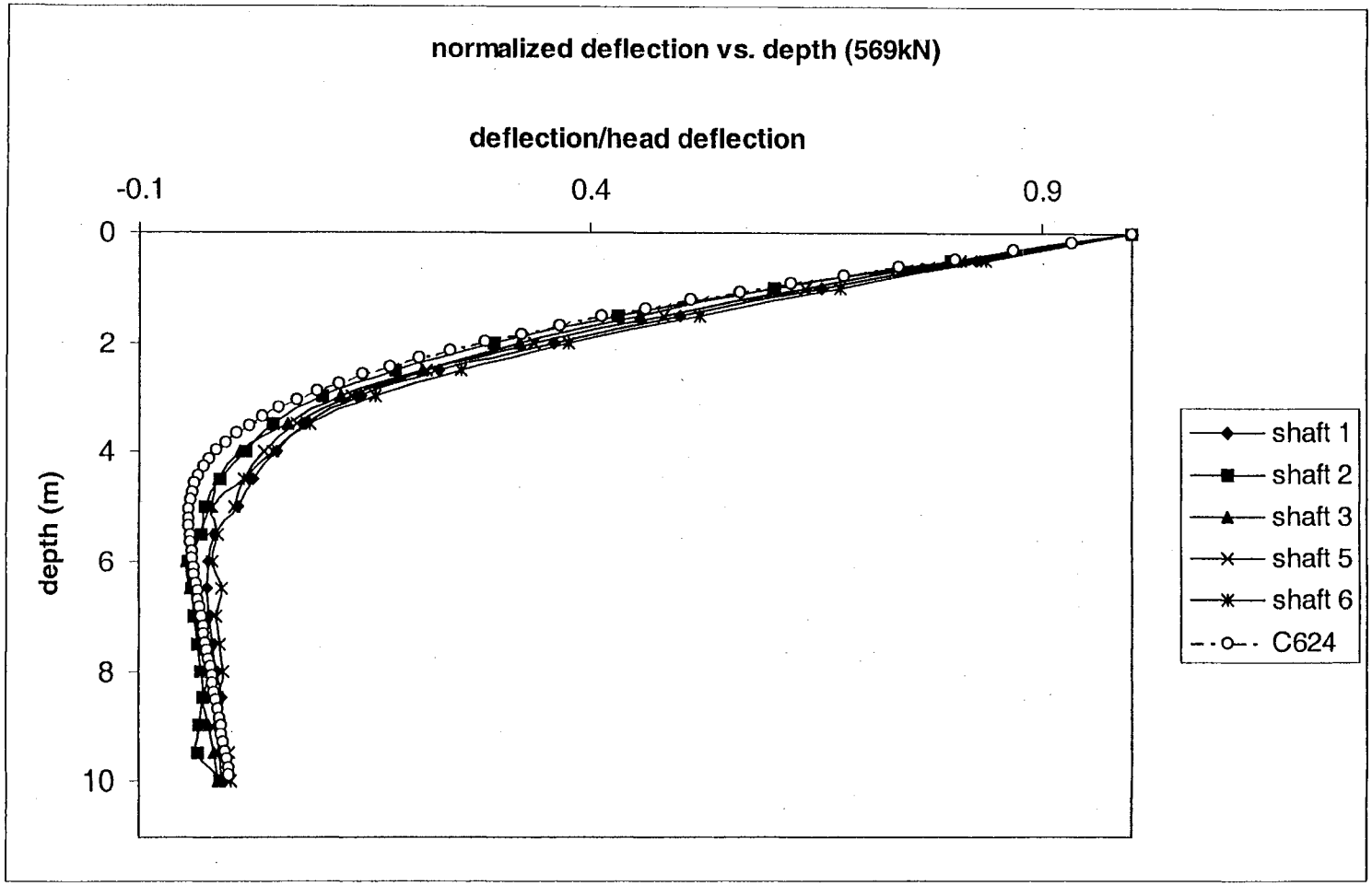

Figure 5.27

SPT Normalized Deflection vs. Depth for 569 kN Load

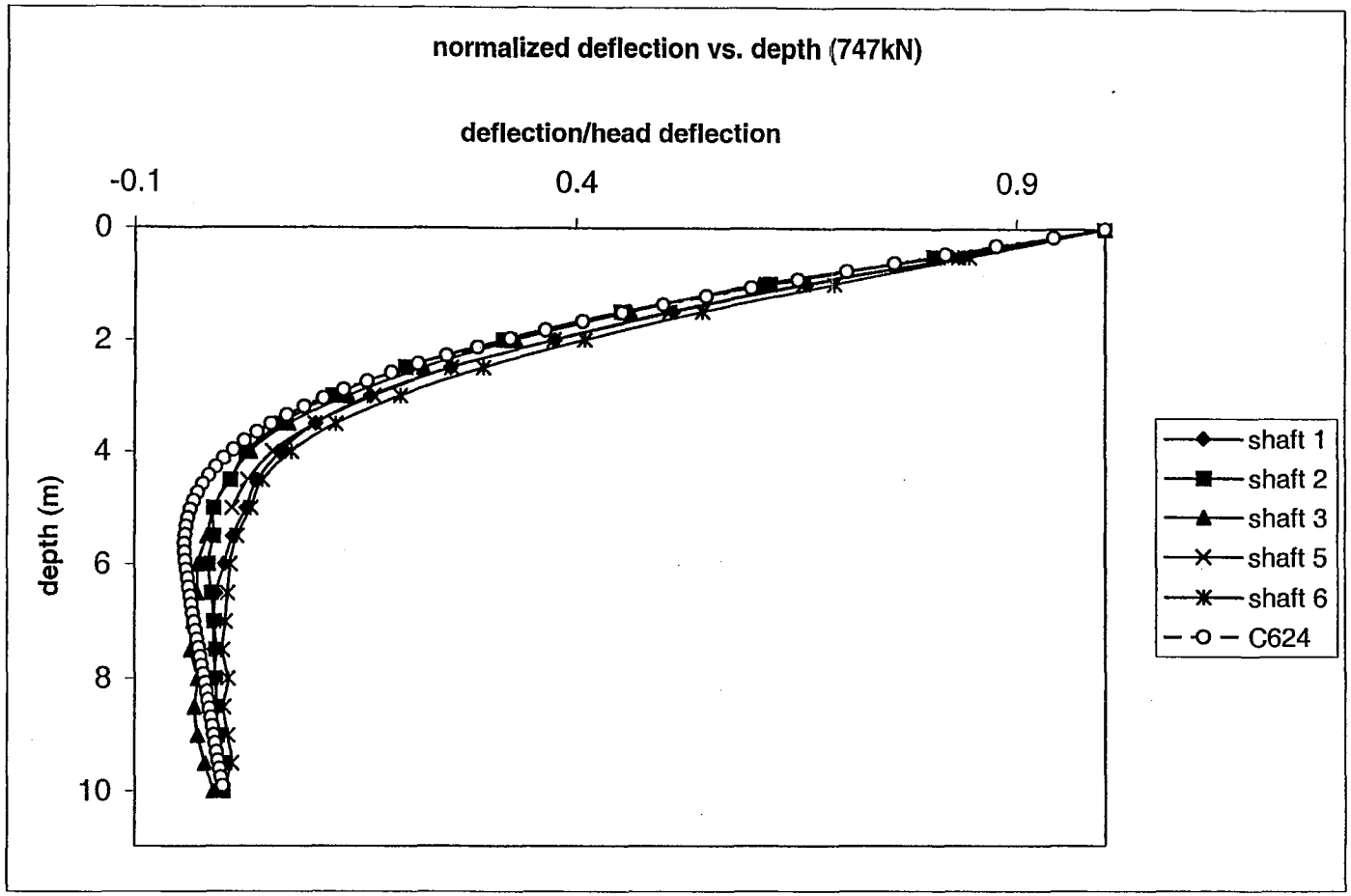

Figure 5.28

SPT Normalized Deflection vs. Depth for 747 kN Load

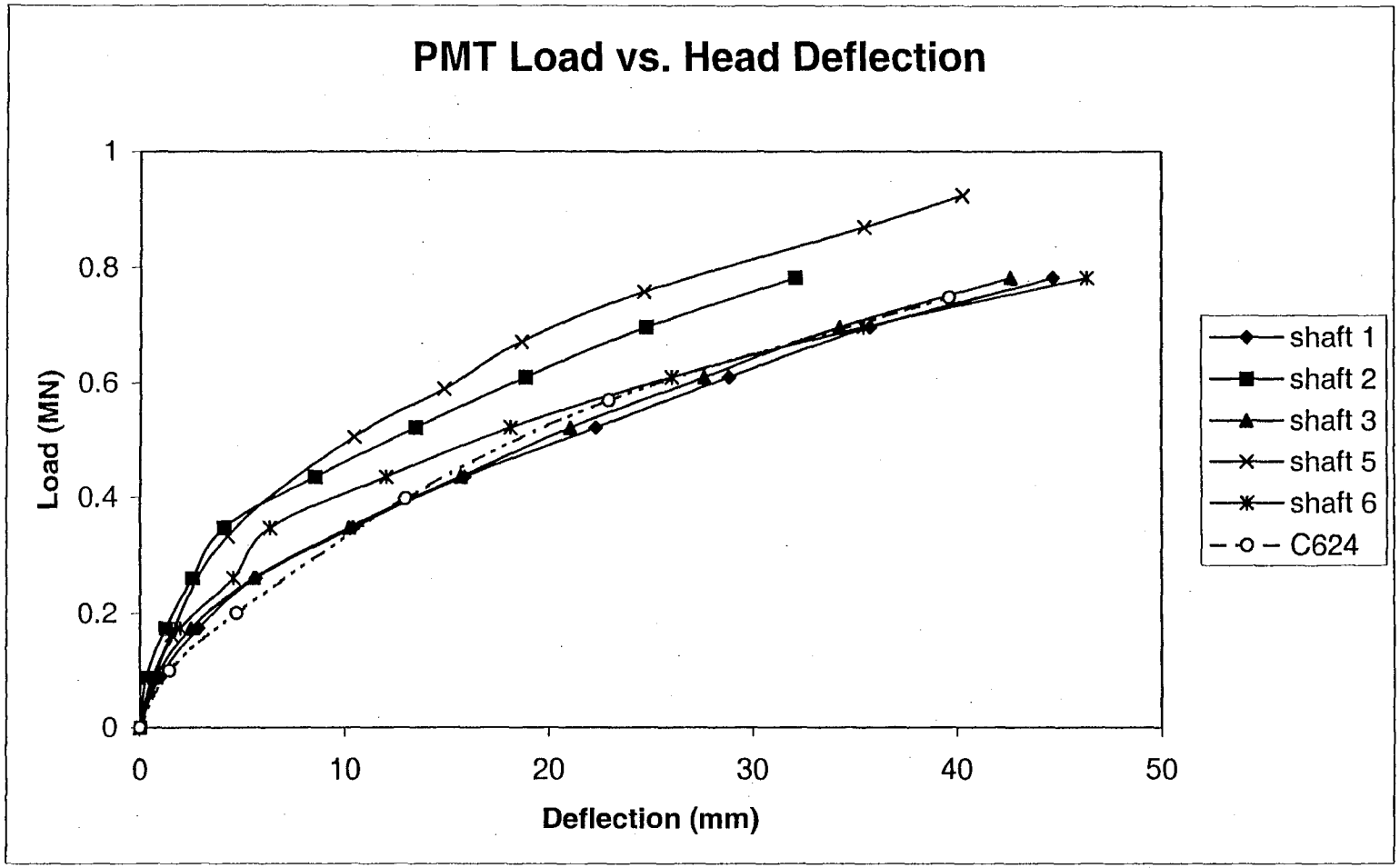

Figure 5.29

PMT Load vs. Head Deflection

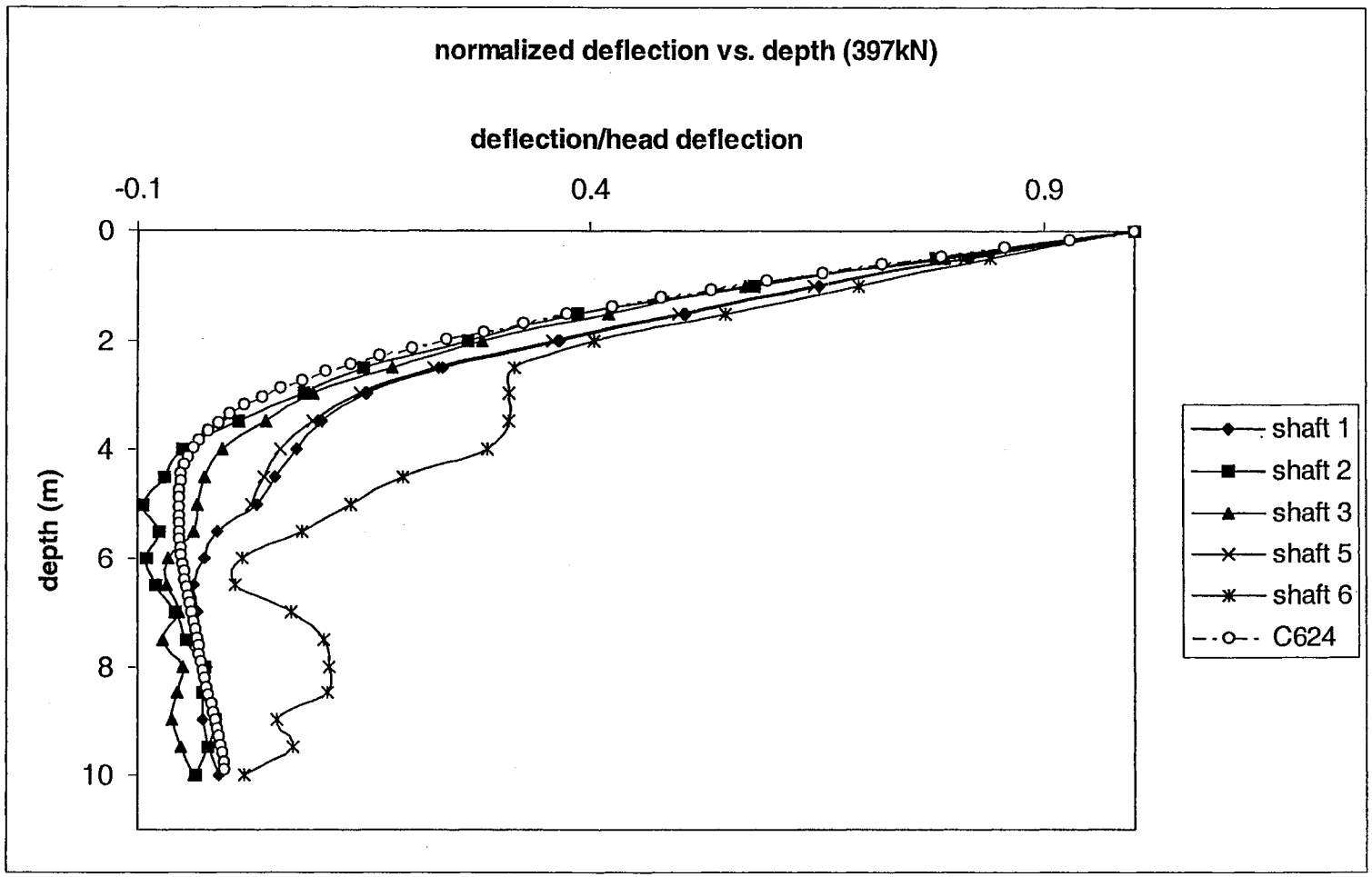

Figure 5.30

PMT Normalized Deflection vs. Depth for 397 kN Load

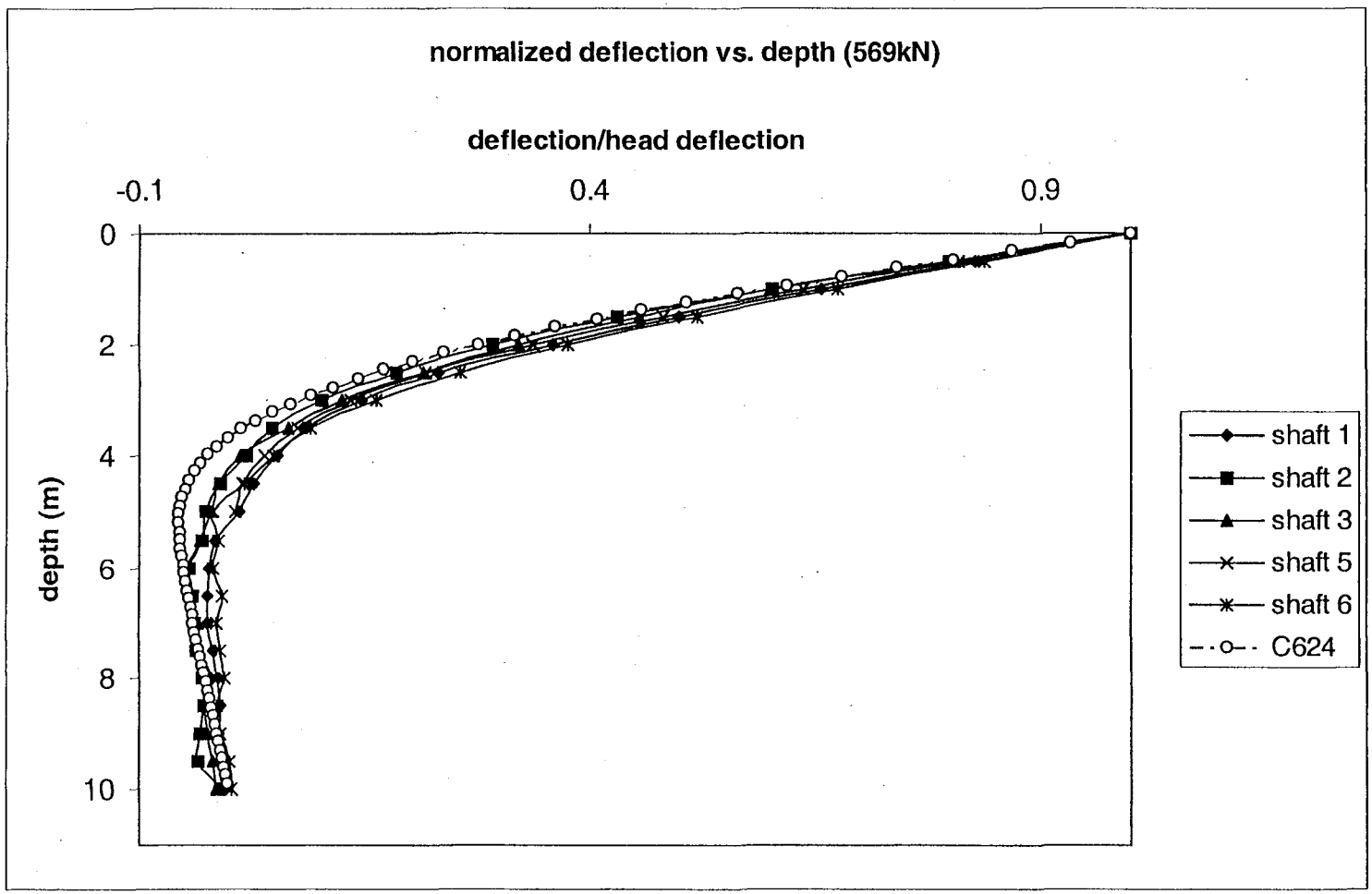

Figure 5.31

PMT Normalized Deflection vs. Depth for 569 kN Load

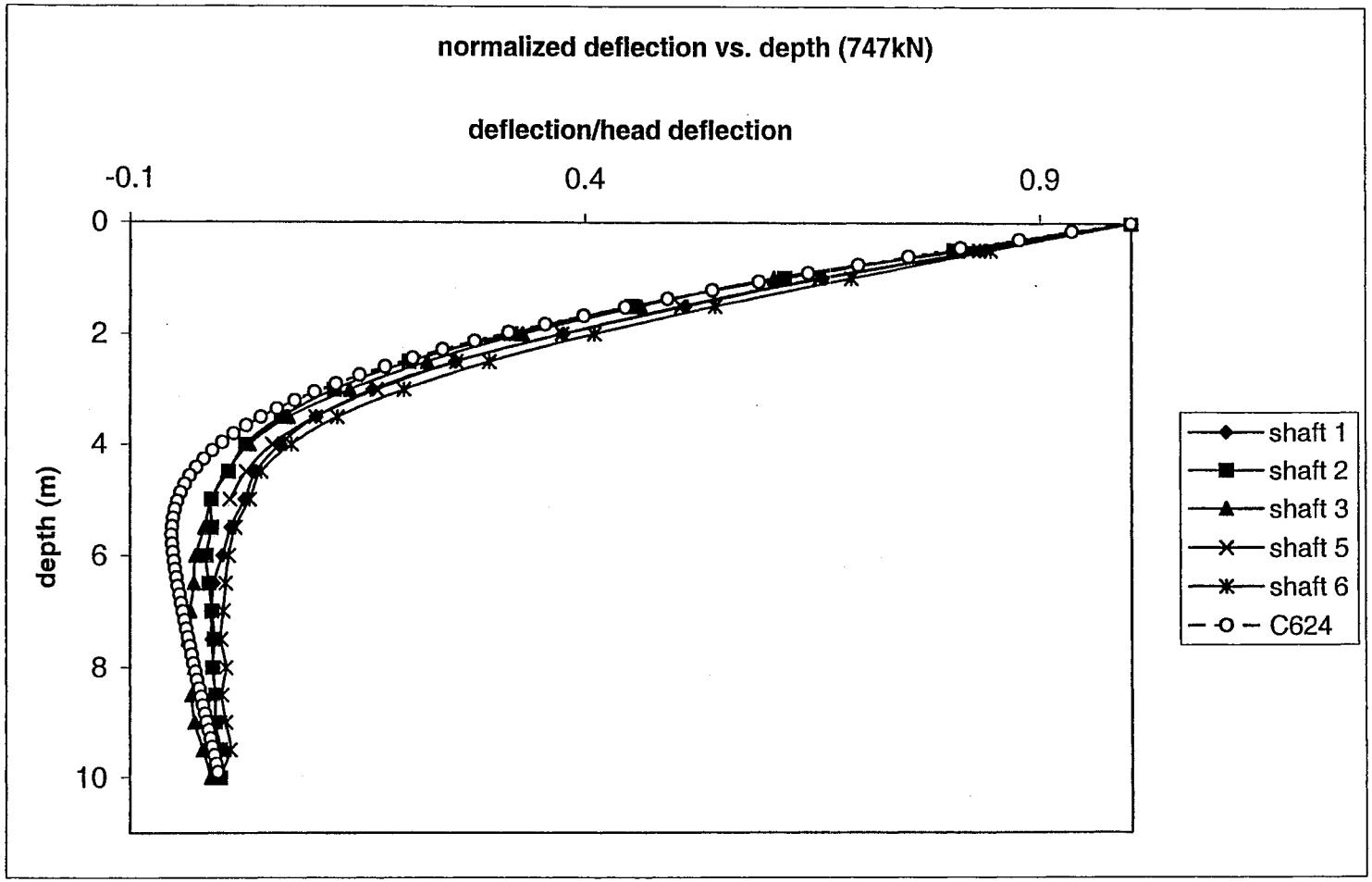

Figure 5.32

PMT Normalized Deflection vs. Depth for 747 kN Load

5.6 Sensitivity to EI

COM624 calculates EI based on the input concrete compressive strength (f'_c). The program calculates the initial concrete modulus as 57,000 $(f'_c)^{0.5}$. For this research, the concrete strength was approximately 4500 psi. In order to evaluate the influence of this parameter, some sensitivity tests were performed using COM624.

Presented in figure 5.33 are deflections calculated in COM624 for concrete strengths of both 4500 and 5500 psi. The plot is the deflection versus depth produced using the DMT equation with a 569 kN load. Notice that the deflections are almost identical. Small differences in the measurement of concrete compressive strength do not appear to significantly influence the computations.

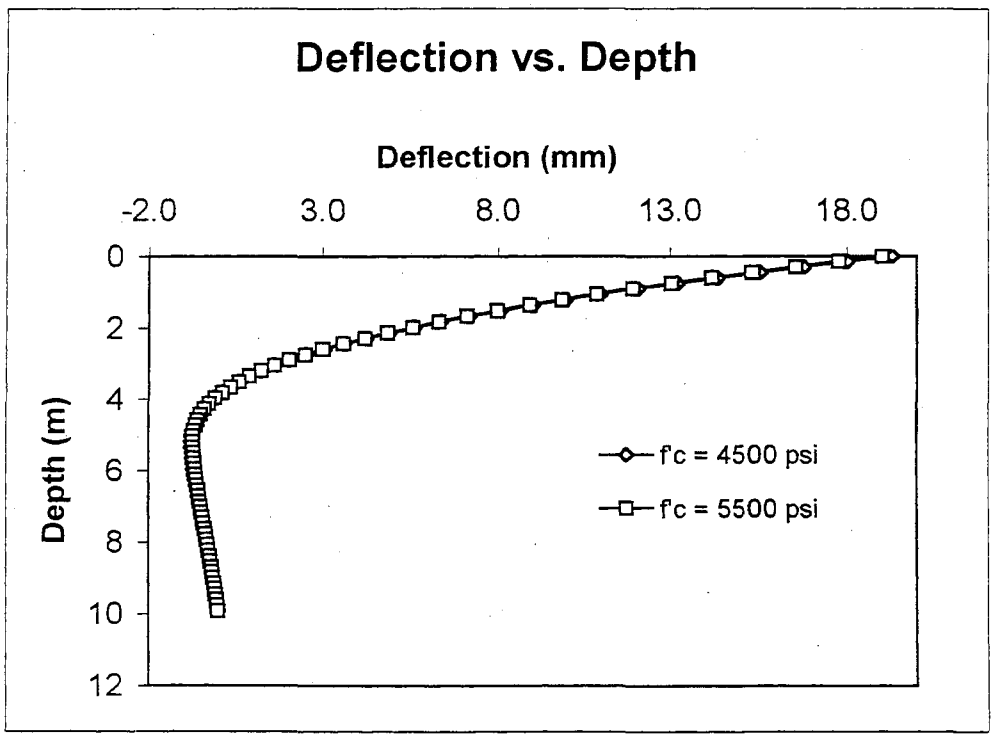

Figure 5.33

Deflection vs. Depth with Varying Concrete Strength

5.7 Summary

COM624 lacks a criterion for computing p-y curves for residual soils. A formulation has been presented which can be used to compute p-y curves based on correlations with four types of in-situ test data developed from the Spring Villa Test Site. Using these p-y curves, COM624 becomes a useful tool in predicting pile behavior in Piedmont residual soils.

The presented criterion was formed using full-scale lateral load tests and in-situ tests performed in residual soil. A simple relationship shown in equation 5.3 relates p with k (E_S = k/b) and y. A logarithmic degradation of E_S was assumed to account for the non-linear decrease in soil stiffness with increased load and deflection. The model was adjusted to back fit the data from the test site. The equation in a general form is as follows:

$$p = (E_S)(b)(y)$$

where:

$$E_S = E_{Si} \text{ ; for y/b} < 0.001$$

$$= E_{Si}\left[1 - \lambda \ln\left(\frac{y/b}{0.001}\right)\right] \text{ ; for } 0.001 < \text{y/b} < 0.0375$$

$$p = p_{ult} \text{ ; for y/b} > 0.0375$$

$$p_{ult} = (b)(y)[1 - 3.624\lambda]$$

$$\lambda = -0.23$$

$$E_{Si} = (0.076)(E_{DMT})$$

$= (0.118)(q_c)$

$= (22)(N_{SPT})$

$= (0.235)(E_{PMT})$

b = diameter of pile

y = deflection

The results using this criterion match the data collected in the field to a degree sufficient for design of laterally loaded drilled shafts. The shape of the deflected pile is captured quite well by all four equations. Also, the head deflections calculated using these equations are conservative. Since the equations produce similar results, each one should be equally useful in design.

CHAPTER 6

SUMMARY AND CONCLUSIONS

6.1 Summary

Six Full-scale load tests and several in-situ tests were performed at the Auburn University Geotechnical Research Site. The data from the in-situ tests were used to create a criterion for developing p-y curves for Piedmont residual soils. Equations to develop these p-y curves were formed using the DMT, CPT, SPT, and PMT. Linear p-y curves were used in COM624 to match the deflections measured in the field tests. A trend was observed between the in-situ data and the slope of these p-y curves. A simple relationship, equation 5.3, was used to relate p and y. The equations were then formed by accounting for the decrease in soil stiffness with increasing deflection, and by incorporating the in-situ test data to form each equation. The five non-defective load tests served as a basis for checking the accuracy of this criterion by using COM624 to predict the deflections from these input p-y curves.

6.2 Conclusions

The objectives of this research were to analyze the load tests performed at the Spring Villa geotechnical test site located in Opelika, Alabama and from the analysis, to give recommendations for computing p-y curves for laterally loaded piles in the piedmont

residuum. A criterion for developing p-y curves was developed using in-situ test data from the site. The criterion produced results which were similar to the field test data. The results were conservative and sufficient for design of laterally loaded piles. The data suggest that a useful criterion has been developed for Piedmont residual soils.

6.3 Recommendations for Further Research

The following recommendations are made concerning the developed criterion for p-y curves in Piedmont residual soils:

1. These p-y criteria need to be implemented into COM624 or LPILE using a new subroutine.
2. Additional tests need to be conducted in other areas of the Piedmont. The residual soils in which this research was conducted lies in one localized area of the Southern Piedmont. Different ranges of shaft diameter need to be tested. Most important, more tests need to be performed in a range of different soil stiffness and A-horizon thickness.
3. It is important to compare future test results with a variety of in-situ tools, since the cross-correlations may also vary.
4. Field test data is needed for other silty soil geologic conditions similar to the Piedmont.

There is much further research needed involving the development of p-y curves for residual soils.

REFERENCES

Matlock, H. (1970). "Correlations for Design of Laterally Loaded Piles in Soft Clay", 2nd Annual Offshore Technology Conference, Houston, Texas, pp 577 – 594.

Mayne, P.W., and Brown, D.A. "Site Characterization of Piedmont Residuum of North America".

O'Neill, M.W., and Reese, L.C. (1999). Drilled Shafts: Construction Procedures and Design Methods, U.S. Department of Transportation, Federal Highway Administration, McLean, Virginia.

Reese, L.C. (1997). Handbook on Design of Piles and Drilled Shafts Under Lateral Load, U.S. Department of Transportation, Federal Highway Administration, McLean, Virginia.

Reese, L.C., Cox, W.R., and Grubbs, B.R. (1974). "Field Testing of Laterally Loaded Piles in Sand", 6th Annual Offshore Technology Conference, Houston, Texas, pp 459 – 472.

Reese, L.C., Cox, W.R., and Koop, F.D. (1974). "Analysis of Laterally Loaded Piles in Sand", 6th Annual Offshore Technology Conference, Houston, Texas, pp 473 – 483.

Reese, L.C., Cox, W.R., and Koop, F.D. (1975). "Field Testing and Analysis of Laterally Loaded Piles in Stiff Clay", 7th Annual Offshore Technology Conference, Houston, Texas, pp 671 – 690.

Reese, L.C., and Welch, R.C. (1975). "Lateral Loading of Deep Foundations in Stiff Clay", Journal of Geotechnical Engineering Division, 101:7, pp 633 – 649.

Robertson, P.K., and Mayne, P.W. (1998). "Geotechnical Site Characterization", Proceedings of the First International Conference on Site Characterization, Atlanta, Georgia, pp 1229 – 1234.

Sowers, G.F. (1954). "Soil Problems in the Southern Piedmont Region", Proceedings, ASCE, Vol. 80, separate 416, pp 1 – 16.

Sowers, G.F. (1963). "Engineering Properties of Residual Soils Derived from Igneous and Metamorphic Rocks", Proceedings, 2nd Pan American Conference on Soil Mechanics and Foundation Engineering, Rio De Janeiro, Brazil, Vol. 1, pp 39 – 61.

Sowers, G.F., and Richardson, T.L. (1983). "Residual Soils of the Piedmont and Blue Ridge", Transportation Research Record, No. 919, Washington, D.C., pp 10 – 16.

Vinson, J.L., and Brown, D.A. (1997). Site Characterization of the Spring Villa Geotechnical Test Site and a Comparison of Strength and Stiffness Parameters for a Piedmont Residual Soil, Auburn University Highway Research Center, Auburn, Alabama.